A NUMERICAL SIMULATION OF

DIESEL AUTOIGNITION

by

Mark A. Theobald

B.A. Kalamazoo College
(1975)

M.S.E. University of Texas at Austin
(1977)

Submitted to the Department of
Mechanical Engineering
in Partial Fulfillment of the
Requirements of the Degree of

DOCTOR OF SCIENCE

at the

MASSACHUSETTS INSTITUTE OF TECHNOLOGY

February 1986

Signature of Author: _____
Department of Mechanical Engineering, 31 January 1986

Certified by: _____
Wai K. Cheng, Thesis Supervisor

Accepted by: _____
Ain A. Sonin, Chairman, Departmental Graduate Committee

A NUMERICAL SIMULATION OF

DIESEL AUTOIGNITION

by

Mark A. Theobald

Submitted to the Department of Mechanical Engineering on
31 January 1986 in partial fulfillment of the requirements
for the degree of Doctor of Science in Mechanical Engineering.

ABSTRACT

The autoignition behavior of an evaporating liquid fuel spray in a high pressure, high temperature environment typical of a diesel engine cylinder was examined experimentally and numerically. The ignition delay and high speed photographic data on diesel combustion were obtained for a typical diesel fuel using a Rapid Compression Machine. The autoignition kinetics model for gasoline knock developed by the group at the Shell Research Centre, and modified by Schäpertöns and Lee, was installed in the KIVA computational fluid dynamics code from the Los Alamos National Laboratory. The methodology was extended to predict diesel autoignition for heavy fuels. Two-dimensional calculations for dodecane fuel were compared to the spray ignition experiments of Hiroyasu. Two- and three-dimensional calculations were compared to the MIT experiments for a rapid compression machine. Correct trends for ignition delay versus temperature and pressure were found. Features of diesel autoignition were reproduced: they include the sensitivity of ignition sites and times to the random influence of turbulence and droplet-size distribution, the presence of multiple ignition sites, the apparent rapid spread of the enflamed area, and the approximate location of ignition.

Thesis Advisor: Dr. Wai K. Cheng

Title: Associate Professor of Mechanical Engineering

ACKNOWLEDGEMENTS

I thank the members of my thesis committee: Professors Judson Baron, Ahmed Ghoniem, John Heywood, and especially my advisor Wai Cheng for their sound counsel and unfailing availability during this research project. Professor James Keck provided insight and advice on the kinetics of autoignition.

The computations described herein were performed during my stay with Group T-3, Theoretical Fluid Dynamics at Los Alamos National Laboratory. Richard Gentry had carried out 3-D simulations of combustion in the rapid compression machine (RCM) prior to my arrival. He provided several of the specialized code updates listed in Appendix A as well as training on the CRAY system. T. Daniel Butler exhibited intense interest in the project and dispensed excellent advice on all matters. Group Leader Hans Ruppel gave permission to visit and foraged office space and priority computer time on the CRAY 1S. It is a pleasure to acknowledge helpful discussions with the authors of the computer code KIVA: Anthony Amsden, Peter O'Rourke, John Ramshaw, and John Dukowicz.

Experimental and computational work at the Sloan Automotive Laboratory at MIT was made possible by assistance from staff members Don Fitzgerald, Duane Page, Jim Watts, and Salvatore Albano. Fellow students Eric Balles and Kurt Colella carried out the particular experiments in the rapid compression machine which are described here. They, along with student Peregrine White, made major improvements to the RCM. These three also kept alive the spirit de corps of those who have known the frustrations (and dangers) of working with this experimental apparatus. My office-mates Cmdr. Al Brown, Genie Hainsworth, Ioannis Kyratzoglou, and James Moller offered many helpful suggestions. Finally, my wife Ruth Anne made the whole venture worthwhile.

This research was supported by the Industrial Consortium for Engine Research at the Sloan Automotive Laboratory. The members of the Consortium were:

Caterpillar Tractor Company,
Cummins Engine Company,
Deere & Company,
Gulf Research & Development Company,
Peugeot Societe Anonyme, and
Regie National des Usines Renault.

Representatives of these companies met at MIT four times per year for progress reviews. They provided constructive criticism and enthusiasm for this research.

This thesis is dedicated to the memory of my grandfather
Glenn Edward Theobald.

QUOTATION

...Instead we proceed with a mixture of optimism and utilitarianism: optimism, in the sense that we produce only finitely many numbers, subject them to only a few tests, and hope (with some justification) that they would have satisfied the remaining unmade tests; utilitarianism, in the sense that one of the tests that might have been applied is whether or not the random numbers yield an unbiased or a reliable answer to the Monte Carlo problem under study, and it is really only this test that interests us when we are ultimately concerned only with a final numerical solution to a particular problem. Taken in this second vein, the other tests are irrelevant; the numbers produced need not satisfy them. The more of the irrelevant tests we ignore, or indeed deliberately permit to be violated, the easier and cheaper it may become to generate the numbers, which now of course are no longer genuinely random but only 'pseudorandom' or 'quasirandom'. It is simply a question of sacrificing ideality to expediency. In Monte Carlo work justice will have been done if the final verdict is fair, i.e. the answers come out approximately right.

J. M. Hammersley and D. C. Handscomb
on the generation of random numbers
in Monte Carlo Methods,
(Barnes & Noble, New York, 1964).

TABLE OF CONTENTS

LIST OF TABLES

LIST OF FIGURES

LIST OF PLATES

CHAPTER I

INTRODUCTION

The diesel engine has become one of the prime movers of the modern industrial world since its invention in 1892. So it is perhaps surprising to find that the combustion process at the heart of this engine is rather poorly understood on a detailed, quantitative basis. This disparity between utility and intimate knowledge of the process is caused by the difficulty in seperating for study the coupled, near-simultaneous physical mechanisms which transpire within the complex combustion event. In the terms of fluid mechanics, the combustion process in a modern diesel involves the mixing of a transient, turbulent jet of evaporating fuel droplets into a swirling bulk flow of air at high temperature and pressure. The fuel and air mix to form a reactive atmosphere, which autoignites and then burns under diffusion control. The reactive medium is compressible and the high-speed fuel jet provides a source of mixing for combustion. The resulting combustion process in an engine must provide a satisfactory compromise between the conflicting demands of low pollutant emission, high specific power output, and good fuel economy at both high and low loads.

The difficulty of achieving both high efficiency and low levels of emissions has forced a renewed attack on the combustion problem using the new arsenal of supercomputers. This thesis represents a skirmish in an ongoing battle.

The basic diesel combustion process for a typical four-cycle, direct injection, reciprocating engine will now be described. The events are illustrated in Figures 1.1 and 1.2. Typical pressure records and heat release rate diagrams are given in Fig. 1.3. High speed photographs of a diesel combustion event are given in Plates 1-4 of Chapter V. During the intake stroke, air is drawn by the descending piston through an inlet valve and into the combustion chamber. Bulk motion of the air may be imparted by specially-shaped inlet tracts or shrouded valves. The inlet valve then closes as the piston begins to ascend. The piston compresses air plus any residual burned gases to high pressure and temperature. Liquid fuel is sprayed into the hot air by means of a high pressure fuel injector. The liquid spray disintegrates into small droplets which evaporate as they spread into the chamber. The resulting fuel vapor mixes with the air. The time delay during which the fuel is prepared for burning is often termed the physical delay. Precursor chemical reactions are believed to occur during and after the fuel mixing stage, causing an additional time delay referred to as the chemical delay. The fuel then autoignites, that is, combustion begins without an external source of ignition energy. The fuel which was mixed sufficiently with air to within combustible limits (said to be "pre-mixed") burns very quickly. The remaining unmixed or unevaporated fuel is burned more slowly and then only as it is properly prepared. The later stage of diesel combustion is described as being "mixing-controlled" or limited by the rate at which the fuel may be mixed with air. In the

engine, the high pressure gases derived from combustion drive the piston downward thereby delivering useful work to the crankshaft. The exhaust valve then opens and the piston rises to pump exhaust gases from the chamber, at which point the entire four-stroke cycle is repeated. An examination of the autoignition process in the diesel forms the subject of this thesis. The examination is carried out by means of numerical simulation or modeling.

Numerical modeling, that is, the numerical solution of differential or partial differential equations describing particular features of an engine process, offers several advantages for engine research, design, and development. To the analyst or researcher, the numerical model offers the possibility of isolating the effects of certain physical phenomena, for example, mass diffusion or heat conduction, in ways that may be difficult or impossible to achieve in a "real" experiment. Data with extreme resolution in space or time may sometimes be computed when a physical measurement is difficult to make. A model may also act as a heuristic tool to show trends or point out important features in a process. For the engine designer, models offer the possibility of reducing the number of prototypes built; the chance to optimize a design without the extensive and costly testing now required. Large commercial airliners are designed using computational fluid dynamics (CFD) models solved on a computer. The results of these calculations have reduced the amount of wind tunnel testing needed to optimize a design. It may be hoped that combustion engine design can eventually be so well understood as to allow a similar reduction of effort and cost to be made.

Particular interest in computing diesel autoignition stems from the need to improve the combustion predictions in present numerical models.

The autoignition event in the diesel engine controls the heat release schedule; therefore the timing of the event is important in correctly predicting the work output possible. Also, the rapid pressure rise found in the premixed burning stage is a major contributor to the noise associated with diesel engines.[1] Modern engine designs have tended to shorten the ignition delay period and decrease the relative magnitude of premixed burning because of high pressure and temperature conditions in the cylinder, and by the use of high-pressure, multi-nozzle injectors. The ignition delay in modern turbocharged engines is of the order of one-half millisecond, representing only about three degrees crank angle at 1000 RPM. The ability to predict the absolute ignition time is then perhaps of less interest than is the eventual ability to calculate the sensitivity of the autoignition event to different fuels. The location of the ignition event may also have an effect on the initial rate of flame spreading in the cylinder, and thus influence the rate of pressure rise.

A second major reason for interest in simulating diesel autoignition is to attempt to understand the wide scatter in the experimental data found in the literature. Researchers over the last fifty years have not been able to determine, in a quantitative manner, the mechanism(s) dominating autoignition under given (though often poorly known) conditions. The research effort of this thesis would address this issue and contribute to improving the present understanding of diesel combustion.

Goals and Scope

The goals of this thesis are

> to exercise an existing autoignition chemistry model in the

environment of an evaporating spray,

> to investigate whether the autoignition model may be extended appropriately to the heavier fuels of interest in diesel combustion,

> to investigate whether the proper scaling of ignition delay with temperature and pressure may be reproduced by the numerical simulation, and

> to examine the features of a multi-dimensional simulation of the diesel ignition process under conditions representative of current diesel geometry and practice.

Because of the lack of complete understanding of the physics and chemistry as well as the uncertainty in the parameters used by the model, the simulation of the autoignition of an evaporating spray is not a precise exercise. However, this is believed to be the first attempt to simulate the autoignition of a fuel spray directly and consistently from the underlying physical principles.

The interest in the present work is focused on the autoignition event in an evaporating spray. Computations are continued only to the time of autoignition or slightly beyond. No attempt is made to carry through the entire combustion period. The main reason for this limitation is the inadequacy of the present turbulence model for describing the flow once large amounts of heat are released. This limitation should be relaxed as more complicated turbulence models are included in the parent program. Similarly, the geometry is limited to two simple cases: the two-dimensional axisymmetric jet and the centrally-located injection jet found in the simple pancake-shaped combustion chamber of the MIT rapid compression machine. Compression and inlet valve flows are not addressed in this work

and all combustion takes place at constant volume. Thus the flows in an operating engine are approximated only near top center.

Organization

The thesis is organized in the following way. Prior investigations related to the present work are cited in Chapter II. The synthesis of the autoignition model is explained in Chapter III. Experiments from the literature and work at MIT to which the computations will be compared are described in Chapter IV. The present author contributed to major modifications of the MIT rapid compression machine and to early entries in the data base. The description of this apparatus is expanded to reflect that work. The results of the calculations and their comparison to experimental data are contained in Chapter V. Conclusions and recommendations for further work are summarized in Chapter VI. Finally, the computer codes used to perform the autoignition calculations are listed in the Appendices. These codes are augmentations of the KIVA program.[2] Superscript numbers throughout the text refer to the references listed in numerical order at the end of the thesis. All figures appear in order following the references.

CHAPTER II

REVIEW OF PREVIOUS STUDIES

Combustion in the diesel engine involves, as explained earlier, the combustion of an evaporating spray of liquid droplets in a turbulent flow field with moving boundaries. The combustion event is initiated by chemical reactions characteristic of the specific fuel in the diesel environment. Thus a complete revue of the literature applicable to the modeling of diesel combustion would comprise synopses of turbulence, computational fluid dynamics, spray and droplet mechanics, the fuel properties as well as the thermodynamics of fluids at high temperatures and pressures, and combustion chemistry. In addition it would be necessary to examine the experiments performed in each of these areas in order to glean information on the correctness of the models or to calibrate unknown coefficients in the models. Instead, in the summary to follow, four main areas of research will be highlighted. These are combustion modeling, autoignition experiments, autoignition chemistry, and the efforts to couple the autoignition chemistry with fluid motion. Excellent review papers are available for many of the subject areas and these are cited for brevity. Then specific papers most relevant to the present work are outlined in more detail.

COMBUSTION MODELING

In the effort to understand combustion better, the engineering community constructs models of the component processes. That is, a given process is simplified conceptually to the point where descriptive differential equations may be written. Correlations and dimensional analysis of an effect are also used to quantify a process. A general review of models applied to engine combustion has been given by Heywood in a recent symposium.[3] A model of a phenomenon may arise in several ways. So-called phenomenological models are defined by Blumberg, et. al.[4] as assemblies of "seperate, physically-based submodels of important identifiable phenomena". In contrast to this approach is the practice of solving the governing conservation equations for the physical region of interest, often termed the multidimensional approach. A review of the application of phenomenological models to engine combustion including diesels is given by Blumberg, et. al. It may be noted that phenomenological models have proved to be difficult to apply in describing diesel autoignition. This fact may be attributed to the complexity and close coupling of the underlying physical processes, especially in the geometric aspect of the fuel spray, which cannot be described easily by such models. The method to be used in this thesis is the multidimensional approach utilizing computational fluid dynamics (CFD). Reviews of the application of CFD methods to combustion have been provided by Aggarwal and Sirignano,[5] Oran & Boris,[6] and Kahlil.[7] Oran & Boris give particular attention to the difficulty of describing the propagation of flames in CFD models. They point out the important roles played by numerical diffusion

and the effects of the wide range of time scales which tend to degrade the solutions. Reviews specific to internal combustion engines were given by Butler et. al.[8] and Bracco and O'Rourke.[9] Methods for describing and simulating fuel sprays (necessary for detailed simulations of diesel combustion) were reviewed by Elkobt[10] and Faeth.[11]

Two- and three-dimensional simulations of diesel combustion have been carried out by several investigators. See, for example, the papers of Gosman,[12] Duggal and Kuo,[13] and Amsden, et. al.[2] The results from this type of computation are yielding new and detailed information on the mixing processes in diesel combustion. The treatment of combustion in these investigations has taken two main forms: either (1) The assumption is made that a single Arrhenius rate equation adequately describes the entire course of ignition and combustion, or (2) The simplification is imposed that the chemical reaction time is instantaneous relative to fluid dynamic mixing time (e.g. the eddy breakup model[14] is employed). The first method has proved difficult to implement with a reasonable reaction rate that results in the proper flame spread and heat release rate.[12] The second description also is not sufficient, particularly for very cold starting conditions when ignition delay apparently becomes much longer than the mixing time.[15] The use of separate chemical reaction descriptions for autoignition and main combustion may ultimately resolve these conflicts.

AUTOIGNITION EXPERIMENTS

Autoignition is the onset of combustion in a reactive medium without the introduction of an external initiating source. Autoignition may be triggered, as it is in diesel engines, by quickly compressing the mixture.

Autoignition has been observed to be either a one- or two-stage event depending on the physical conditions and the fuel. The first stage of ignition, which may or may not be present, is characterized by the appearance of one or more cool flames. The cool flame liberates a small amount of heat and blue light. Second-stage ignition appears after a certain delay and the bulk of the reaction heat is then liberated.

The elapsed time between the beginning of fuel injection and some indicator of the onset of combustion is termed the ignition delay. One may conceive of this delay as stemming from two separate sources. The physical delay is that period required for some portion of the fuel spray to evaporate and mix with air to proportions which can sustain combustion. The time required for the chemical reactions to run to completion is termed the chemical delay. Because many chemical reactions exhibit an exponential dependence on temperature while physical processes such as mixing are not as sensitive to temperature, one then expects that the ignition delay at high temperatures would consist in the main of physical delay, while at low temperatures chemical delay would dominate the total. Indeed the data of some investigators seem to show a temperature dependence congruent with this explanation.[16]

The working definition of ignition delay is often intimately tied to the method used to detect the onset of ignition. If a photodetector or photographic film is used to record ignition, then the "illumination" delay, the time elapsed before light is detected, becomes the operational definition. The time to a detectable pressure rise, either in absolute terms or relative to the case of no combustion (motoring, in an engine) is termed the "pressure-rise" delay. In practice various smoothing methods may be applied to the raw pressure data before identifying the change in

slope on the pressure record. Each definition may yield slightly different values depending on the particular experiment.[17] When calculating autoignition times via a chemical kinetics scheme, other definitions of autoignition time may be needed. In the simulation of their experiment in a rapid compression machine (RCM), the group at the Shell Research Centre defined the first-stage autoignition delay τ_1 (time to cool flame) as the time delay from the attainment of top center conditions to a maximum in the radical species population.[18] Their corresponding measurement in the RCM was the time to the small pressure rise associated with the cool flame.[19] Shells's definition of the onset of second-stage (hot) ignition was the time after top center τ_{total} at which the (homogeneous) cylinder contents reached a computed temperature of ~1100 K. The relevant experimental measurement was the time to the large pressure increase associated with second-stage ignition.

The traditional correlation form for the ignition delay τ has been of the simple Arrhenius form

$$\tau = Ap^{-n} \exp(E/RT).$$

Here A is a constant, p is the pressure, n is a constant, E is an activation energy, R is the universal gas constant, and T is the temperature. The results for one experimental device using one fuel can usually be expressed in this form. When one attempts to compare spray ignition data from different experimenters (see, for example, Spadaccini and TeVelde[20]), it becomes apparent that the values of the parameters A, n, and E are not unique for a given fuel. Evidently the physical arrangements of the experiments also influence the data.

The standard method of rating the autoignition quality of a fuel is the cetane number scale.[21] The current standard rates a fuel between values of

15 and 100 (increasing values indicate an increasing susceptibility to autoignition, a desirable feature for a diesel fuel) based upon experiments in a standard engine. This rating method has never been entirely satisfactory and a number of alternative rating methods have been proposed.[22]

A great deal of basic autoignition data has been gathered for application to the homogeneous charge engine. See, for example, Taylor, et. al.[23] Much of the autoignition data in the literature on sprays concerns the determination of the ignition delay in steady combustors suitable for use in gas turbine engines. While of interest, these combustors are physically quite different than high pressure diesel injectors and make the data of limited use for the present purposes. Nevertheless, the exhaustive work of Mullins[24] in measuring ignition delays for many fuels is noted. The more recent experimental work of Spadaccini and TeVelde[20] for a steady, gas turbine-type combustor points up the importance of the details of fuel/air mixture preparation on the measured ignition delay.

There exists in the literature a vast array of measurements of ignition delay for particular practical engines and engines specially modified for diagnostic data. See, for example, Lyn and Valdmanis.[25] But the general utility of these data is compromised when one recognizes that each engine has a somewhat different combustion chamber shape, injector type, and fuel and cylinder conditions.

For the purpose of investigating the computation of ignition delays in sprays, an experiment with a simple geometry is desirable for comparison. Several experimenters have utilized combustion bombs or rapid compression machines outfitted with injectors to examine autoignition. See, for

example, the work of Hurn and Smith[26] and Kobayashi, et. al.[27] The most complete set of experimental data for the autoignition of diesel-type fuels in a simple geometry is that of Hiroyasu and coworkers.[28] These data will be compared with computations in Chapter V. A disadvantage of much of the experimental work on autoignition is that the pressure rise and rate of flame spreading are usually unreported, making it difficult to compare more than just the time to ignition between computation and exeriment.

AUTOIGNITION KINETICS

The creation of the existing chemical models for autoignition was mainly inspired by the increasingly critical need to understand and quantify the phenomenon of knock in the spark-ignition engine. Knock is believed to be the autoignition of premixed charge compressed between an advancing flame front and the cylinder wall. Fundamental theoretical studies of hydrocarbon combustion have involved the cataloging of a large number of chemical reactions that may occur between the fuel and air and the many intermediate species. The resulting set of up to several hundred equations must then be integrated numerically. The solution of such large sets of equation sets may yield little insight into the limiting reactions in the problem. These enterprises have generally been limited to the lighter hydrocarbon fuels such as methane because the number of possible reactions escalates rapidly with the molecular weight of the fuel. No such studies are available for the heavy fuels typical of diesel combustion. The description of combustion at high temperatures ($T > 1000$ K) generally involves more equations but less conceptual difficulty than for ignition at

lower temperatures.[29] Westbrook and Dryer[29] have summarized the state of understanding for high temperature combustion.

The important work of the research group of Halstead, et. al.[18,30] at the Shell Research Centre has resulted in a kinetics-based model (henceforth to be referred to as the Shell model) for hydrocarbon autoignition based on the degenerate branched chain mechanism as outlined by Semenov.[31] This model (to be described more fully in Chap. III) employs generic molecular species which obviates the accounting for every conceivable reaction. The model is able to simulate the important phenomena of high-pressure autoignition: cool flames, multiple cool flames, and second stage ignition. The large amount of simplification involved in the Shell model has prompted several attempts to put the fitted parameters (reaction rates, etc.) on a firmer, more fundamental basis. Cox and Cole[32] have refined the Shell model by improving estimates of the chemical reaction rates involved using newer data from the chemical literature.[33] The cost of this endeavor has been to increase the number of reactions from 8 to 15, some of which are equilibrium reactions. Keck and coworkers[34] are also working to improve estimates of the chemical rates involved.

The parameters for the Shell model have been matched to data for several fuels of interest for spark ignition engines. It should be possible to repeat this fitting procedure for the heavier fuels used in diesel engines. Required for this undertaking would be experimental autoignition data for premixed heavy fuels over a range of temperatures and pressures. Unfortunately such data do not seem to exist. Some autoignition measurements have been carried out for diesel-weight fuels at very low pressures (the order of 100 Torr) for investigations of cool

flames by employing low pressure injection. The heavy fuels are difficult to vaporize, especially at high pressures, without heating them sufficiently to cast doubt on the resulting ignition data. See, for example, the paper of Wilk, et. al.[35] The composition of diesel fuel is often uncertain. Practical fuels are refined from crude oil and contain many hundreds of different compounds, each boiling at a different temperature.[36] As in spark ignition work, it is a standard practice in computations or laboratory experiments to substitute a pure fuel for the practical fuel. For the computations reported here, dodecane was chosen to represent the physical properties of diesel fuel. Other pure fuels have been used for this purpose including tridecane, tetradecane, and hexadecane.

THE COUPLING OF AUTOIGNITION KINETICS WITH CFD METHODS

The first step toward coupling the Shell autoignition model with a description for fluid motion was taken by its authors, Hirst and Kirsch.[37] They carried out preliminary calculations by estimating the rate at which gaseous fuel and air mix under the conditions found in a diesel cylinder. The ignition parameters used for the fuel were basically those for 70 Primary Reference Fuel (cetane number = 25), but the parameters were modified in an unspecified way. By varying the mixing rate coefficient they were able to compute ignition delays in the practical range of 1 millisecond.

Schäpertöns and Lee[38] made the large step of linking the autoignition kinetics with an existing CFD program for two-dimensional gas motion in a premixed charge. Their contributions are utilized in the present work and

are outlined in detail in Chapter III. These authors were able to simulate knocking conditions in a rapid compression machine and in practical engines. They properly identified trends in knock sensitivity with temperature and compression ratio. Natarajan and Bracco[39] have followed a similar methodology also to examine knock in homogeneous charge engines. They also were able to generate the correct trends for autoignition behavior in a combustion bomb, a rapid compression machine, and a spark-ignition engine. Some of the problems encountered by both groups as well as their suggestions will be discussed in Chapters III and V. No similar investigations are known for the parallel but perhaps more complicated case of diesel autoignition. It is this gap in the logical progression that the present work is meant to fill.

CHAPTER III

SYNTHESIS OF THE AUTOIGNITION MODEL

The coupled fluid mechanics and chemistry model exercised in this thesis was synthesized from several components which had been presented independently in the literature. The features and manner of integration of the components for the synthesis are explained in this chapter. A complete fluid mechanics, droplet dynamics, and chemistry equation solver was provided by the KIVA code developed at Los Alamos National Laboratory.[40,41] The features of this code are summarized below. The autoignition model of the Shell Research Centre with the significant modifications of Schäpertöns and Lee was installed in the KIVA code for specific application to diesel ignition. Other modifications were made for use with the case of diesel combustion. The modified Shell model was extended here to the use of fuels with higher molecular weights than for the fuels studied by Shell. The Shell model and the modifications of Schäpertöns and Lee will now be summarized. More detailed information is available in the original papers.[18,30,38]

AUTOIGNITION KINETICS--The Shell Model

The Shell autoignition model makes use of the following generic molecules:

RH, hydrocarbon fuel of chemical formula C_nH_{2m},

R^*, radical formed from the fuel,

B, branching agent,

Q, intermediate species, and

P, burned products, consisting of CO, CO_2, and H_2O in specified proportions,

where the superscript * denotes a radical. In addition, the local concentrations of O_2 and N_2 are needed to compute the reaction rates. The eight equations comprising the model are:

Function	Equation	Rate Coefficient	
Initiation	$RH + O_2 \rightarrow 2R^*$	k_q	(1)
Propagation	$R^* \rightarrow R^* + P$	k_p	(2)
	$R^* \rightarrow R^* + B$	$f_1 k_p$	(3)
	$R^* \rightarrow R^* + Q$	$f_4 k_p$	(4)
	$R^* + Q \rightarrow R^* + B$	$f_2 k_p$	(5)
Branching	$B \rightarrow 2R^*$	k_b	(6)
Linear termination	$R^* \rightarrow$ nonreactive species	$f_3 k_p$	(7)
Quadratic termination	$2R^* \rightarrow$ nonreactive species	k_t	(8)

All rate coefficients take the Arrhenius form k= A exp(-E/RT) with the exception of k_p, which has a form compounded from three seperate rates:

$$k_p = \frac{1}{1/[k_{p1}(O_2)] + 1/k_{p2} + 1/[k_{p3}(RH)]} \quad , \qquad (9)$$

where () denotes molecular concentration in, for example, moles/cm^3, and k_{p1}, k_{p2}, and k_{p3} are the rate coefficients for the propagation steps first order in (O_2), unimolecular, and first order in (RH), respectively. The propagation path includes the heat release appropriate to the consumption of one $-CH_2$ group from the original fuel molecule. The rate of heat release in a volume V is

$$\Omega = \xi V k_p (R^*) \quad ,$$

where ξ is the heat release per propagation cycle equal to 9.4×10^4 calories per cycle. The entire model requires 26 rate and concentration parameters to be fitted for each fuel of interest. Part of the parameters were set by appealing to known chemical reaction rates and activation energies. The remainder were chosen by matching the results of the numerical integration of the equation set to experimental data. The Shell experiments which lead to this fitting were carried out for a premixed charge in a rapid compression machine (to be described in Chapter IV). The six fuels surveyed by Shell were primarily of interest for use in spark ignition engines. These fuels were:

Fuel Name	Fuel Constituents	RON†	MON††
100 PRF*	100% isooctane	100	100
90 PRF	90% isooctane;10% heptane	90	90
70 PRF	70% isooctane;30% heptane	70	70
99.6 TRF**	10% isooctane;16% heptane;74%toluene	99.6	88.5
89.5 TRF	0% isooctane;30% heptane;70%toluene	89.5	77.9
2-Methylhex-2-ene (100%)		90.4	78.9

* Primary Reference Fuel
** Toluene Reference Fuel
† Research Octane Number
†† Motor Octane Number

The parameters determined by Shell for the 70, 90, and 100 RON pure research fuels are listed in Table I.

THE SCHÄPERTÖNS AND LEE MODIFICATIONS OF THE SHELL MODEL

The modifications of the Shell model performed by Schäpertöns and Lee balance the mass in the reaction equations and provide guidance in the use of decision rules for applying the Shell model in the context of a multidimensional computation. Equations (2)-(5) are mass-balanced by defining the molecular weights of the generic species B, R^*, Q, and P. The mass used to form these species must ultimately originate from the fuel and oxygen. Therefore the main propagation step [incorporating Eqs. (2)-(4)] is rewritten as

$$R^* + (\Lambda+1)(1/m\ RH + pO_2) \rightarrow qP + f_1 B + f_4 Q + R^*, \qquad (10)$$

where $\Lambda = (f_1 MW_B + f_4 MW_Q)/(MW_{RH}/m + pMW_{O2})$, MW_x denotes the molecular weight of species x, and the coefficients are $p = (n(2-\lambda) + m)/2m$ and $q = (n/m + 1)$. The coefficient λ determines the burned products mixture via $(CO)/(CO_2) = \lambda/(1-\lambda)$, with $\lambda = 0.67$. The reaction rate coefficient for

Eq. (10) is k_p and the reaction rate is $k_p(R^*)$. Mass-balancing is accomplished by defining:

$$MW_R = (MW_{RH} + MW_{O2})/2,$$
$$MW_B = 2\ MW_R,$$
$$MW_Q = MW_B, \text{ and}$$
$$MW_P = (n/m\ \lambda\ MW_{CO} + n/m\ (1-\lambda) MW_{CO2} + MW_{H2O})/q\ .$$

The nonreactive species in the termination equations are assumed to be equivalent to nitrogen. Therefore Eqs. (7) and (8) become

$$R^* \rightarrow (MW_R/MW_{N2})N_2, \text{ and} \qquad (7a)$$
$$2R^* \rightarrow 2(MW_R/MW_{N2})N_2. \qquad (8a)$$

For consistency in the above modifications, the heat release per propagation cycle is increased by the factor $(A+1)$ accounting for the increased consumption of the reactants.

The solution of the above set of chemical equations within the fluid model is complicated by the wide differences in the relative rates of reaction. Specifically, the branching reaction [Eq.(6)] is often much faster than the reactions forming the branching agent [Eqs. (3) and (5)]. The Shell group integrated their ordinary differential equations by means of a special variant of the Gear method.[42] Schäpertöns and Lee dealt with the problem by dynamically adjusting the chemistry subcycle time in the chemistry equation solver. The KIVA program used as a basis for the present work did not contain a chemistry subcycle. A chemistry subcycle

was added to KIVA using the formulation taken from the RICE code,[43] which also formed the basis of the REC code used by Schäpertöns and Lee.[44] Specifically, tthe total rate of change of (B) due to chemistry,

$$d(B)/dt = -k_B(B) + f_1 k_p(R^*) + f_2 k_p(R^*)(Q) \quad ,$$

is used to set the chemistry time step. The chemistry time step (in seconds) Δt_c is

$$\Delta t_c \leq x(B)/[\, d(B)/dt \,] \quad , \tag{11}$$

where x is a fraction in the range 0.5 - 1. A value of x=0.5 indicates that the local value of (B) is allowed to change by 50% over the time Δt_c. The chemistry subcycle time Δt_c is an integer submultiple of the main time step. In general, more subcycles are required as the local temperature increases. The fluid is not allowed to move during the chemical subcycling, but themodynamic quantities within the cell are adjusted. A typical overall fluid time step is 4 μs for the 2-D spray problems to be described. The segment of the code subject to the CFL limit (to be described below) would subcycle approximately 10 times during this fluid step. The chemistry routine would subcycle from 1 to 50 times over this period depending on temperature. The heat release rate is quite small over most of the autoignition period, particularly for single-stage ignition, and this feature is believed to be the reason why the subcycling seems to work well. When the rate of heat release becomes large, the overall fluid time step is reduced to retain accuracy.

The other set of modifications suggested by Schäpertöns and Lee is a method of interfacing the autoignition model with a standard one-step kinetics model for the main heat release (high-temperature combustion). For the premixed case studied by Schäpertöns and Lee, and during the premixed combustion phase in the case of the diesel, a reactive mixture surrounds an autoignition site. This surrounding mixture may either autoignite or burn more slowly as a flame propagates across the region. The rules determining which mechanism dominates in the computation were suggested to be:

> The main heat release reaction is only active for temperatures higher than 950 K. This rule ensures that autoignition dominates at low temperatures.

> The autoignition model may be active at all temperatures, but the reaction rates are limited to their values at 950 K. Physically, the kinetic process tends toward quasi-equilibrium at these fast rates, and is therefore not sensitive to the rates themselves.

> The autoignition model is locally inhibited if a computational cell has a temperature lower than 900 K and a Q-concentration less than 10^{-7} mole/cm^3. This rule was used by Schäpertöns and Lee to prevent immediate knock in their homogeneous mixture when the reactive mixture is compressed by an advancing (hot) flamefront.

EXTENSION OF THE AUTOIGNITION MODEL FOR USE WITH DIESEL COMBUSTION

The Shell model and the modifications described above were intended for use with computations for homogeneous fuel-air mixtures, in which the

entire medium is capable of supporting combustion. For the case of diesel combustion considered here two types of changes were required.

First, the decision rules mentioned above were altered. Because of the wide range of temperatures and species concentrations encountered during diesel autoignition, it is not necessary or desireable to subcycle in every computational cell. The issue of computational efficiency is more critical in a 2 or 3-D diesel problem for which droplet dynamics and evaporation must be calculated as well as the fluid motion and chemistry. The subcycle time is set locally as described above unless one of the following conditions is encountered.

> No subcycling is performed if the cell is very lean, or oxygen starved, or already burned. Subcycling is also inhibited if the population of B is very low or the temperature is high. The cutoff limits for subcycling are

$$(B) \leq 10^{-15} \quad \text{moles/cm}^3 \quad ,$$
$$(RH) \leq 10^{-10} \quad \text{moles/cm}^3 \quad , \text{ and}$$
$$(O2) \leq 10^{-7} \quad \text{moles/cm}^3 \quad .$$

> The autoignition equations are disabled in cells with a temperature greater than an externally specified limit.

> A maximum number of subcycles is allowed, such as 200.

> No chemistry solution (either main heat release or autoignition) is performed if

$$(O_2) \leq 10^{-10} \quad \text{moles/cm}^3 \quad ,$$

$(RH) \leq 10^{-10}$ moles/cm^3 ,or

$T \leq 300$ K .

> The autoignition model may be turned off a short period after ignition has occurred. This time duration depends on the problem being investigated, but one or two milliseconds is probably a sufficiently long period for all autoignition events in the computing mesh to have been completed.

> The autoignition event is detected by recording the time and position of the first cell to exceed a trigger temperature of 1100 K. This temperature was used by Shell to define the second-stage ignition.

The second set of modifications was required because there is little or no overlap between the fuels studied by Shell and the fuels reported in experiments for diesel autoignition. The quantities needed to mass-balance the modified Shell model for use with several heavier fuels (all of straight-chain chemical form) are given in Table II. The kinetics parameters for diesel-type fuels are not known. Therefore the parameters of the Shell fuels were modified slightly to use as estimates for a model diesel fuel (dodecane). This procedure is discussed in Chapter V. It was found possible to keep the kinetic rates well-within the range of parameters given by Shell. In the present work, the contributions of the generic trace species R^*, B, and Q to the specific heat of the mixture were ignored.

The main heat release equation used in the present work was

$$2\ C_8H_{18} + 25\ O_2 \rightarrow 16\ CO_2 + 18\ H_2O\ ,$$

for the primary reference fuels, and

$2\ C_{12}H_{26} + 37\ O_2 \rightarrow 24\ CO_2 + 26\ H_2O$ for doodecane. The rate of reaction for the main heat release in both cases was taken to be[45]

$d\omega/dt = -5 \times 10^{12} \exp(-15{,}780/T)\ (\text{fuel})\ (O_2)$. Other parametric fits for reaction rates are available for fuels lighter than decane.[29]

THE FLUID DYNAMICS EQUATIONS SOLVED BY THE PROGRAM "KIVA"

The KIVA program solves the unsteady Navier-Stokes equations for a compressible gas in two or three spatial dimensions. The conservative form of these equations is retained by using a finite volume formulation. Coexisting with the gas is a spray of evaporating liquid droplets which exchange mass, momentum, and energy with the gas. The spray is assumed to be thin enough that the volume displaced by the droplets may be neglected. The equations governing the flow are tabulated here for completeness. Dimensional quantities are used throughout the code, which is set up to accept all input values in CGS units. The documentation for the code[40] contains more detail should it be required.

The conservation equations are written in vector notation. A three-dimensional Cartesian coordinate system is employed. The unit vectors in this system are $\hat{i}$, $\hat{j}$, and $\hat{k}$ in the x, y, and z directions, respectively. The position vector is

$$\underset{\sim}{x} = x\,\hat{i} + y\,\hat{j} + z\,\hat{k} \quad .$$

The vector operator $\underset{\sim}{\nabla}$ is

$$\underset{\sim}{\nabla} = \hat{i}\,\partial/\partial x + \hat{j}\,\partial/\partial y + \hat{k}\,\partial/\partial z \quad .$$

The fluid velocity vector is

$$\underset{\sim}{u} = u(x,y,z,t)\,\hat{i} + v(x,y,z,t)\,\hat{j} + w(x,y,z,t)\,\hat{k},$$

where t is time. The total fluid density (in the gaseous phase) obeys the continuity equation

$$\frac{\partial \rho}{\partial t} + \underset{\sim}{\nabla}\cdot(\rho \underset{\sim}{u}) = \dot{\rho}_S \quad ,$$

where $\dot{\rho}_S$ is the rate of change of the fuel vapor due to spray evaporation or condensation. The continuity equation for each species m satisfies the equation

$$\frac{\partial \rho_m}{\partial t} + \underset{\sim}{\nabla}\cdot(\rho_m \underset{\sim}{u}) = \underset{\sim}{\nabla}\cdot[\rho D \underset{\sim}{\nabla}(\rho_m/\rho)] + \dot{\rho}_m^C + \dot{\rho}_S \delta_{m1} \quad ,$$

where D is the species diffusivity (assumed to be the same for all species), $\dot{\rho}_m^C$ is the rate of change of ρ_m due to chemical reactions, δ_{ij} is the Kronecker delta, and species 1 is assumed to be the fuel. The momentum equation for the fluid mixture is

$$\frac{\partial}{\partial t}(\rho \underset{\sim}{u}) + \underset{\sim}{\nabla}\cdot(\rho \underset{\sim}{u}\underset{\sim}{u}) = - \underset{\sim}{\nabla} p + \underset{\sim}{\nabla}\cdot \underset{\approx}{\sigma} + \underset{\sim}{F}_S \quad ,$$

where p is the fluid pressure, $\underset{\approx}{\sigma}$ is the viscous stress tensor, and $\underset{\sim}{F}_S$ is the momentum per unit volume per unit time transferred from the spray droplets to the fluid.

The equation for internal energy is

$$\frac{\partial}{\partial t}(\rho I) + \underset{\sim}{\nabla}\cdot(\rho I \underset{\sim}{u}) = - p \underset{\sim}{\nabla}\cdot \underset{\sim}{u} + \underset{\approx}{\sigma} : \underset{\sim}{\nabla} \underset{\sim}{u} - \underset{\sim}{\nabla}\cdot \underset{\sim}{J} + \dot{Q}_C + \dot{Q}_S + \dot{Q}_T \quad ,$$

where I is the specific internal energy of the fluid (not including chemical energy), $\underset{\sim}{J}$ is the heat flux vector, where $\dot{Q}_C$ is the chemical heat release, $\dot{Q}_S$ is a source term from the spray interaction, and $\dot{Q}_T$ is a source

term from the turbulence model. The heat flux is

$$\underline{J} = - K\underline{\nabla}T - \rho D \sum_m h_m \underline{\nabla}(\rho_m/\rho) \quad ,$$

where K is the thermal conductivity, T is the absolute temperature, and h_m is the partial specific enthalpy of species m.

The state relations in the code are those of an ideal gas mixture. The enthalpy of each species as a function of temperature (from the JANAF Tables[46] or other sources) is loaded into the program. The vapor pressure and liquid enthalpy, both as functions of temperature, are also stored in the program.

The system of chemical reactions included in the program is of the form

$$\sum_m a_{mr} \chi_m \rightleftharpoons \sum_m b_{mr} \chi_m \quad ,$$

where χ_m stands for one mole of species m, and a_{mr} and b_{mr} are the stoichiometric coefficients for the rth reaction. Both kinetic and equilibrium reactions may be accomodated.

For turbulent flow the above conservation equations are retained, but turbulent contributions are added to the laminar values of all transport coefficients. The program presently provides a subgrid scale model with one equation for the turbulent kinetic energy. The k-ε model is being added to the code. The turbulence model used in the spray computations performed here was that of constant diffusivity. The turbulent diffusivity was assumed to be equal to that for a turbulent gas jet, given by Schlicting (see, for example, Ref. 58) as

$$D_t = 0.0161\left(\frac{\pi d^2}{4} U_{inj}^2\right)^{1/2} \quad , \qquad (12)$$

where U_{inj} is the injection velocity and d is the nozzle diameter. The turbulent kinetic energy was taken to be 20% of the mean kinetic energy.

The spray droplet description used in KIVA is one of the more complicated models available. Probability distributions are employed to describe droplet size and the angle at which droplets are injected. Turbulent velocities (random in both magnitude and direction) affect the droplets to simulate turbulent dispersion. Droplets may collide causing either coallescence or an exchange of momentum. Droplet breakup is not simulated. The spray is assumed to be sufficiently thin such that the volume displaced by the droplets may be neglected. Each droplet has a single temperature. Computational parcels, each of which represents many droplets of identical temperature and size, are utilized to reduce the requirements on computer memory.

The drop distribution function f is defined such that

$$f(\underline{x},\underline{v},r,T_d,\underline{u}',t)\ d\underline{v}\ dr\ dT_d\ d\underline{u}'$$

is the probable number of droplets per unit volume at position $\underline{x}$ and time t with velocities in the interval $(\underline{v},\underline{v}+d\underline{v})$, radii in the range $(r,r+dr)$, temperature in the range (T_d,T_d+dT_d), and gas turbulence velocities in the interval $(\underline{u}',\underline{u}'+d\underline{u}')$. The probability destribution for the occurrence of the droplet radius r at injection is

$$f(r) = (1/\hat{r})\exp(-r/\hat{r}),$$

where $\hat{r}$ is the number-averaged droplet radius. The Sauter mean radius (SMR), the radius of a droplet having the same volume-to-surface area ratio as the entire spray, is equal to $3\hat{r}$. The gas turbulence velocity $\underline{u}'$ is used in calculating the drag and evaporation rate for the droplet. It is assumed that each component of $\underline{u}'$ follows a Gaussian distribution with mean square deviation (2/3)q. The time evolution of f is given by the spray equation

$$\frac{\partial f}{\partial t} + \underline{\nabla}\cdot(f\underline{v}) + \underline{\nabla}_{\underline{v}}\cdot(f\underline{F}) + \frac{\partial}{\partial r}(fR) + \frac{\partial}{\partial T_d}(f\dot{T}_d) + \underline{\nabla}_{\underline{u}'}\cdot(f\dot{\underline{u}}') = \dot{f}_{coll} \quad ,$$

where the quantities $\underline{F}$, R, $\dot{T}_d$, and $\dot{\underline{u}}'$ represent the time rates of change (following an individual droplet) of velocity, radius, temperature, and gas turbulence velocity, respectively. The droplet acceleration $\underline{F}$ is the product of the inertial gas force on the droplet and a drag coefficient C_D, divided by the mass of the droplet:

$$\underline{F} = \frac{3}{8}\frac{\rho}{\rho_p}\frac{|\underline{u} + \underline{u}' - \underline{v}|}{r}(\underline{u} + \underline{u}' - \underline{v})\, C_D \quad , \text{ where}$$

$$C_D = \begin{cases} \dfrac{24}{Re_p}\left(1 + 1/6\, Re_p^{2/3}\right) & , \quad Re_p < 1000 \\ .424 & , \quad Re_p > 1000 \end{cases} ,$$

and Re_p is the particle Reynolds number. The droplet temperature is determined via the energy balance equation for the droplet

$$\rho_p \frac{4}{3}\pi r^3 c_\ell \dot{T}_d - \rho_p\, 4\pi r^2\, RL(T_d) = 4\pi r^2 Q_d \quad ,$$

where c_ℓ is the liquid specific heat, $L(T_d)$ is the latent heat of vaporization, and Q_d is the rate of heat conduction to the droplet surface per unit area. The heat conduction rate to the droplet is given by the Ranz-Marshall correlation[47]

$$Q_d = \frac{K_{air}(\hat{T})(T - T_d)}{2r} Nu_p \quad , \text{ where } \hat{T} = (T+2T_d)/3 ,$$

$$Nu_p = \left(2.0 + 0.6\, Re_p^{1/2} Pr_p^{1/3}\right)\frac{\ln(1 + B_p)}{B_p} \quad ,$$

and B_p is the mass transfer number $B_p = \dfrac{Y_1^* - Y_1}{[\,U\, 1_1^*}$.

Here Y_1 is the fuel mass fraction and Y_1^* is the fuel mass fraction at the

droplet surface. The rate of change of the droplet radius is

$$R = -\frac{(\rho D)_{air}(\hat{T})}{2\rho_p r}\frac{Y_1^* - Y_1}{1 - Y_1^*}\,Sh \quad , \text{ where Sh is the Sherwood number,}$$

$$Sh = \left(2.0 + 0.6\, Re_p^{1/2} Sc_p^{1/3} \right) \frac{\ln(1 + B_p)}{B_p} \quad .$$

The Schmidt and Prandtl numbers are

$$Sc_p = \frac{\mu_{air}(\hat{T})}{\rho D_{air}(\hat{T})} \qquad \text{and} \qquad Pr_p = \frac{\mu_{air}(\hat{T})\, c_p(\hat{T})}{K_{air}(\hat{T})} \quad ,$$

where c_p is the local specific heat at constant pressure and temperature.

The mechanism of thermal radiation is neglected in the calculation.

The above set of coupled equations must be solved sequentially in order to generate a time-dependent, spatially-resolved description of the fluid and droplet motions and states.

METHODS OF SOLUTION USED BY THE PROGRAM "KIVA"

Provided here is a brief description of the character of the numerical methods used in KIVA. The reader or potential user is referred to the program documentation and its supporting publications for a comprehensive description of the methods.

The KIVA code solves the governing equations on a Cartesian mesh applicable to cylindrical or planar geometries in two or three dimensions. In three dimensions the mesh consists of arbitrary hexahedrons whose size may vary in space and time. An elaborate staggered mesh system is used to

locate velocities at the cell nodes and thermodynamic quantities at cell centers to allow accurate setting of the boundary conditions. Spatial differencing of the equations is performed by a donor cell (or "upwind differencing") method. The spatial accuracy is between first and second order depending on parameters set by the user based upon convection conditions in the test problem. The temporal accuracy is first order. The code primarily uses explicit solution techniques. Time-step size is controlled automatically during program execution to ensure that the stability and accuracy criteria explained below are satisfied.

The spatial differencing in the code is based on the arbitrary Lagrangian-Eulerian (ALE) technique.[68] The fluid solution is advanced by one time step by means of three phases of calculation: (A) The first phase is an explicit Lagrangian calculation, except that the mesh vertices are not moved. The effects of diffusion, chemistry, and spray behavior are included in this phase. (B) The second phase is an iteration method to adjust pressure gradients to the next time level. This iteration consists of sub-time steps, each of which conforms to the Courant stability condition that limits sound waves from traveling more than one cell per time step. The overall time step is not limited by this condition. The mesh vertices are moved to their new Lagrangian positions at the end of phase B. (C) In the third phase, the mesh can be moved to follow, for example, a moving piston. Convective fluxes are computed to keep track of fluid moving between cells as the mesh moves. These calculations are also subcycled if the fractional change in cell mass caused by the motion is large.

The three phases of calculation for advancing the solution time by Δt impose a number of individual stability criteria on the method. These will

be listed for a uniform Cartesian mesh. Approximate analog criteria are used for nonuniform meshes. Diffusion of mass and energy is calculated with time step Δt, the overall fluid time step. This calculation is explicit in the ℓ and R directions and implicit in the $\jmath$ direction (the azimuthal direction in an engine cylinder, where computational cells may be very thin near the axis). The stability limit is

$$\Delta t \leq \frac{1}{2\alpha} \left(\frac{1}{\Delta x^2} + \frac{1}{\Delta y^2} \right)^{-1} ,$$

where α stands for the mass diffusivity D, the thermal diffusivity $K/(\rho c_p)$, or the diffusivity of turbulent kinetic energy μ/ρ. Convection is calculated explicitly with the stability condition

$$\Delta t \leq \min \left(\frac{\Delta x}{|u - b_x|}, \frac{\Delta y}{|v - b_y|}, \frac{\Delta z}{|w - b_z|} \right) ,$$

where b_x, b_y, and b_z are the three components of the grid velocity. This condition restricts the flux volume in any coordinate direction to values less than the cell volume. The propagation of sound waves on the mesh introduces a stability requirement for the subcycle time step δt of

$$\delta t \leq a^{-1} \min(\Delta x, \Delta y, \Delta z) ,$$

where a is the sound speed. Diffusion of momentum is calculated explicitly with a viscous subcycle time Δt_{vs}. The stability requirement is

$$\Delta t_{vs} \leq \frac{1}{2} \left(\frac{1}{\Delta x^2} + \frac{1}{\Delta y^2} + \frac{1}{\Delta z^2} \right)^{-1} \left[\frac{2\mu + \lambda}{\rho} \right]^{-1} ,$$

where μ and λ are the viscosity coefficients. Factors of safety of approximately 2.0-2.5 are used with respect to the above stability criteria to make sure that the time steps are well below the equalities listed. In addition to the stability criteria, an accuracy criterion is applied to

guarantee that the fractional change of internal energy due to chemistry is small over a time step. Accuracy conditions on the spray model must be examined by increasing the resolution using more spray particles.

Velocity boundary conditions are calculated by the code for slip, no-slip, or turbulent law of the wall conditions. Available thermal boundary conditions are either adiabatic or fixed-temperature walls with turbulent law of the wall heat transfer and thermal conduction.

The droplet equations are solved by means of a Monte Carlo simulation using a discrete particle method. For the discrete particle method, the continuous distribution function f is replaced by a discrete approximation. Computational particles representing a number of identical physical droplets are injected into the mesh. These particles are tracked in the Lagrangian sense and are allowed to exchange mass, momentum, and energy with the cells in which they are located. Each parcel of droplets is assigned an initial droplet size and trajectory within the spray angle by random sampling from the appropriate distributions. The parcels move through the flowfield where they are affected by gas motion, collisions, and evaporation. Turbulent velocities are applied to the particles based on random sampling from a third distribution. Particles are tracked until the associated droplets have evaporated or have struck a wall, at which time they are deactivated and no longer influence the solution.

KIVA was written specifically for use on the CRAY computer. Vector arithmetic is utilized wherever possible to reduce the execution time greatly. Processing time remains substantial, however. The three-dimensional calculations described in Chapter V required approximately one CPU hour each on the CRAY-1S.

Table I
Optimized Parameter Values for the Shell Model[30]
(Only Primary Reference Fuels Listed)

A_i (cm, mole, s units) or E_i (cal/mole).
Other quantities are dimensionless.

Parameter	90 RON PRF	100 RON PRF	70 RON PRF
A_{p1}	1.0×10^{12}	1.0×10^{12}	1.0×10^{12}
E_{p1}	0	0	0
A_{p2}	1.0×10^{11}	1.0×10^{11}	1.0×10^{11}
E_{p2}	1.5×10^{4}	1.5×10^{4}	1.5×10^{4}
A_{p3}	1.0×10^{13}	1.0×10^{13}	1.0×10^{13}
E_{p3}	850.	850.	850.
A_q	1.2×10^{12}	4.0×10^{13}	7.0×10^{11}
E_q	3.5×10^{4}	4.0×10^{4}	3.5×10^{4}
A_B	4.4×10^{17}	6.5×10^{15}	3.4×10^{18}
E_B	4.5×10^{4}	4.0×10^{4}	4.7×10^{4}
A_t	3.0×10^{12}	3.5×10^{12}	2.5×10^{12}
E_t	0	0	0
A_{f1}	7.3×10^{-4}	7.3×10^{-4}	1.6×10^{-6}
E_{f1}	-1.5×10^{4}	-1.5×10^{4}	-1.5×10^{4}
A_{f2}	180	180	180
E_{f2}	-7.0×10^{3}	-7.0×10^{3}	-7.0×10^{3}
A_{f3}	1.47	2.2	0.75
E_{f3}	1.0×10^{4}	1.0×10^{4}	1.0×10^{4}
A_{f4}	1.38×10^{4}	1.25×10^{4}	8.89×10^{5}
E_{f4}	3.0×10^{4}	3.0×10^{4}	3.0×10^{4}
x_1	1.0	1.0	1.0
y_1	0.0	0.0	-0.5
x_3	0.0	0.0	0.0
y_3	0.0	0.0	0.0
x_4	-1.0	-1.0	-1.3
y_4	0.35	0.35	1.0
n	7.90	8.00	7.67
m	8.90	9.00	8.67

Table II

Parameters for Schäpertöns and Lee's Adaptation of the Shell Model

Fuel	n	m	p	λ(n/m)	(1-λ)(n/m)	MW_{RH}	MW_R	MW_B	MW_Q
heptane	7	8	1.082	.5862	.2888	100	66	132	132
70 PRF	7.67	8.67	1.088	.5927	.2919	109.8	70.9	141.8	141.8
90 PRF	7.90	8.90	1.090	.5947	.2929	112.6	72.3	144.6	144.6
100PRF	8	9	1.091	.5956	.2933	114	73.0	146	146
dodecane	12	13	1.114	.6185	.3046	170	101	202	202
tridecane	13	14	1.118	.6221	.3064	184	108	216	216
tetra-decane	14	15	1.121	.6253	.6253	198	115	230	230
hexa-decane	16	17	1.126	.6306	.3106	226	129	258	258

CHAPTER IV

DESCRIPTION OF EXPERIMENTS USED AS A DATA BASE

Summarized in this chapter are the experiments (from the literature as well as from the MIT Rapid Compression Machine) that will be used in Chapter V to gauge the behavior of the results from computations with the autoignition model. The experiments are described in order of increasing spatial resolution from zero-dimensional (homogeneous) to two- and three-dimensional geometries.

ZERO-DIMENSIONAL EXPERIMENT

The experiments for fitting the kinetics parameters to the Shell model were carried out in a rapid compression machine using a premixed fuel/air charge.[19,48] A rapid compression machine (RCM) provides a method to compress a gas quickly and therefore with little initial heat loss. The RCM is a "single-shot" device intended to simulate the compression stroke of an internal combustion engine. Combustion occurs at constant volume; the compression piston is usually not allowed to rebound. The arrangement

of the Shell rapid compression machine is shown in Figure 4.1. Dual opposed pistons were forced to top center and held there by larger pistons under pneumatic drive. The mixture was compressed into a clearance volume of height and diameter of 3.81 cm (1.5 in.). The compression ratio was 10:1 and the compression time was approximately 10 milliseconds. The cylinder pressure was measured by means of a piezoelectric pressure transducer. The piston position was measured as a function of time using an optical detector. The elapsed time was measured from when the pistons approached top center until a pressure rise due to combustion was registered in the cylinder. This quantity was therefore a "pressure-rise" autoignition delay. Light from within the cylinder was sensed through a window by a photomultiplier tube. The premixed charge was preheated and introduced into the cylinder at controlled pressure through a 0.5 micron filter to remove potential ignition-promoting dust particles. The cylinder walls were maintained at a temperature of 373 K. The combustion pistons were unlubricated to eliminate contamination by oil. Two typical pressure traces are shown in Figure 4.2(a) and 4.2(b) for two- and one-stage ignition events, respectively. This experiment was idealized by ignoring the presence of boundary layers and compression vortices in the cylinder such that the conditions were considered to be spatially uniform, or having a spatial dimensionality of zero. The experimental data reported by Shell included bulk temperatures computed under this same assumption.

TWO-DIMENSIONAL EXPERIMENT

The cylindrical combustion bomb used by Hiroyasu[28] for measuring the autoignition times of fuel sprays is shown in Figure 4.3. Fuel was

injected along the cylinder axis. The inside diameter and length of the cylinder were 18 cm and 54 cm, respectively. The cylinder walls were heated electrically and the air within the bomb was stirred using a fan in order to eliminate temperature gradients. The initial air temperature and pressure were adjustable over the ranges 673-973 K and 1-31 atm. abs, respectively. Ignition was detected by a photodetector such that the "illumination" time delay was measured. A high-speed movie camera was used to verify that the detector accurately registered ignition sites from any position in the cylinder. The dynamic pressure in the cylinder apparently was not recorded. The experiments to be compared in Chapter V used a nozzle with a single orifice of diameter 0.5 mm and an injection pressure of 96.8 atm abs. The injector needle-lift was measured via an optical detector.

Experiments to measure the penetration and size distribution of nonevaporating (and non-burning) fuel sprays were reported in 1974 by Hiroyasu and Kadota[49] for the apparatus shown in Figure 4.4. Diesel fuel was sprayed down the cylinder axis to be captured in a sampling medium. A photo-microscope was then utilized to count and measure the spray droplets as a function of axial and radial distance. The cylinder had a diameter and height of 20cm and 65 cm, respectively. A hole nozzle of diameter 0.3mm was used with a valve opening pressure of 97.7 atm abs.

THREE-DIMENSIONAL EXPERIMENT

The rapid compression machine in use at the Sloan Automotive Laboratory is intended to simulate the compression and combustion phases of a diesel engine. The advantage of this device over an engine is the relative ease

with which the geometric, thermodynamic, and injection parameters may be varied. The primary purpose of the machine is to provide a diagnostic tool for improving the understanding of the diesel combustion process. Therefore the RCM was designed with a particularly simple geometry for ease of optical access rather than with all of the complicating features of a practical engine. A schematic diagram of the machine is given in Figure 4.5. The machine consists of a combustion chamber, at the far right in the diagram, whose piston is forced to top center by air pressure acting on the driving piston. The driving piston is first preloaded while the common shaft through the machine is restrained mechanically. The shaft is then released quickly to provide a very swift compression event. A hydraulic retarder limits the forward speed of the piston shaft and provides a velocity profile which approximates the half-sinusoid profile of a reciprocating engine. The combustion piston is locked at top center by a set of non-return pawls, after which fuel is injected directly into the cylinder by a single-shot injector. Autoignition and combustion take place at constant volume. The cylinder pressure is measured as a function of time while high speed movies may be taken through a transparent, flat cylinder head. The compression chamber geometry and the optical view from the camera are shown in Figure 4.6. The RCM was designed and built by Rogowski[50] and coworkers in 1961 but has been modified by a succession of researchers for various purposes including the study of stratified-charge combustion. The most recent of modifications, which have been carried out as the earlier part of this thesis, will now be described.

The RCM was returned to operation at a high compression ratio by White.[51] The clearance volume is now a right circular cylinder with a diameter of 10.16 cm (4 in.) and a height of about 2.5 cm (1 inch). The

combustion piston carries three gapless, bronze-loaded Teflon rings. No lubricating oil is needed. Contamination of the combustion results by residual lubricating oil is thereby avoided. A new air tank was installed to provide pneumatic drive suitable for use with the new compression ratio of 16:1 plus supercharging of the intake air. The higher driving force required in turn a new mechanism for restraining the tailshaft prior to firing. See Figure 4.7. A toggle latch was installed by the present author to replace the former starting mechanism, which consisted of a shear pin broken by a ballistic pendulum. The toggle is unlocked by an air cylinder under solenoid control.

A new fuel injector, the UFIS injector (Universal Fuel Injection System) by American Bosch,[52] was installed in the RCM. This injector utilizes special hydraulic circuits to provide amplification of the rail pressure and a well-behaved fuel cut-off at the end of injection. The injector is operable under a wide range of conditions. The injection pressure, fuel quantity, and mass-flow profile may be adjusted. Injection is triggered by means of an internal solenoid. A mechanical stop was added for the fuel metering piston to achieve reliable "single-shot" operation. The fuel injector was located on the cylinder axis. Five hole-nozzles with orifice size 0.22mm were evenly spaced in the azimuthal direction and defined a cone angle of 126 degrees. The injection pressure upstream of the nozzles was calculated from the rail pressure[53] to be 613 atm. abs. The mass of fuel injected for these experiments was a total of 0.148 g through the five nozzles. The injection pulse was nearly a square wave[54] with a duration of about 3 milliseconds. The evolution of the fuel handling system may be found in the various Sloan Automotive Lab reports.[55]

A new digital sequencer was constructed to control the operation of the machine. A block diagram of the sequencer is shown in Fig. 4.8. The sequencer consists of two TTL digital clocks, several timing modules (DCI model 324), and power switching circuits. Each timing module has selectable setpoints to permit adjustment of the relative time delays between events in the sequence. Special attention was paid to eliminating sources of electromagnetic interference in the test cell. Such interference could accidently trigger unwanted events and damage equipment or personnel. All power switching is performed by solid state relays. Solid state relays generate less interference and operate faster than mechanical relays. Direct current is used wherever possible and the reverse voltages generated by switching inductive loads are clamped by diodes and capacitors. The switching sequence will now be described.

Before the shaft of the RCM is allowed to move, several other events must first take place. The "pre-firing" clock starts the high speed movie camera, waits for the camera to attain a useable speed, then closes the intake air valve and releases the tailshaft from the toggle latch. The initial motion of the tailshaft is detected by a photodetector/light emitting diode pair to enable the second clock. The "post-firing" clock lights the flash bulbs for illuminating the fuel spray, signals the fuel injector, and post-triggers the analog-to-digital converter.

Timing and cylinder pressure data from the experiment are digitized at 25 kHz and recorded on a VAX 750 computer. The heat release model of Gatowski, et. al.[66] is used to generate profiles of heat release versus time for the experiment. This model includes the effects of a temperature-dependent ratio of specific heats and the entrapment of gases at wall temperature within crevices in the combustion chamber. Photographic data

realizeable from the movies include the visible spray penetration, time to autoignition, visible enflamed area, and swirl velocity (via following small glowing particles and reaction zones).

Prior to firing the machine, intake air flows into the cylinder through a shrouded poppet valve in the head and out through three radial exhaust ports at the bottom of the cylinder. The intake air and cylinder walls may be heated or cooled. The cylinder is conditioned before an experiment so that intake and exhaust air temperatures are identical, thereby indicating the absence of temperature gradients down the long cylinder. The swirl velocity in the cylinder was estimated at bottom center by illuminating pinwheels of various diameters with a stroboscope. The indicated rotational speed was about 4000 RPM. Because the piston and cylinder head are both flat, it is assumed that the swirl at top center is also about 4000 RPM. The fuel utilized in these experiments was a standard test fuel supplied by Caterpillar with a cetane number of 47. The fuel was doped with copper oleate to improve the visibility of the hot combustion products for photography.

CHAPTER V

COMPARISON OF CALCULATED RESULTS AND EXPERIMENTAL DATA

Computations were carried out using the experimental parameters described in Chapter IV. The calculations are described and compared with the experimental data in the order of increasing spatial dimensions. The kinetic equations describing autoignition were first installed in KIVA and tested using zero-dimensional (homogeneous) calculations. The changes in the kinetics parameters necessary to describe diesel-type fuels were investigated. Then two-dimensional computations were carried out using dodecane as a typical fuel. The effects of varying several spray and kinetics parameters were examined in this configuration. Finally, exploratory calculations were performed in three dimensions for an experiment from the MIT rapid compression machine.

ZERO-DIMENSIONAL CALCULATIONS

The autoignition computation may be carried out without spatial resolution, that is, evolving only in time, for a homogeneous mixture when boundary layer effects may be neglected. The following computations, based

on the Shell experiments, were performed for a single cylindrical computational cell (see Fig. 5.1) assuming a homogeneous charge. The initial conditions correspond to the top-center conditions of the Shell RCM experiment. Halstead, et. al.[18] have shown that the extent of reaction during the compression stroke has a negligible effect on the computed time to ignition. The wall of the cylinder was held at the temperature found in the experiment. Bulk heat removal from the mixture was the only boundary effect considered. The cell dimensions and molar density for the computation were chosen to enable direct comparison with the Shell data.

The Shell autoignition equations in the modified form due to Schäpertöns and Lee have been added to the KIVA program. In addition, a subcycling step has been added to the chemistry routine for following rapid changes in the species concentrations. These changes were essentially minor modifications to the kinetic chemistry subroutine (CHEM) to allow the use of nonstandard rate expressions specific to the Shell model, to add the decision steps discussed in Chap. III, and to repeat the update of the state variables in order to follow the ignition event while subcycling. It must first be verified that the modified program and equations do in fact reproduce the Shell results. A positive answer would indicate that first, the program was executing as intended (without "bugs") and second, that the integration time step was short enough to yield reasonable results for the stiff set of equations. The fidelity to the Shell results is illustrated in Figure 5.2 for the case of 90 RON fuel at a charge density of 3.2×10^{-4} mole/cm^3, for varying postcompression temperatures. The total ignition delay is underpredicted at high temperatures (small 1/T). The Shell results are reproduced with about the same accuracy as the calculations of Schäpertöns and Lee. The lack of exact reproducibility at high temperature

is caused by using a time sub-step longer than desired for integrating the stiff equation set. This situation is illustrated in Figure 5.3, where a more restrictive criterion for the specification of the stepsize (x=0.5, instead of x=1.0, in Eq. (11) of Chap. III) has been used to repeat the calculation of Figure 5.2. The resulting accuracy is improved, but very small time steps are prohibitively expensive for 2 or 3 dimensional calculations.

The two characteristic types of ignition events for this temperature and pressure regime are shown in Figs. 5.4 and 5.5. The two-stage event at lower temperatures exhibits first a local maximum in the radical concentration (R^*) corresponding to the existance of a cool flame, followed by the hot ignition. Two seperate peaks are visible in the diagram of the rate of heat release versus time. The single-stage ignition at higher temperatures has only one peak in both (R^*) and the heat release rate. There is a smooth transition between these two types of ignition as the temperature is varied. The conditions at top center in a diesel cylinder are high temperature and high pressure, which would tend to favor a hot, single-stage ignition as shown in Fig. 5.5, as opposed to the two-stage ignition shown in Fig. 5.4.

The fuels investigated by Shell were suitable for homogeneous charge engines. The ignition delays for these fuels are much longer than the delays for diesel-type fuels in identical environments. It was necessary, therefore, to investigate how the parameters of the Shell kinetics model might be adjusted in order to describe fuels which autoignite much more easily. The effect on autoignition time of the rates of branching, formation of intermediate species, and initiation were tested.

Variation of Parameters Controlling Second-Stage Ignition

(a) 70 RON vs 90 RON fuels; The Rate of Branching

The rate at which the branching agent B decomposes to the radical R^* could conceivably decrease the second-stage autoignition time, and indeed, the results for 70 RON fuel are fitted with a larger branching preexponential factor that those for 90 RON fuel. Ignition calculations were performed using the ignition parameters given by Shell for 70 RON fuel, which autoignites in about one-half the time of 90 RON fuel under the same conditions. These results are compared with the 90 RON calculations as well as the Shell data in Figure 5.6. The present calculation reproduces the Shell calculation well. The 70 RON fuel parameters require much faster branching (by a factor of about eight times) than for the 90 RON fuel. The increased stiffness of the equation set represents an added burden for the chemistry subcycling, which responds to the time rate of change of the concentration of B. This rate is generally dominated by the branching rate alone with coefficient k_b. Thus it is more expensive to evaluate the 70 RON case and, in attempting to fit autoignition data for heavier fuels, it would be computationally preferable not to increase the branching rate. Nevertheless, the effect of increasing only the branching rate was examined for one case. Starting from the set of 90 RON parameters, the branching rate k_b alone was increased to the the rate for 70 RON fuel. The results are shown in Figure 5.7. Faster branching alone (at least for these values of the other parameters) appears to shorten τ_1 (time to cool flame) while slightly increasing the total delay. Because of the comparative insensitivity of the total delay to k_b, and noting the

computational disadvantage of fast branching, the option of adjusting the branching rate was not pursued.

(b) The Rate of Formation of the Intermediate Species Q

According to Halstead, et. al,[18] the second-stage ignition is triggered by the growth of the intermediate species Q to sufficiently high concentrations. The parameter most directly influencing the formation of Q is the preexponential factor A_{f4}. Shown in Fig. 5.8 are the results for varying temperature, pressure, and values of A_{f4} for a premixed charge of 90 RON fuel at a concentration of ϕ=0.9. The pressures used here cover a part of the pressure range of Hiroyasu's jet experiments and include the high temperature range of the RCM at MIT. The delay period is found to be quite sensitive to the value of A_{f4} over the entire range of pressure and temperature.

(c) The Rate of Initiation

Cox and Cole[32] state that second-stage ignition is also sensitive to the rate of initiation of the entire ignition process. The initiation rate pre-exponential A_q was varied between the values appropriate for 90 RON and 100 RON fuels (with 90 RON fuel parameters, otherwise). Note in Table I that 100 RON fuel has a larger branching multiplier, but also has a higher activation energy E_q, than the corresponding values for 90 RON fuel. The results are shown in Figure 5.9, where it may be observed that A_q is also a powerful influence in changing the computed time to second-stage ignition.

(d) The Physical Properties of Heavier Fuels

The fuels generally used for diesel combustion have significantly different physical properties than the fuels used with spark ignition. The values of the following properties are usually higher for diesel fuels: viscosity, molecular weight, surface tension, and liquid density. The vapor pressure is usually lower for diesel fuels. The specific fuel parameters should be described in order to properly account for their effects, particularly in view of the intimate coupling between fluid dynamics, droplet behavior, and the chemistry kinetics in diesel combustion. Tables of physical properties from Vergaftik[57] for heptane, dodecane, tridecane, and hexadecane were incorporated into KIVA (see Appendix C). Tables of physical data were already available at Los Alamos for n-octane and tetradecane. These fuels were next coupled with with the Shell kinetics scheme.

The Shell kinetics scheme is general in the sense that the main unit of interest is the $-CH_2$ group from a long-chain hydrocarbon molecule. The scheme, therefore, has the correct structure to be generalized to heavier fuels. Schäpertöns and Lee have mass-balanced the kinetics scheme in order to make it compatible with CFD codes, which require mass conservation. Their adaptation is extended here to the heavier molecules by changing the values of m,n,p, and the molecular weights of R, B, Q, and RH to conform to the heavier fuels. If the kinetic parameters are fixed, there will still be indirect effects on the ignition delay because of the lower temperatures due to higher fuel specific heats or reduced reaction rates caused by lower fuel molar concentrations for the same equivalence ratio. The effects of molecular weight and specific heat are shown in Fig. 5.10, where a

comparison is made between the computed ignition times of dodecane and 90 RON fuel at the same mixture temperature, pressure, and equivalence ratio ϕ, using the kinetic parameters of the 90 RON fuel. The concentrations of fuel and oxygen on a molar basis, which are the quantities directly affecting the kinetics scheme, are different in the two cases. The autoignition times are therefore quite different. Nearly identical results are recovered for the two fuels when the molar concentrations are matched, (thereby changing the equivalence ratio of the dodecane mixture) as shown by the two triangles in the figure. Note that it is not consistent to simply employ alternate fuel data tables in KIVA while retaining the 90 RON or other Shell values of the parameters m, n, p, q, and MW_{RH}, etc., because quantities must be expressed on both molar and mass bases throughout the program.

The extension of the autoignition kinetics model to heavier fuels is reasonable in view of the available experimental data. Hurn and Smith[26] have shown that, for the pure paraffins and alpha olefins, the autoignition time is a smoothly decreasing function of the number of carbon atoms in the chain, for the range of seven to sixteen carbon atoms. See Fig. 5.11. The pressure-rise delay measured by Hurn and Smith also varied in a smooth manner with the cetane rating of the fuel. This simple behavior was not exhibited by more complex pure fuels, however. This thesis will be confined to the use of one paraffin, dodecane (with twelve carbon atoms), as a sample fuel.

Summary of the Zero-Dimensional Calculations

The zero-dimensional calculations described above served the following purposes. First, they verified that the kinetics scheme, as installed in the KIVA code, functioned in a manner consistent with the Shell results. Next, the sensitivity studies showed the strong dependence of the time to second-stage ignition on the values of A_{f4} and/or A_q. The values of these parameters were kept well-within the range used by Shell in fitting the reference fuels. In the applications to follow, an attempt is made to calculate the temperature and pressure dependence of the autoignition time of a spray of dodecane. Only the value of A_{f4} will be varied to match the experimental data. This parameter most directly affects second-stage ignition and reflects the influence of the fuel structure on the ignition event. While it is probably true that the adjustment of a single parameter is too simple to give an accurate accounting of the kinetics of heavy fuels, in view of the uncertainties in the kinetics, it is the most reasonable course of action at this time.

TWO-DIMENSIONAL CALCULATIONS

As an introduction to the calculations, it is helpful to examine first the physical event. Shown in Figure 5.12 is a segment of the high speed movies taken by Hiroyasu of an igniting fuel spray. Hiroyasu described the ignition event in his experiment (translated from Japanese):

> After some period of time from the beginning of injection, a small luminous nucleus appears at some point in a spray. The location of the first appearance of a small nucleus is almost limited to the peripheral portion in a spray. Nonreproducibility of the location is due to the fact that the spray ignition is a statistical phenomena governed by many processes as atomization, mixing of fuel droplets with air, evaporation of fuel droplets and chemical reaction. Photographic inspection showed us that the evaporation of fuel ended around a

luminous nucleus before its appearance. Soon after the first appearance of luminous nucleus, consecutive appearance of small luminous nuclei occurs at different positions in a spray. Simultaneously, the size of flame nuclei increases resulting in abrupt spread of flame over the spray.

This is the physical behavior which the computations are intended to simulate.

The Penetration of a Non-evaporating Spray

An accurate description of the autoignition of a fuel spray must ultimately rely on an accurate description of the spray behavior itself. In order to verify that the computer program was operating as documented, a computation performed previously by O'Rourke[58] and expanded upon by Kuo[59] was repeated. Hiroyasu's spray penetration experiment[49] for a nonevaporating, noncombusting spray of diesel oil was simulated. The spray inlet boundary conditions used by O'Rourke, in conjunction with the aerodynamic spray breakup theory of Reitz,[60] were used to set the spray variables at injection. The turbulent diffusivity in the spray was assumed to be equal to that for a turbulent gas jet and set according to Eq. (12) of Chap. III. The turbulent kinetic energy was taken to be 20% of the mean kinetic energy. The turbulent Prandtl and Schmidt numbers were set to unity. These same methods were used in all of the autoignition calculations which follow. All other input conditions were matched with O'Rourke's calculation including cell sizes on the stretched computational mesh (see Fig. 5.13) and the rate of injection of computational particles. (The dark bands appearing on the left of Figs. 5.13, 5.15, 5.21, and 5.22 are the result of insufficient resolution in reprinting the densely packed

mesh cells from the microfiche storage medium used by the computer. Two to three mesh cells in the radial direction are obscured.) The mesh was axisymmetric about the injector with the smallest cells located nearest the injector nozzle. The walls of the mesh were held at the constant ambient temperature and slip velocity conditions were applied. The end wall of the mesh opposite the injector was solid in this computation as opposed to the outflow boundary used by O'Rourke. This geometry was a reasonable approximation to the actual cylinder for spray penetration distances small compared to the length of the mesh, and was used because no change in the code was required. The results are shown in Fig. 5.14 where the present calculation is compared against both Hiroyasu's data and O'Rourke's calculation using an entirely different computer program on a different computer. The agreement between calculation and data is good. The spread between the two calculations is typical of that shown by O'Rourke as caused by using different random number sequences in the injection model. From this brief test and the extensive set of published results of the model, it was concluded that the spray model was performing properly.

Autoigniting Jet

The geometry considered in the two dimensional calculations is that of an axisymmetric fuel jet spraying down the axis of a cylinder. The conditions on the mesh boundary were a wall temperature fixed at the initial gas temperature (as in the experiment) and a slip velocity condition on all solid walls. The method of setting the inlet boundary conditions for the spray was that of O' Rourke.[58] The droplet size (SMR) for the spray was calculated for each set of chamber conditions using the method of Reitz.[60]

The mesh used for most of the autoignition computations is shown in Fig. 5.15. This axisymmetric mesh had the same resolution utilized for the spray penetration calculation above, but added more cells in the radial direction at the same cell-stretching rate. The mesh matched the radial geometry of Hiroyasu's combustion bomb but was shorter than the actual bomb. This geometry should be acceptable as long as the events of interest do not occur near the bottom boundary.

The results of the multidimensional calculations are shown by plotting contours of constant values of a given variable. The format for these graphs is given in Fig. 5.16. The mesh outline is shown to define the physical region. Two-dimensional calculations show the mesh as a plane. In three dimensions, the mesh may be shown in perspective or in sections cut from the mesh. The compact heading of the plot is translated as follows. One line of identification is given to label the problem under study. The elapsed time t (in seconds) from the start of injection is given and the variable to be plotted is listed. The units of the variables are: pressure (dynes/cm^2); temperature (K); velocity (cm/s); and species concentration (mole/cm^3). The maximum and minimum values of the variable found anywhere in the mesh section displayed are denoted max and min, respectively. The highest and lowest contour values are labeled H and L in the plot and are listed in the heading. The increment between countours is DQ. Up to ten contours may be drawn in each plot. Strong gradients in the variable are indicated by clustering of the contours.

The autoignition model described earlier does induce high temperature ignition in a fuel spray as for the zero-dimensional case. A fuel spray of 90 RON fuel (with A_{f4} set to the 70 RON value) autoigniting is shown in Figure 5.17. This early calculation was carried out on the small computing

mesh from the spray penetration calculation. Prior to autoignition, one observes the increasing concentration of the intermediate species Q at the future ignition site (note the clustered contours indicating a steep gradient about the site at times of 0.85 and 1.3 ms). The high temperature area appears to spread quickly from an initial site into the vapor sheath surrounding the evaporating spray (see the expanded volume encompassed by the outermost temperature contour between the samples at 1.3 and 2.1 ms). A large temperature gradient exists at 2.1 ms between the burning mixture at 2800 K and the region of the evaporating spray at about 460 K. The region near the centerline of the spray is fuel rich while the outer edge of the burning spray is fuel lean. The contours of equivalence ratio spanning the range 0.5 to 4.5 lie atop one another at 2.1 ms, indicating the sharp gradient in fuel-air mixture. Combustion occurs more slowly (see Fig. 5.18) in the calculation after about 2 ms. The slowed rate of combustion is caused by several factors. The premixed fuel has burned out so that combustion is now mixing limited. The geometry of the experiment did not encourage strong circulation of unburned air into the fuel jet. It is difficult to state whether combustion was complete in the experiment because no heat release data were provided. The calculation showed 56% of the fuel mass remaining unburned at 3.1 ms and 40% unburned at 5 ms.

The computation time requirement to compute (for example) an 8 ms autoignition event on the larger two-dimensional mesh is about 10 CPU minutes on the CRAY. The computation time is set by the calculations for the fluid and drop dynamics. The autoignition chemistry itself does not become a hindrance to quick program execution until very near the autoignition time, when the population of B is changing rapidly. Following autoignition in one region, the chemistry slows the calculation as more and

more cells heat up and in turn require subcycling to follow the autoignition reactions in their locale.

The autoignition delay data of Hiroyasu for a range of pressure and temperatures, for four different fuels, are shown in Fig. 5.19. These data will be the basis for comparison with the calculations described below.

Effect of Statistical Variations on the Autoignition Calculation

The Monte Carlo simulation of the spray model in KIVA uses a (pseudo-) random number generator to select particle sizes from the size distribution, to set the particle trajectory within the spray angle, and to apply turbulent velocities (both magnitude and direction) to the spray parcels. Unless otherwise instructed, the program always begins with a certain number seed. A random sequence is generated with a new value provided for each call to the generator. Therefore the autoignition calculation could be sensitive to the random number sequence. This behavior would agree qualitatively with the observations of experimenters that the ignition site and ignition time vary as unknown (and presumably statistical) functions of turbulence, thermal fluctuations, etc. Borisov[61] has attempted to estimate the sensitivity of autoignition to statistical fluctuations in temperature, radical concentration, the presence of contaminating particles, and fluid-dynamic disturbances. He concluded that, for branched chain reactions in fuel vapor/air mixtures, any one of these mechanisms is capable of causing observable fluctuations in ignition data under typical experimental conditions. Hiroyasu's ignition delay data are mean values for 5 to 10 repetitions of the experiment at each condition. No statistical parameters were reported for the range or

variance of the data. The measured illumination delay was sensed from anywhere in the entire combustion bomb such that the variation in position of the ignition sites was also unreported. One would expect that the high temperature, high pressure data (where the kinetic reactions are the fastest) would be most sensitive to variations in the particle sizes and paths. This sensitivity is shown in Fig. 5.20. Three statistically independent executions were performed for:

a) 880 K, 30 atmg, 400 computational particles/ms,

b) 750 K, 30 atmg, 400 computational particles/ms, and

c) 880 K, 30 atmg, 800 computational particles/ms.

An injection rate of 400 particles per millisecond was found by O'Rourke (and repeated by this author) to be adequate for simulating spray penetration accurately. The ignition results show wide variation at the high temperature and less variation at the lower temperature as expected. The variation may be reduced substantially by doubling the particle injection rate as shown. The higher rate was used for all two-dimensional computations which follow. The three-dimensional calculations used an even higher rate (1300 partiicles/ms) to compensate for an extra dimension of turbulence velocity. The variance of a Monte Carlo simulation decreases as 1/n, where n is the sample size. Because all of the fluid variables must be computed independent of the number of spray particles, it is cheaper to make a single computation with a large number of spray particles than to make repeated calculations (with different random numbers) with a small number of particles. It should be pointed out that our computational experience is insufficient in order to decide how much randomness may be

realistic, as compared to the statistical nature of the experimental data. In attempting to fit the kinetics parameter A_{f4} for a fuel, a small variation in ignition time at high temperatures is required. For this reason, the two-dimensional calculations in the sections to follow utilized the higher particle injection rate (800 particles/ms).

The ignition locations for the runs with different random number sequences are shown in Figs. 5.21-5.22. The spray tip has passsed these locations to about 8-10 centimeters penetration. The ignition locations vary, but not dramatically. All of the two-dimensional computations performed to date show the spray igniting toward the rear of the jet; no instances of ignition near the tip have been observed. The predicted location is reasonable when compared to Fig. 5.12, Hiroyasu's description above, and other descriptions in the literature.[36] Because of a lack of specific experimental data, however, a definitive comparison is lacking.

Part of the effect of changing the injection rate of computational parcels may be observed in Fig. 5.23. Here the total vapor mass is plotted as a function of time for the results at 880 K. The 3 runs at 400 particles/msec show a very large variation in vapor mass, indicating the importance of the statistical variations on the gross features of evaportation for the entire spray. At the same time one notices the importance of local conditions, because the spray with the highest total vapor mass does not necessarily ignite first.

On The Use of Bulk Temperature in the Shell Results

Because of the presence of the thermal boundary layer on the cylinder wall, Keck has shown that the core temperature in the rapid compression

machine used in the Shell experiments may have been of the order of 50 K higher than the reported bulk temperature computed from pressure data.[34] The effect of this potential temperature error would be to shift the experimental ignition times to the left in a τ vs 1/T plot. Keck has rescaled the ignition data and found that the data collapse is improved by correcting the temperature. The implications for the Shell model predictions are less clear. An attempt was made to shift the temperatures used in the exponential equation rates by 50 K. The resulting delay times were then extremely long unless the second stage kinetic rates were boosted by very large multipliers (of the order of 3200 X the 90 RON value). It is believed that the temperature difference cannot be adjusted out of the model unless other of the parameters fitted to the data are also altered. The exponential temperature dependence of the reaction rates is difficult to overcome for a simple readjustment. Therefore the data of Shell were utilized exactly as they were published. This question of the bulk temperature should be examined in any subsequent experiments to be performed.

Sensitivity of the Autoignition Behavior to the Q Formation Rate

The autoignition behavior was explored using dodecane as the fuel. The values of A_{f4} tested were:

$A_{f4} = 8.89 \times 10^5$	64 X 90 RON value (= 70 RON value)
1.38×10^6	100 X 90 RON value
2.07×10^6	150 X 90 RON value
4.14×10^6	300 X 90 RON value

6.90×10^6 500 X 90 RON value.

The resulting behavior is shown in Figs. 5.24 and 5.25. The responses of the kinetic scheme to variations in A_{f4} are nonlinear and depend on the temperature and pressure. For ignition in an evaporating jet, however, the ignition delay is influenced by the physical processes of evaporation and mixing. As shown in Fig. 5.24(a), the delay τ decreases slightly with increasing A_{f4} both at 750 and 880 K. This variation in τ is much less than that obtained in similar calculations with a homogeneous charge (see Fig. 5.8). These τ values are compared to the experimental data of Hiroyasu in Fig. 5.24(b).

To fit the kinetic parameters to Hiroyasu's data over the pressure and temperature range, the value of A_{f4} was set based on matching a mid-temperature, mid-pressure point (750 K, 20 atm abs) as closely as possible. The value of A_{f4} was set to 2.07×10^6 (150 X the 90 RON value). The results are shown in Fig. 5.25. The general trends of increasing ignition delay with decreasing temperature and pressure are well-represented, considering that the matching is done by adjusting a single parameter.

The delay for 10 atmg and T=670 K appears to be too high, causing the slope of the trend to change. Examining the contour plots of the species concentration and temperature explains the reason for this behavior. See Fig. 5.26. At this low temperature and pressure, a significant portion of the liquid fuel spray has hit the end wall prior to evaporation and mixing. (Droplets which hit the wall are removed from the computation and have no further effect.) The mixing of whatever fuel has evaporated is restricted by the end wall, and potential reaction sites are cooled by the wall. This was the only case found where autoignition was predicted to occur so close

to the end wall. All other cases showed ignition sites within half the mesh length of the injector. The probable ignition delay for the 10 atmg, 670 K condition is then (by extrapolation) about 13.5 ms, if the mesh were longer. This question could be resolved only by using a longer mesh with the corresponding penalty in computation time; an outflow boundary would be of no use here.

An estimate of the sensitivity of the dodecane results to the random number sequence at this A_{f4} setting for 880 K, 30 atmg was generated. Three computations with varying shifts in the initial point of the sequence gave delays of 0.98, 1.01, and 1.06 milliseconds (listed in order of magnitude), showing little variability. The values plotted in Fig. 5.25 are therefore believed to be good representations of the mean values.

The slopes of the Arrhenius plots of τ do not exactly match the experimental data, which have an apparent activation energy of 8.64 kcal/mole independent of pressure (at high pressures). This behavior probably indicates that attempting to fit the heavier fuel to the Shell scheme by adjusting only one parameter may be too simplistic. However, the kinetics scheme does provide the correct behavior and reasonable values of τ for the complicated case of autoignition in a spray.

A second possible explanation for the disagreement in slopes would be the underprediction of the ignition delay at high temperature, caused by an excessively-large time substep in the chemistry routine. This possibility was checked by repeating several of the calculations at high temperature using the more restrictive timestep criterion ($x=0.5$ instead of $x=1.0$). The predicted delay was changed by less than 10%, which cannot explain the slope obtained.

The matching of the kinetic parameter was not repeated for Hiroyasu's other fuels. The physical properties of the "light oil" fuel used by Hiroyasu were undefined. Thus additional unknowns would have entered the calculation because detailed tables of physical properties are required for the code. The experimental data for hexadecane were quite close to those for dodecane, so close that, given the present accuracy demonstrated for dodecane, we could not hope to resolve them. Finally, the data for heptane showed such long delays that the mesh size and time duration required would have made the computation extremely expensive. Instead, a few illustrative tests were made by varying physical parameters.

The Sensitivity of the Autoignition Behavior to Physical Parameters

The effect of halving the Sauter mean radius, with all other parameters held constant, was examined for the conditions of 880 K, 10 atmg. The results are shown in Fig. 5.27. Decreasing the mean radius from 6 to 3 microns shortened the ignition delay from 3.58 to 2.51 ms. The ignition for the 6 micron drops actually occured after the end of injection (at 3 ms). The penetration of the evaporating spray also decreases with the smaller droplets. The total vapor mass increases more rapidly for the small droplets; the small droplets evaporate faster. For this setting of the kinetics parameter (A_{f4}= 2.07 X 10^6, as for the temperature/pressure sweep) the droplet size appears to be important in determining the ignition delay. (This result, and the results of the following calculations, will be discussed at the end of this section.)

The sensitivity of the ignition results to the vapor pressure of the fuel was tested. The data table of vapor pressure versus temperature for

dodecane was altered artificially by reducing the vapor pressure to one-half of the correct value, simulating a less volatile fuel. No other physical properties were altered, in particular, the latent heat of evaporation was kept constant. The Sauter mean radius for these calculations was 2 microns. The results, for two different values of the kinetics parameter A_{f4}, are shown in Figs. 5.28 and 5.29. The ambient conditions for this test were 880 K at 37 atmg, the conditions for the RCM experiment. The data show a 20-60% reduction in total fuel vapor mass during the period from injection to ignition, but a very small effect on the ignition delay. The position of the ignition sites was also essentially unchanged by the change in vapor pressure.

The effect of variations in the constant diffusivity on the ignition delay, total fuel vapor mass, and droplet penetration are illustrated in Fig. 5.30 and 5.31. The constant diffusivity value (10^{-3} m^2/s) was raised and lowered by 20% about the value calculated from Hinze's correlation. All of the quantities appear to be insensitive to this variation of diffusivity in the present calculation. This is rather misleading because the numerical diffusivity is significant in the present calculation. The calculation has employed essentially an upwind differencing scheme to prevent temperature overshoots caused by the large temperature and velocity gradients near the nozzle. The numerical diffusivity in the vicinity of the ignition site may be estimated as $0.5u\delta x$, where u and δx are the velocity and grid spacing transverse to the jet. This diffusivity value is estimated to be $\sim 10^{-2}$ m^2/s, and is much larger than the input value for the diffusivity. Therefore the diffusive nature of the above computations should be the same.

In summary, the above calculations show that, for the same effective diffusivity, which, in this case, is governed by the numerical diffusion, the ignition delay is not sensitive to an artificial lowering of the fuel vapor pressure, but decreases by more than 40% when the droplet SMR is lowered from 6 μm to 3 μm. These observations will be discussed next.

The autoignition of a fuel-air mixture is a result of the processes of evaporation, mixing, and chemistry. If the same kinetic scheme is used, the factors which influence the ignition delay would be the temperature and composition history of the fuel-air mixing process. Consider first the evaporation of a single fuel droplet. For simplicity, assume the evaporation process to have a Lewis number of 1 so that the evaporation may be described by the diffusion of the vapor, since in this case, the temperature profile would be similar. Then dimensional analysis would give

$$dm/dt = [p_s D_L d /(RT_d)]\, f(Re_p) \quad ,$$

where dm/dt is the evaporation rate, p_s is the saturation vapor pressure, D_L is the laminar mass diffusivity, d is the droplet diameter, R is the gas constant of the vapor, T_d is the droplet surface temperature, and Re_p is the Reynolds number based on the relative velocity of the drop to the charge. For a dilute suspension with N droplets, the total evaporation rate would be proportional to N. If the fuel flow rate is constant, then $N \sim d^{-3}$. Therefore, the total evaporation rate is

$$dm_t/dt \propto [p_s/(T_d d^2)]\, f(Re_p).$$

If the fuel spray is not dilute, however, the above relationship will no longer be true and the evaporation is mixing limited. When the evaporation rate is changed by changing p_s, with the latent heat kept constant, T_d does not change much because of the exponential dependence in the Clapeyron relation. Therefore $dm_t/dt \propto p_s$ in the dilute limit. The calculation,

however, shows that when p_s is lowered by a factor of 2, dm_t/dt only changes by about 20% (see Fig. 5.28). This suggests that the evaporation process is mixing limited.

That the evaporation is mixing limited is further evidenced in the calculation involving a change in the drop size. The effect of convection on the evaporation from spheres in the laminar flow regime is $f(Re_p) \sim \sqrt{Re_p}$. The droplet velocity for the two cases may be estimated from the penetration velocity (Fig. 5.27), and is not significantly different for the two cases. Therefore $f(Re_p) \sim \sqrt{d}$. Then $dm_t/dt \sim d^{-3/2}$. The calculation (Fig. 5.27) showed $dm_t/dt \sim d^{-1}$, again suggesting a mixing limited process.

In the runs involving the variation of vapor pressure, since the droplet initial diameters were kept the same, the mixing rate, which is driven by the momentum transfer from the fuel jet to the air, would not change substantially. Hence the evolution of the temperature and composition field for the two cases would be the same, because the process is mixing limited. The ignition delay, therefore, would be the same.

For the runs involving the change of droplet diameter, however, the momentum exchange between the fuel spray and the air is much faster for the smaller diameter droplets, resulting in a higher mixing rate. It is this process, rather than the faster evaporation, that is responsible for the significant shortening of the delay time.

The Simulation of the Conditions of the Rapid Compression Machine in Two Dimensions

In preparation for the three-dimensional calculations of the RCM experiment to follow, the spray conditions for that simulation were also

executed in two-dimensions using the geometry of Hiroyasu's bomb. Some of these results have just been discussed. This paragraph concerns the specification of the kinetic rates. The kinetic rate carried throughout the analysis so far, $A_{f4} = 2.07 \times 10^6$, was the value that gave the best fit to the Hiroyasu data for the overall pressure and temperature range. At the RCM conditions, which are at the end of the fitted temperature range and outside the pressure range, this value of A_{f4} would yield an ignition delay about one-half the measured value. While this value of A_{f4} will be used in one of the three-dimensional calculations for consistency, it was also desired to choose another rate that would cause the RCM results to be matched approximately, so that the timing of the pressure traces or photographs and the computations could be compared. The ignition delays, computed in two and three dimensions for the RCM conditions with dodecane fuel, were

A_{f4} Value	Multiple of 90 RON Rate	2-D Calculation τ - ms	3-D Calculation τ - ms
2.07×10^6	150	0.534	0.439
8.89×10^5	64	0.678	-
2.21×10^5	16	1.12	1.02

The value 2.21×10^5 was used to match the RCM results in two of the three-dimensional calculations. The ignition delays in three dimensions are somewhat shorter than for two dimensions, but are reasonably close considering the difference in grids, the increased numerical diffusion in 3-D, and hence the change in mixing.

The two-dimensional calculation using the value $A_{f4} = 2.21 \times 10^5$ produced the autoignition event shown in Fig. 5.32. The contour plots are for a time of 1.15 ms, just beyond the ignition delay of 1.12 ms. In this

calculation, there appear to be two seperate sites for ignition. This situation is indicated by two sets of closed contours of (Q) about two physical positions. Two perturbations in the temperature contours at these sites are also present. The site farther from the injector attained a temperature of 1100 K (taken as the definition of ignition) first, but it was trailed closely by the second site. This result is qualitatively similar to the pictures from Hiroyasu's experiment, where more than one ignition site may appear as the spray is enflamed. This was the only case in the computed results generated to date where such a clear seperation between two sites has been found. Ignition in the two-dimensional jet is seen to take place well back from the tip of the jet, on the periphery of the jet where the average equivalence ratio is approximately 0.5. The computed location of ignition will be seen to be somewhat different in the three-dimensional geometry of the RCM.

THREE-DIMENSIONAL CALCULATIONS

The top center conditions in the rapid compression machine for experiments numbered 3.09 and 3.10 are now described. These two experiments were intended to be two independent realizations of the same event, that is, a measure of the repeatability of the experiment. In fact, conditions in the two experiments were slightly different. The conditions and measured ignition delays were:

Experiment	Bulk Temperature-K	Pressure at Injection-atm abs.	Pressure-rise Ignition Delay-ms
3.09	878	38.3	1.24
3.10	861	37.6	1.12

The bulk temperature was computed from the measured pressure at injection, the known initial air mass in the cylinder, the assumption that an insignificant amount of mass was lost during compression, and the approximation that crevices account for 1% of the clearance volume, with the trapped gas at the wall temperature. The assumption of no mass loss is a good one for static conditions, but has not been verified for the dynamic compression. The initial conditions assigned in the three-dimensional numerical simulation were 880 K at 38.3 atm abs., thereby being most representative of experiment 3.09.

Reproductions of the high speed movies from these experiments are included as Plates 1 to 4. Shown in Plates 1 and 2 are the full combustion events, with time increasing as indicated. Plates 3 and 4 are enlargements of the ignition events, being the first two frames from the preceding plates. Pressure traces from the two experiments are overlaid in Figs. 5.33 and 5.34. The oscillating behavior of the magnified pressure trace (Fig. 5.34) is due to the acoustic ringing of the combustion chamber, with the correct resonant frequency.

T. Butler and R. Gentry have carried out three-dimensional calculations for this RCM experiment using tetradecane and dodecane as model fuels. These computations employed a one-step kinetic equation, that is, without an autoignition model.[62] The computing mesh for both the earlier and the present three-dimensional calculations is shown in Fig. 5.35. The cylinder geometry is periodic in the azimuthal direction with five equally-spaced sprays. Therefore only one-fifth of the entire cylinder need be computed. The front and back boundaries of the mesh are periodic. The number of mesh cells is 20 radial by 12 azimuthal (for 1/5 of the cylinder) by 20 axial for a total of 4800 cells. The resolution for the entire cylinder is

equivalent to that provided by 24,000 cells, a number considerably higher than most other 3-D simulations in the literature. This resolution was required because initial results by Butler and Gentry predicted an unrealistically short spray penetration. The cause of the reduced penetration was the momentum exchange process between the spray and the gas in the computational cell. The cells in this mesh are basically wedge-shaped. For a uniform mesh, the amount of mass in a cell increases approximately as the square of the radius. Therefore as the spray spreads and slows, it encounters ever larger cells with which to exchange momentum. Because there is no sspatial resolution within a cell, the velocity of the droplets decreased radically towards the outer radii unless sufficient resolution was available.

The initial swirl field in the cylinder was estimated for the calculation in the following way. As mentioned earlier, the geometry of the RCM includes no squish regions. Then, except for friction at the cylinder wall and head, and the effect of turbulent dissipation, the angular momentum of the initial swirl should be nearly constant during the compression process. The swirl velocity estimated at bottom center should then be representative of the velocity at top center if no mass is lost during compression. In fact, the swirl measurement by means of a pinwheel at bottom center is approximate because the flowfield is fully three-dimensional as it issues from the shrouded valve and travels down the cylinder to the exhaust ports. Yet another estimate of the swirl may be obtained by following the paths of enflamed areas and small glowing particles during combustion. These two estimates are plotted in Fig. 5.36 along with a theoretical swirl profile from Ref. 63 for decaying swirl in a cylinder. The two swirl estimates show reasonable agreement. The

theoretical profile is a solution for the Navier-Stokes equations assuming the effective viscosity ν_t uniform in space and slowly varying in time. The form of the solution is

$$\text{Tangential velocity} = KJ_1\left[\frac{\lambda r}{R}\right] \exp\left[\frac{-\nu_t \lambda^2 t}{R^2}\right] ,$$

where J_1 is a Bessel function, r is the radial coordinate, R is the cylinder radius, t is time, λ is an eigenvalue of J_1, and K is a constant. The value of λ was adopted from experiments in a cylinder of size close to the RCM clearance volume. The value of K was adjusted to approximate the RCM swirl data. The theoretical swirl profile fitted to the measured values was used to set the swirl field for the computation at top center. The initial swirl in the computation is shown in Fig. 5.37.

The turbulent diffusivities were set using the constant diffusivity model as was done for the two-dimensional calculations. The 3-D grid is coarse compared to the 2-D grid used earlier. As a result, the effects of numerical diffusion caused by truncation errors are larger for the 3-D calculation and in fact dominate the diffusion.

The line source model of Chatwani and Bracco[64] was used to provide the best available description of the breakup of the spray. This model simulates the solid liquid core that is presumed to exist at the center of a thick spray as a line source of mass. The Sauter mean radius of the spray distribution was taken to be 2 microns. This radius is about five times larger than the radius computed on the basis of Reitz' aerodynamic breakup theory that has been used throughout the two-dimensional computations. The spray penetration was found to be inadequate on the 3-D mesh when the smaller radius was tried, presumably for the reason discussed above.

Run A

The first three-dimensional calculation was performed using a value of A_{f4} equal to 2.07 X 10^6. This value, which was used throughout the two-dimensional calculations, resulted in a computed ignition delay of 0.439 ms. As described earlier, the computed delay is about one-half of the measured delay. Selections of the output from the computation are shown in Fig. 5.38 and 5.39. Qualitatively, the solutions do not differ significantly from the results of Butler and Gentry.[62] The present solution burns faster and earlier because of the ignition model, resulting in a pressure trace that rises too early. See Fig. 5.40, where pressure traces for all three-dimensional computations are summarized and compared against the experimental pressure trace. The computed ignition site is underneath the spray, near the tip. This same region also burns first in the calculation without the ignition model, indicating that temperature and conditions for mixing are most favorable at this location under the set of ambient conditions.

Run B

The second calculation was carried out with A_{f4} set to 2.21 X 10^5, the value which in two-dimensions gave an ignition delay matched to the experiment. The computed delay for three-dimensions was 1.02 ms, slightly less than the 1.12 computed in two-dimensions and less than the measured value of 1.24 ms. The autoignition model was only applied in regions where the temperature was below 1000 K. This procedure is necessary because once ignition starts at one computational cell, the mixture would burn to a very

high temperature. If no cutoff mechanism is introduced, the neighboring cell will be ignited in the next time step, causing a very fast pseudo-flame spreading rate. This point will be further discussed in the next section. The result for the cylinder pressure at early times is compared in Fig. 5.40. The initial pressure rise is not quite time-aligned with the data, because the criterion of ignition in the computer program may not be quite the same as the detection of the start of the pressure rise in the experiment. The rate of pressure rise is more gentle, compared to the calculation without autoignition, and the value is comparable to the observed value. The spatial plots have a solution similar to Run A except for the timing. The reaction zones have the same shapes and are similarly distorted by the swirl at later times.

Run C

Run B was repeated for the same value of A_{f4}, but without the temperature limit in place. That is, the autoignition model explained in Chapter III was applied at all temperatures until a cell had burned out. The kinetic rates for the autoignition kinetics were still limited to their values at 950 K. The inhibition condition of Schäpertöns and Lee (for high temperatures at low Q concentrations) had also been removed earlier. The results are show in Figs. 5.40-5.42. Ignition again occurs at about the same area as before, but now a very violent gas motion, with large pressure gradients occurs. The results suggest the explosion of a hemispherical "cap" of premixed fuel at the tip of the fuel jet. The vapor sheath about the jet burns very quickly. Cold fuel continues to be sprayed into the chamber, but the droplets are evaporated and burned very quickly due to the

high temperatures. Temperatures of up to 3400 K were recorded in the calculation near autoignition, which then decreased to about 3100 K. The seemingly high temperature appeared because no equilibrium chemistry equations were used in the computations; such use would have decreased the temperature.

Discussion

The three-dimensional calculations show qualitative behavior characteristic of the experiment. That is, the shapes of the reaction zones match the photographic evidence fairly well. The behavior near the ignition time is not matched well. In the experiment, the fuel jet ignites along at least the outer two-thirds of its length within 0.13 ms of the first visible reaction site (see Plates 3 and 4). The computations (except for Run C) show a much slower burning progression up the jet. The predicted ignition site, at a radius of 0.6 times the cylinder radius and a distance of 0.2 times the clearance height above the piston, is consistent with the evidence in the photographs, although there is considerable variation between the behavior of the different jets. The apparent ignition sites in the experiment were at radii from 0.4-1.0 times the cylinder radius. The axial position of the sites could not be determined from the photographs. The entire jet does light quickly in Run C, but the violence of this event is not physically correct, as may be seen from the steep rise of the pressure trace. It may be said that the results of Runs B and C bracket the experimental data in terms of cylinder pressure and flame spread. Further refinement of the calculation appears to hinge on finding the appropriate method for simulating the flame spread mechanism

correctly. The physical mechanism describing the flame propagation and the numerical behavior of the simulation will be described next.

To set the stage for the discussion, several order of magnitude estimates are first made. The reaction is initiated in a region of size L. The value of L may be estimated as $(D\tau)^{1/2}$, where D is the effective (turbulent) diffusivity relevant to the mixing process ($\sim 10^{-3}$ m^2/s, from turbulent jet correlations as applied to the present case) and τ is the ignition delay (~ 1 ms); hence L~1 mm. The acoustic speed, a, in the unburned region (880 K) is ~600 m/s. The heat release reaction time scale estimated from the homogeneous charge calculations (see Fig. 5.5) is τ_c~0.1 ms. Since L/a (~ 1.67 μs) is much smaller than τ_c, the combustion takes place locally at constant pressure, while emitting a pressure disturbance δp, which travels at speed a. To estimate δp, and the associated δT, the velocity δu_0 of the expanding burn region may be estimated as

$$\delta u_0 \sim L(T_u/T_b)^{1/3}/\tau_c \sim 15 \text{ m/s}.$$

The corresponding acoustic pressure δp is $a\rho\delta u_0$, and the temperature rise is

$$\delta T/T \sim (\gamma-1)\, \delta u_0/a \sim 0.8\% ,$$

which amounts to a 5 to 10 K temperature rise adjacent to the flame front.

Several mechanisms for the flame propagation are plausible. Their compatibility with the observation that the flame spreads over a distance s of about 5 cm (the RCM cylinder radius) in τ_s ~ 0.1 ms will be examined.

(i) Diffusion: This mechanism is too slow. The diffusion distance is $(D\tau_s)^{1/2}$. Unless D is unreasonably high (~ 10^5 X the laminar value), this mechanism cannot explain the phenomenon.

(ii) (Almost) Simultaneous Ignition from Multiple Sites: This possibility has been ruled out with the results of runs A and B. In these

runs, the autoignition had been suppressed only at the cells with temperature > 1000 K, i.e., the burned cells and its immediate neighbors. The ignition kinetics were maintained in the rest of the computational domain. No extensive simultaneous ignition sites occurred. Therefore, within this model, simultaneous autoignition is an unlikely mechanism to explain the observed flame spread.

(iii) Direct Acoustic Excitation: The flame spreading rate $s/\tau_s \sim 500$ m/s is of the same order as a. The acoustic pressure, however, decays as the square of the distance. The temperature perturbation at the distance s = 5 cm would be

$$\delta T/T \sim [(\gamma-1)\delta u_0/a]\ (L/s)^2 \sim 3 \times 10^{-6}$$

and $\delta T \sim 3 \times 10^{-3}$ K. This small temperature rise should not influence the kinetics appreciably.

(iv) A Coupled Acoustic/Chemistry Mechanism: The mixture surrounding an autoignition site has almost the same characteristics as those at the site. Specifically, the autoignition reactions in the vicinity have almost reached the ignition conditions when the first site ignites. The temperature increase from the pressure wave radiated from the site, although small, ($\delta T \sim 5$ to 10 K in the vicinity of the ignition site), is sufficient to accelerate the reactions in the immediate surroundings. The resulting acceleration will propagate the high temperature region at sonic speed in the unburned mixture. The effect is similar to a Chapman-Jouguet wave, except that propagation is sonic instead of supersonic, and there is no shock wave - the chemical reaction is propagated by "acoustic" heating rather than shock heating. Attenuation of the pressure wave would be prevented by energy feeding into the wave from the autoignition heat release. This mechanism is suggested to be the appropriate explanation for the behavior seen in the experiment.

The numerical behavior of the apparent flame propagation and pressure rise of Run C may be examined in light of the above discussion. The maximum flame propagation speed may be obtained from Fig. 5.41, in which the flame front had propagated through ~4 cm in 0.06 ms. This corresponds to a propagation speed of 660 m/s, which is comparable to the acoustic speed. Therefore the computation captures favorably the acoustic/chemistry coupled flame propagation mechanism. The pressure rise rate, however, is considerably faster than what has been observed in the experiment (Fig. 5.40), corresponding to a very high heat release rate. This apparent rapid heat release may be attributed to the numerical model, in which the constituents in a computational cell are assumed to be a homogeneous mixture at the mean stoichiometric value. In reality, the mixture is not uniform, and a substantial mass fraction may have a different local stoichiometric composition from the mean value. Therefore the heat release rate calculated should be considered as an upper bound.

In practice, it is impossible to have a grid resolution which would resolve the local composition to the molecular mixing level in flows of high Reynolds number, such as in the present case. To properly account for the distribution of compositions within the computational cell, a suitable probabilistic model could be devised. Progress in the formulation of a hybrid probabilistic/multidimensional fluid mechanical model is underway (Ref. 69).

The difficulty with the coexistence of autoignition and main heat release kinetics is, as in the present set of calculations, to distinguish under what conditions autoignition may progress quickly through a reactive (premixed) medium. In the RCM experiments, it appears that this fast propagation or flame spreading is realistic. For calculations of flame

spread in a homogeneous charge engine, the result could be predicting knock for all combustion events, an unrealistic conclusion. Two ways of limiting the rate of pressure rise and for controlling the behavior of autoignition in a pre-mixed region have been described.

Schäpertöns and Lee were apparently quite successful in selecting criteria for simulating autoignition behavior in premixed combustion. Most of their selection criteria were carried over to the present work. One criterion, the inhibition condition for high temperatures and low Q concentrations, appears to be incompatible with diesel calculations. At the edges of the fuel jets, where autoignition is predicted to occur, temperatures may be high and Q concentrations low. The symptom noticed was that, when the edge of the spray began to autoignite, at a temperature of 900 K, (high enough to trip the inhibition condition with (Q) still low), the calculation would stall. The autoignition reactions were inhibited and an unreasonably long autoignition time would result.

The use of an upper temperature cutoff for the application of the autoignition equations, such as was used here in Runs A and B, also appears to be inappropriate. The idea is to let the autoignition equations run only to a certain temperature (here 1000 K) cutoff, at which point they are turned off and the main heat release equation carries on alone. Natarajan and Bracco have tried a similar scheme with a cutoff of 1600 K. The symptom that this generates is a slow temperature rise during autoignition. That is, once the cutoff temperature is surpassed, the much-slower heat releasse reaction does not continue to raise the temperature sharply as is characteristic of autoignition. On the other hand, the complete removal of this type of condition resulted in Run C, where the entire fuel jet burns rapidly. It should be pointed out that the flame model inherent in the CFD

scheme, that is, a sharp temperature gradient, was in no way changed even in Run C. There is evidence that the CFD scheme always overestimates the flame speed in a premixed charge.[65] Even in the diesel results without an autoignition model (Fig. 5.40), one finds that the rate of pressure rise is excessive once burning is established. Although part of this rise may be explained by the mean stoichiometry effect described above, some refinement in the treatment of the flame itself may be indicated.

Natarajan and Bracco have tried to control the immediate autoignition of the premixed region near a propagating flame by adding a new generic species to the kinetics scheme. This species removes the intermediate Q in regions of high temperature, thus controlling the autoignition of regions near the temperature gradient representing a flame front. While this method is artificial, it may offer an expedient way to generate realistic behavior within the bounds of the computational model. For now, the means to interface the autoignition equations and the propagating flame remain unresolved.

CHAPTER VI

CONCLUSIONS AND RECOMMENDATIONS

The computations reported in this thesis represent the most detailed attempt to date to calculate the autoignition of a fuel spray from the underlying physical and chemical principles. An existing kinetics model for autoignition, the Shell model, has been installed in an existing computational fluid mechanics model, the KIVA code. The kinetics scheme is known to describe the global behavior of the autoignition of a homogeneous fuel-air mixture under engine-like conditions. The code provided detailed descriptions for the transient injection of a fuel spray, including droplet dynamics for an evaporating liquid, fluid motion, and chemical reaction, in up to three spatial dimensions.

The fuels of interest in diesel combustion autoignite more rapidly than fuels for spark ignition engines, but were not among the fuels fitted by Shell with parameter values for their kinetics scheme. The sensitivity of the autoignition time of a homogeneous mixture to the kinetics parameters was examined in order to provide a basis for extending the Shell description to diesel-type fuels. The time delay for second-stage ignition

was found to be very sensitive to the parameters A_{f4} and A_q in the Shell formulation. Parameter A_{f4} was selected for further use because it reflects the fuel structure and directly influences second-stage ignition.

The autoignition delay of an axisymmetric fuel spray was examined by comparing computations using the combined kinetics and fluid models against spray ignition data from the literature. It was found that, for spray ignition, the sensitivity of the ignition delay to the value of A_{f4} was much reduced when compared to the results for a homogenous fuel-air mixture. This difference was ascribed to the limiting effect of the spray mixing process. The sensitivity of the ignition event to several physical conditions was examined. For the conditions used in the computations, it was found that gas temperature, pressure, and the droplet diameter were important in determining the ignition delay. The features of diesel autoignition which were reproduced in the calculations included (1) the correct trends in pressure and temperature dependence for the ignition delay, (2) the approximate correct location of the ignition sites, (3) the variability of ignition time and site location to statistical fluctuations, (4) the appearance of multiple ignition sites, and (5) the rapid enflammation of the vapor sheath surrounding the fuel jet.

Exploratory calculations were performed for a three-dimensional diesel experiment from the MIT Rapid Compression Machine. Qualitative features of the ignition event were simulated including the approximate correct location of the ignition site and the appearance of the high temperature reaction zones. The pressure trace from the experiment was bounded from above and below by the results of testing different decision criteria in the logic determining the relative dominance of the autoignition and main heat release kinetics. The very fast apparent flame spread found in the

experiment was simulated by the calculation providing the upper pressure bound. The nature of the flame spreading is believed to be a coupled acoustic/chemical kinetic mechanism in the autoigniting medium. The calculation yielding the lower pressure bound provided a small improvement in the initial rate of pressure rise relative to a calculation without an autoignition model, but did not simulate the fast flame spreading.

The calculated results for ignition delay were in reasonable agreement with experimental data despite uncertainties in the sub-models. The correct prediction of the absolute ignition delay, particularly for values less than 1 millisecond, is of less practical importance than the ability to be able eventually to predict the sensitivity of ignition delay to the physical and chemical characteristics of the fuel and the physical and geometric conditions under which the fuel is injected. This study represents the first phase in attaining this goal by demonstrating the useful combination of the kinetics and fluids models.

There are major simplifications embodied in the sub-models used here which should not be overlooked and may be improved upon. The constant diffusivity turbulence model is too simplistic, because the single value, which was chosen based on momentum jet correlations, does not apply everywhere in the diesel combustion process. This would be perhaps the easiest area to upgrade in an extension to this work. The k-ε model will be available shortly for use in the KIVA program as an immediate improvement. The kinetics description, particularly for tthe heavier fuels, contains parameters whose values are uncertain. Efforts to quantify better the kinetic rates for autoignition continue by several groups. It may be hoped that this work will put the rates on a more fundamental basis. Results from such endeavors will not be available in the shorter term,

however. The dynamics of the spray and droplet breakup are still being explored, particularly for the physical region near the nozzle where droplet interactions are important. Methods to describe the breakup of droplets, which in diesel autoignition would provide an enhanced rate of mixing between fuel vapor and air, are now appearing in the literature. The spray model could be further improved by replacing the current heat transfer description, the Ranz-Marshall correlation, by newer, more accurate models available from the literature.[66] Finally, the interface in the computation between the autoignition reactions and the flame model requires continued efforts to define the correct compatibility criteria which will give a physically correct result.

The main result of this thesis is an approach or method for studying, in a more-direct manner than possible before, the relative roles of physical and chemical processes in the autoignition of fuel sprays. This method has the following characteristic. It is necessary that the parameters for at least the generic kinetics scheme be known for the fuel. If the kinetics parameters are not known, then the relative controlling behavior of physical and chemical processes predicted may be inaccurate or, at least, the answer will depend on the kinetics values chosen. These parameters are not well-known for diesel-type fuels at this time, and the physical properties for these fuels make it doubtful that experiments for premixed charges can be conducted at high pressures and temperatures in order to define the parameters. The following near-term solution to this quandry is proposed.

Autoignition experiments could be performed for sprays of the lighter hydrocarbons heptane, normal octane, or isooctane. Hiroyasu has already shown results for heptane and mentions results for isooctane, though none

have been published. The pressure rise associated with the autoignition of the spray should be measured. These fuels should then also be premixed and autoignited in a rapid compression machine to define the parameters for the the generic kinetics scheme. Armed with this data base for a common light fuel, computations may be carried out for the spray experiments without the need to estimate the kinetics parameters as part of the spray simulation. As pointed out earlier, these calculations would be expensive at low temperatures (long delays). Useful information on the relative roles of physical effects such as evaporation, droplet size distribution, or swirl versus the chemical rates could then be generated. While the results of such a set of studies would not be immediately applicable for practical diesel fuels, they would provide a solid basis from which to conduct parameter studies incorporating the physical properties of the heavier fuels and extrapolations of the kinetic rates. This progression would improve our understanding and ability to make estimates of the autoignition behavior for the heavier fuels. In the meantime, the method as now extant can be used as a method for conducting more limited sensitivity studies for the physical parameters.

REFERENCES

1. A. Brammer and D. Muster, "Noise radiated by internal-combustion engines," J. Acoust. Soc. Am. 58, 11-21 (1975).

2. A. Amsden, T. Butler, P. O'Rourke, and J. Ramshaw, "KIVA--A comprehensive model for 2-D and 3-D engine simulations," SAE 850554 (1985).

3. J. Heywood, "Engine combustion modeling--An overview," in J Mattavi and C. Amann, eds., Combustion Modeling in Reciprocating Engines, (Plenum Press, New York, 1980).

4. P. Blumberg, G. Lavoie, and R. Tabaczynski, "Phenomenological models for reciprocating internal combustion engines," Prog. Energy Combust. Sci. 5, 123-167 (1979).

5. S. Aggarwal and W. Sirignano, "Numerical modeling of one-dimensional enclosed homogeneous and heterogeneous deflagrations," Computers and Fluids 12, 145-158 (1984).

6. E. Oran and J. Boris, "Detailed modelling of combustion systems," Prog. Energy Combust. Sci. 7, 1-72 (1981).

7. E. Khalil, Modelling of Furnaces and Combustors, (Abacus Press, Tunbridge Wells, 1982).

8. T. Butler, L. Cloutman, J. Dukowicz, and J. Ramshaw, "Multidimensional numerical simulation of reactive flow in internal combustion engines," Prog. Energy Combust. Sci. 7, 293-315 (1981).

9. F. Bracco and P. O'Rourke, "A review of initial comparisons of computed and measured two-dimensional unsteady flame fields," Prog. Energy Combust. Sci. 7, 103-124 (1981).

10. M. Elkotb, "Fuel atomization for spray modelling," Prog. Energy Combust. Sci. 8, 61-91 (1982).

11. G. Faeth, "Evaporation and combustion of sprays," Prog. Energy Combust. Sci. 9, 1-76 (1983).

12. A. Gosman and P. Harvey, "Computer analysis of fuel-air mixing and combustion in an axisymmetric D.I. diesel," SAE 820036 (1982).

13. V. Duggal and T. Kuo, "Three-dimensional modeling of in-cylinder processes in DI diesel engines," SAE 840227 (1984).

14. D. Spalding, "Development of the eddy break-up model of turbulent combustion," Proc. 16th Symp. (Int.) on Combustion, p. 687 (1967).

15. C. Colella, M.S. Thesis, Massachusetts Institute of Technology (1985).

16. F. Stringer, Discussion of SAE Papers 680102 and 690103, Automotive Engineering Congress, Detroit, MI, 8-12 January 1968.

17. N. Henein and J. Bolt, "Ignition lag in diesel engines," SAE 670007 (1967).

18. M. Halstead, L. Kirsch, A. Prothero, and C. Quinn, "A mathematical model for hydrocarbon autoignition at high pressures," Proc. R. Soc. Lond. A 346, 515-538 (1975).

19. A. Fish, A. Read, W. Affleck, and W. Haskell, "The controlling role of cool flames in two-stage ignition," Combust. Flame 13, 39-49 (1969).

20. L. Spadaccini and J. TeVelde, "Autoignition characteristics of aircraft-type fuels," NASA CR-159886 (1980).

21. ASTM D613.

22. N. Henein, A. Fragoulis, and L. Luo, "Correlation between physical properties and autoignition parameters of alternate fuels," SAE 850266 (1985).

23. C. Taylor, E. Taylor, J. Livengood, W. Russell, and W. Leary, "Ignition of fuels by rapid compression," SAE Quart. Trans. 4, 232-274 (1950).

24. B. Mullins, Spontaneous Ignition of Liquid Fuels, (Butterworths, London, 1955).

25. W. Lyn and E. Valdmanis, "The effects of physical factors on ignition delay," SAE 680102 (1968).

26. R. Hurn and H. Smith, "Hydrocarbons in the diesel boiling range," Ind. Eng. Chem. 43, 2788-2793 (1951).

27. H. Kobayashi, T. Kamimoto, and S. Matsuoka, "A photographic and thermodynamic study of diesel combustion in a rapid compression machine," SAE 810259 (1981).

28. S. Igura, T. Kadota, and H. Hiroyasu, "Spontaneous ignition delay of fuel sprays in high pressure gaseous environments," Translation from Trans. Japan Soc. Mech. Engrs. 41, 1559-1566 (1975).

29. C. Westbrook and F. Dryer, "Chemical kinetic modeling of hydrocarbon combustion," Prog. Energy Combust. Sci. 10, 1-57 (1984).

30. M. Halstead, L. Kirsch, and C. Quinn, "The autoignition of hydrocarbon fuels at high temperatures and pressures--Fitting of a mathematical model," Combust. Flame 30, 45-60 (1977).

31. N. Semonov, Chemical Kinetics and Chain Reactions, (Oxford University Press, 1935).

32. R. Cox and J. Cole, "Chemical aspects of the autoignition of hydrocarbon-air mixtures," Combust. Flame 60, 109-123 (1985).

33. S. Benson, "The kinetics and thermochemistry of chemical oxidation with application to combustion and flames," Prog. Energy Combust. Sci. 7, 125-134 (1981).

34. H. Hu and J. Keck, "The explosion of adiabatically compressed combustible gas mixtures in constant volume bombs and rapid compression machines," ICDERS Meeting, August 1985.

35. R. Wilk, R. Cohen, and N. Cernansky, "Ignition studies of dodecane and binary mixtures of dodecane and tetralin," Twentieth Symposium (International) on Combustion, The Combustion Institute, pp. 187-193 (1984).

36. Diesel Fuel Oils, American Society of Mechanical Engineers (1948).

37. S. Hirst and L. Kirsch, "The application of a hydrocarbon autoignition model in simulating knock and other engine combustion phenomena," in J. Mattavi and C. Amann, eds., Combustion Modeling in Reciprocating Engines, (Plenum Press, New York, 1980).

38. H. Schapertons and W. Lee, "Multidimensional modelling of knocking combustion in SI engines," SAE 850502 (1985).

39. B. Natarajan and F. Bracco, "On multidimensional modeling of auto-ignition in spark-ignition engines," Combust. Flame 57, 179-197 (1984).

40. A. Amsden, J. Ramshaw, P. O'Rourke, and J. Dukowicz, "KIVA: A computer program for two- and three-dimensional fluid flows with chemical reactions and fuel sprays," Los Alamos National Laboratory Report LA-10245-MS (1985).

41. A. Amsden, J. Ramshaw, L. Cloutman, and P. O'Rourke, "Improvements and extensions to the KIVA computer program," Los Alamos National Laboratory Report LA-10534-MS (1985).

42. A. Prothero and A. Robinson, "On the stability and accuracy of one-step methods for solving stiff systems of ordinary differential equations," Math. Comp. 28, 145-162 (1974).

43. W. Rivard, O. Farmer, and T. Butler, "RICE: A Computer Program for Multicomponent Chemically Reactive Flows at All Speeds," Los Alamos Scientic Laborator Report LA-5812 (1975).

44. H. Gupta,"REC: A computer program for the computation of combustion in open and divided chamber reciprocating engines with uniform and stratified charges," Aerospace and Mechanical Sciences Department Report No. 1365, Princeton University (1978).

45. R. Diwakar, "Multidimensional modeling applied to the direct-injection stratified-charge engine--Calculation versus experiment," SAE 810225 (1982).

46. D. Stull and H. Prophet, "JANAF Thermochemical Tables," 2nd ed. (U.S. Dept. of Commerce/National Bureau of Standards,NSRDS-NBS 37, June 1971). N.W. Chase, et. al., J. Phys. Chem. Ref. Data 3, 311 (1974).

47. W. Ranz and W. Marshall Jr., Chem. Engr. Progr. 48, 141 and 173 (1952).

48. W. Affleck and A. Thomas, Proc. Inst. Mech. Eng. 183, 1 (1969).

49. H. Hiroyasu and T. Kadota, "Fuel droplet size distribution in diesel combustion chamber," SAE 740715 (1974).

50. A. Rogowski, "A new machine for studying combustion of fuel sprays with controlled air motion," SAE 436F (1961).

51. P. White, M.S. Thesis, Massachusetts Institute of Technology (1984).

52. J. Kimberley and R. DiDomenico, "UFIS--A new diesel injection system," SAE 770084 (1984).

53. J. Van Gerpen, C. Huang, and G. Borman, "The effects of swirl and injection parameters on diesel combustion and heat transfer," SAE 850265 (1985).

54. J. Kimberley, Private communication, 7 November 1985.

55. E. Balles, Chapter 5 of the Third Annual Report of the Industrial Consortium for Engine Research, MIT (1985).

56. J. Gatowkski, et. al., "Heat release analysis of engine pressure data," SAE 841359 (1984).

57. N. B. Vargaftik, Tables on the Thermophysical Properties of Liquids and Gases, (Wiley, New York, 1975).

58. P. O'Rourke, "Collective drop effects on vaporizing liquid sprays," Los Alamos National Laboratory Thesis LA-9069-T (1981).

59. T. Kuo and F. Bracco, "Computations of drop sizes in pulsating sprays and of liquid core length in vaporizing sprays," SAE 820133 (1982).

60. R. Reitz, "Atomization and other breakup regimes of a liquid jet," Ph.D. Thesis 1375-T, Princeton University Dept. of Aerospace and Mechanical Sciences (1978).

61. A. Borisov, "On the origin of exothermic centers in gaseous mixtures," Acta Astronautica 1, 909-920 (1974).

62. T. Butler, "What to Expect from Multidimensional Numerical Simulations," ASME Winter Annual Meeting, Miami, Florida, 19 November 1985.

63. S. Wahiduzzaman and C. Ferguson, "Convective heat transfer from a decaying swirling flow within a cylinder," Paper 86-IHTC-T53, to be presented at the International Heat Transfer Conference, San Francisco, CA, March, 1986.

64. A. Chatwani and F. Bracco, "Computation of dense spray jets," ICLASS-85.

65. T. Butler, Private communication, December 1985.

66. S. Aggarwal, A. Tong, and W. Sirignano, "A comparison of vaporization models in spray calculations," AIAA J. 22, 1448-1457 (1984).

67. S. Haddad and N. Watson, Principles and Performance in Diesel Engineering, (Ellis Horwood Ltd., Chichester, 1984).

68. C. Hirt, A. Amsden, and J. Cook, "An arbitrary Lagrangian-Eulerian Computing Method for all flow speeds," J. Comp. Phys. 14, 227-253 (1974).

69. A. Brown, "Stochastic Mixing Model for Predicting DI Diesel Emissions," Ph.D. thesis proposal, MIT (1985).

CAPTIONS FOR COLOR PLATES

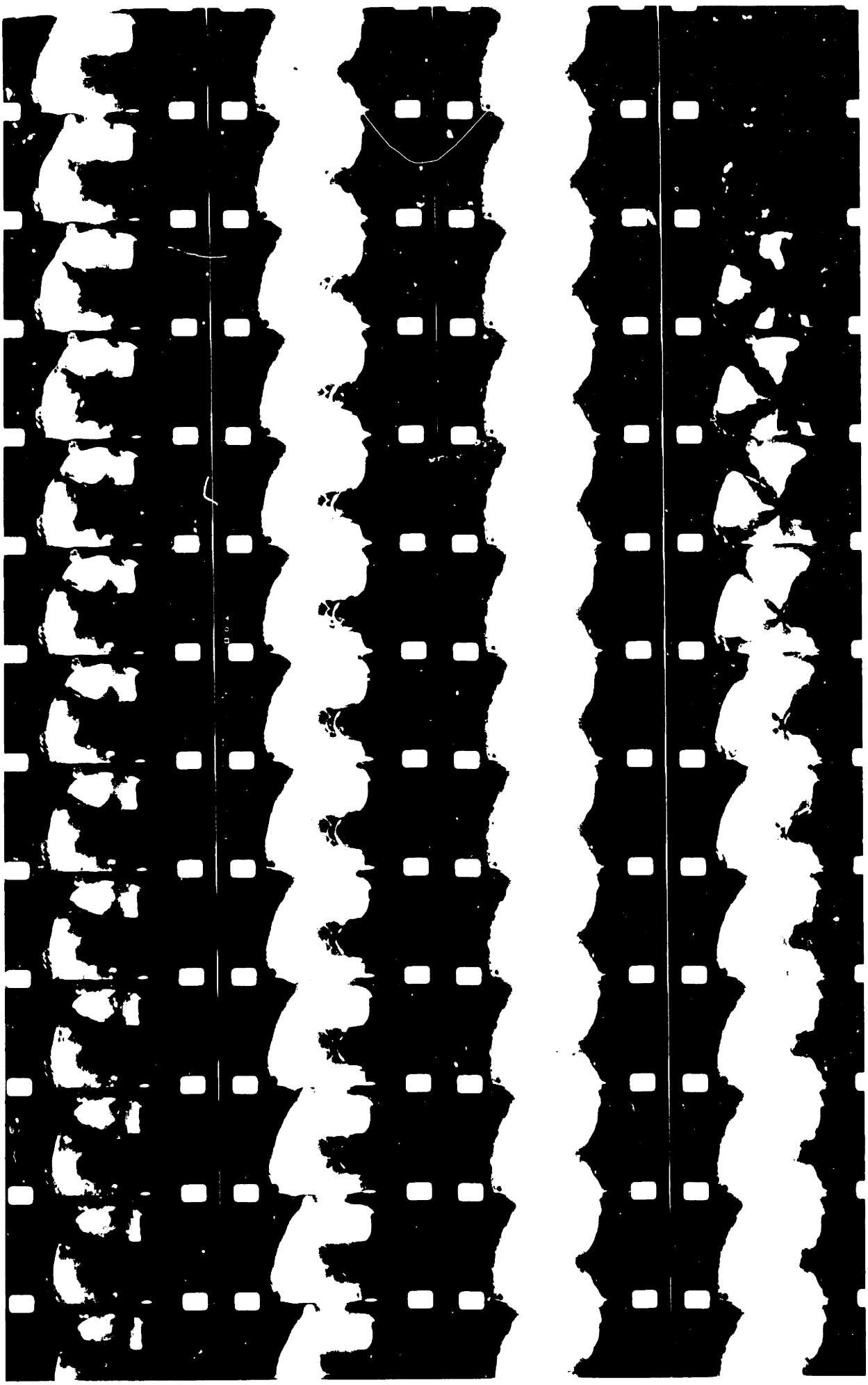

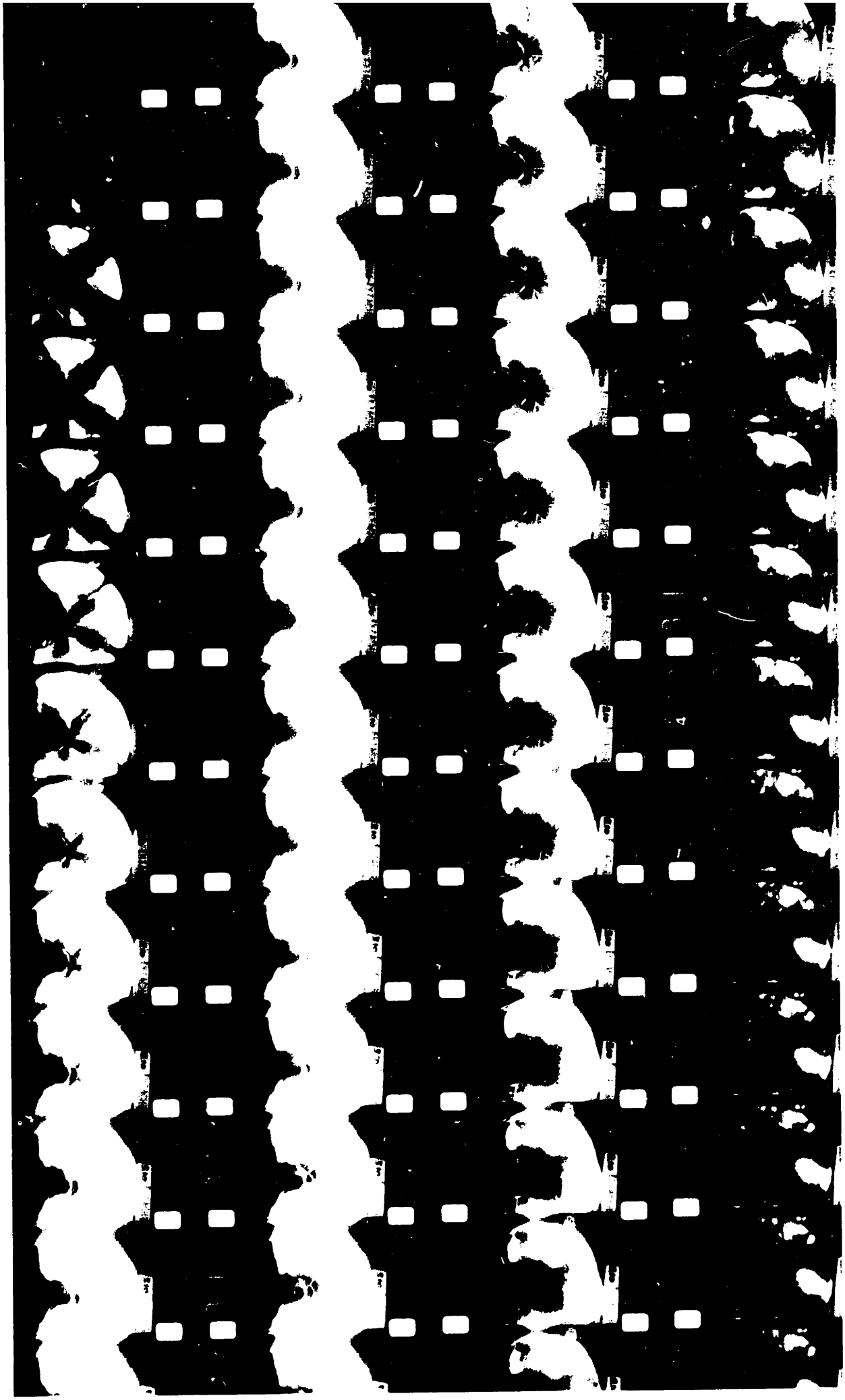

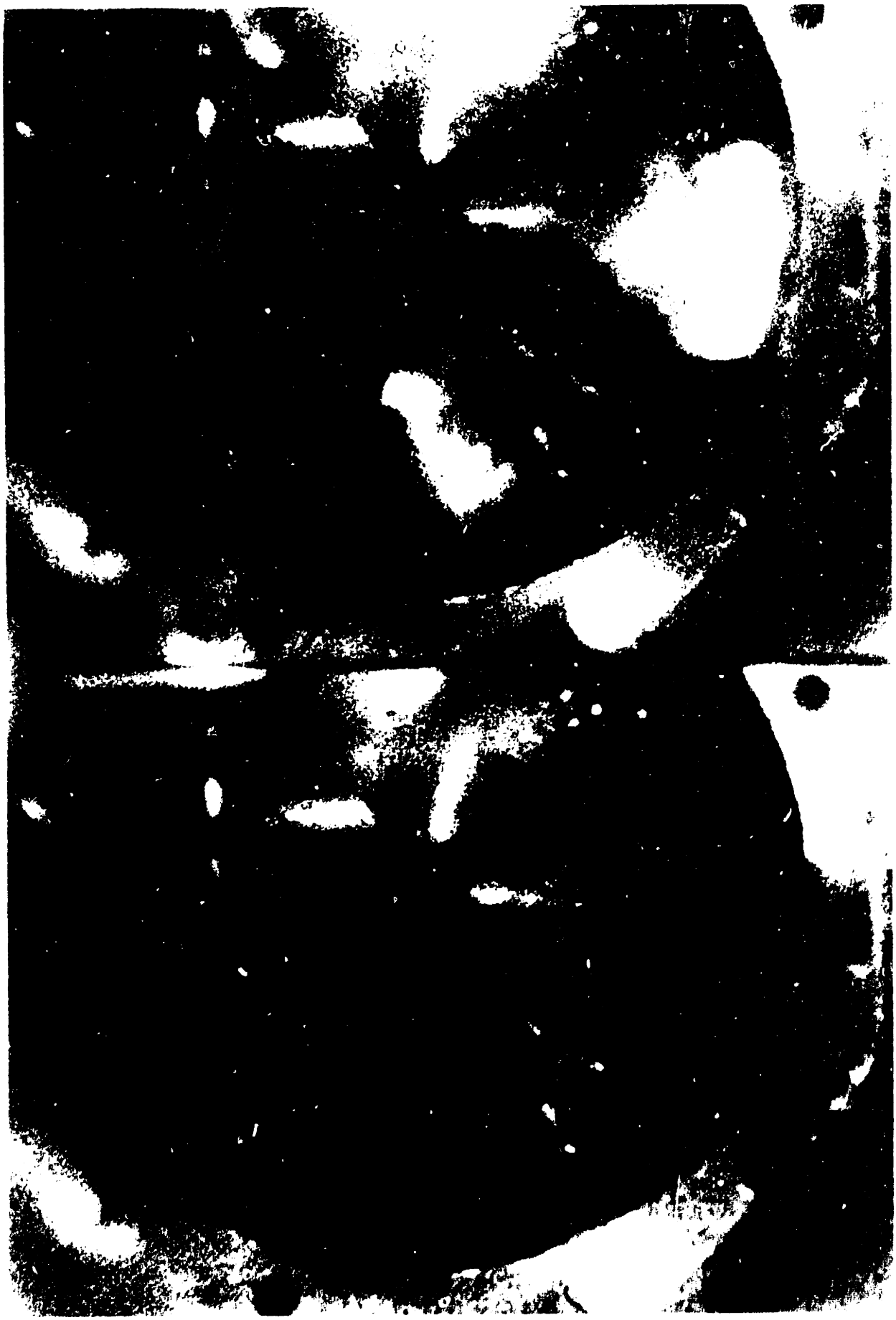

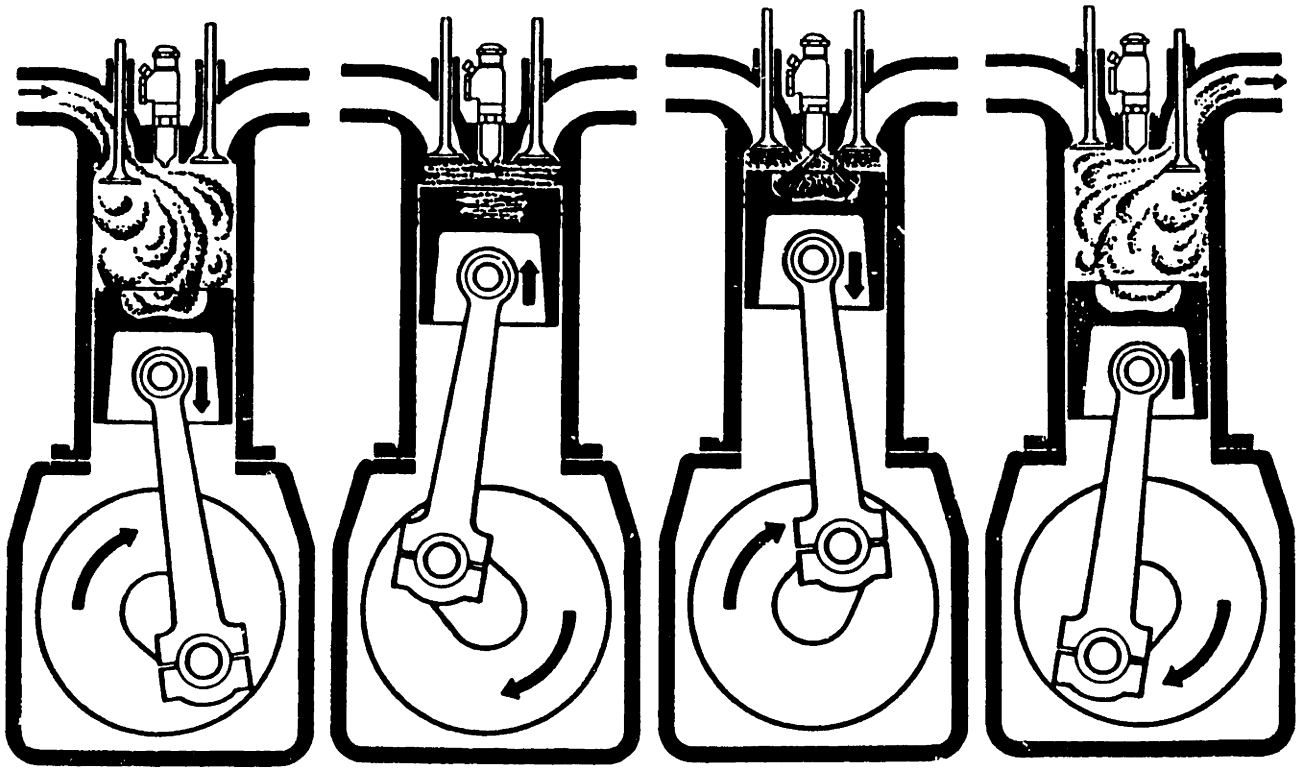

Figure 1.1 The Four-Stroke Diesel Engine (from Ref. 67)

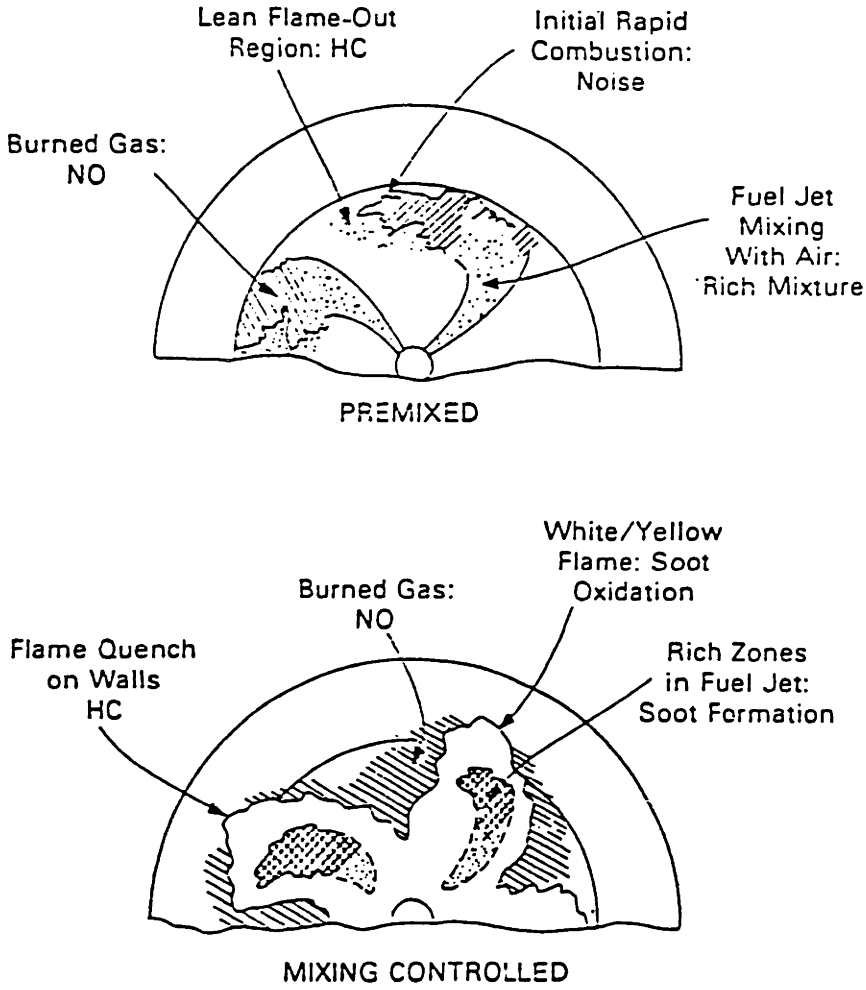

Figure 1.2 The Premixed and Mixing Controlled Phases of Diesel Combustion

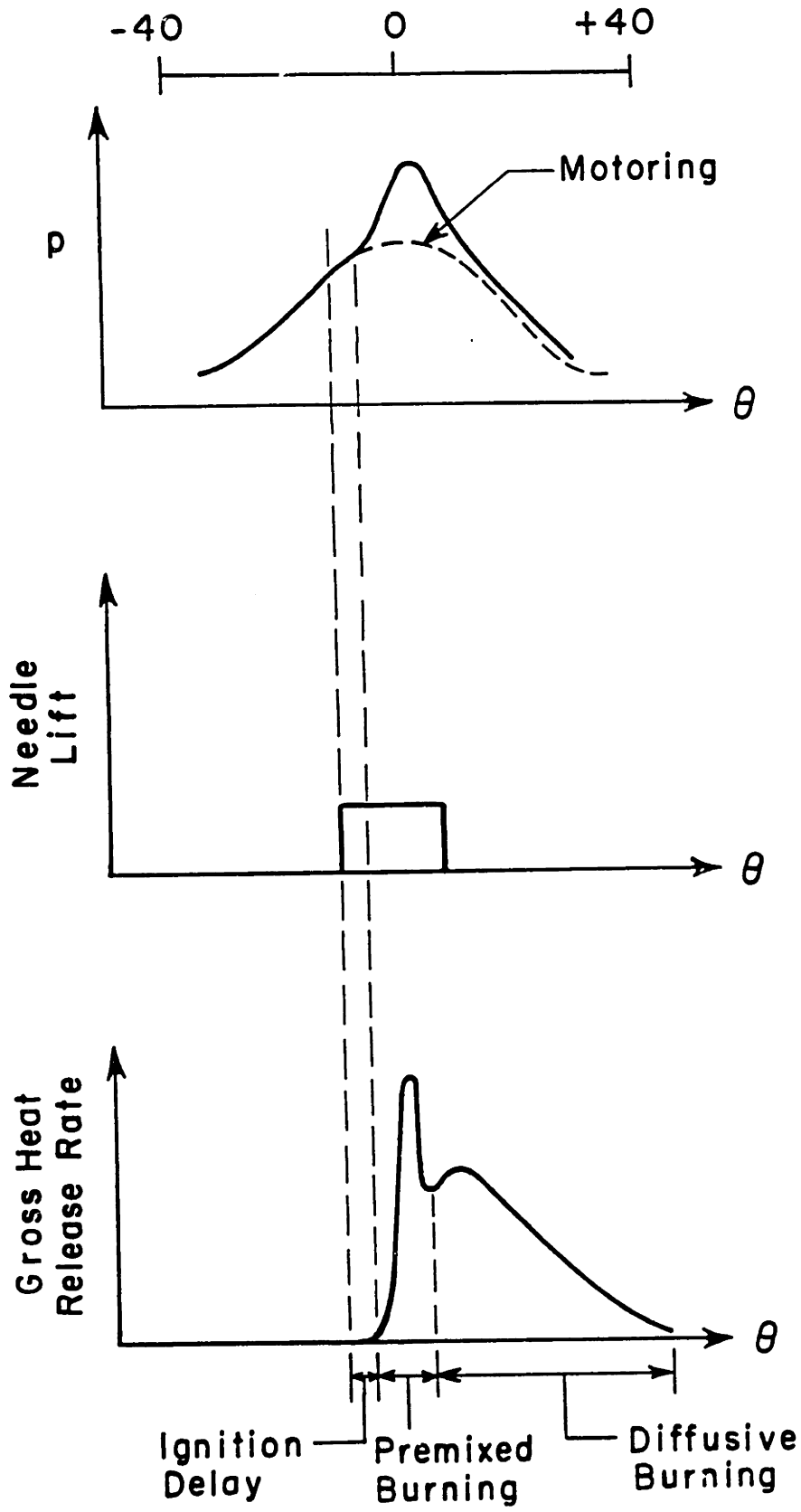

Figure 1.3 Pressure, Needle Lift, and Heat Release Profiles of a Direct Injection Diesel Engine

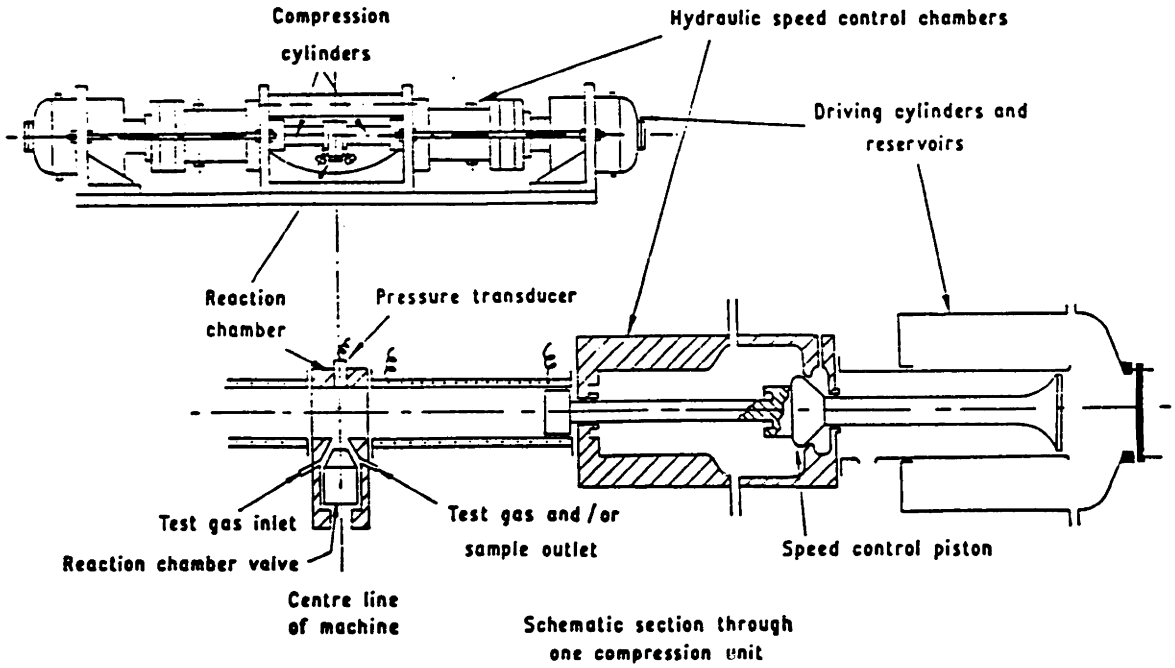

Figure 4.1 Schematic Diagram of the Rapid Compression Machine of the Shell Research Centre

(from Affleck and Thomas[48])

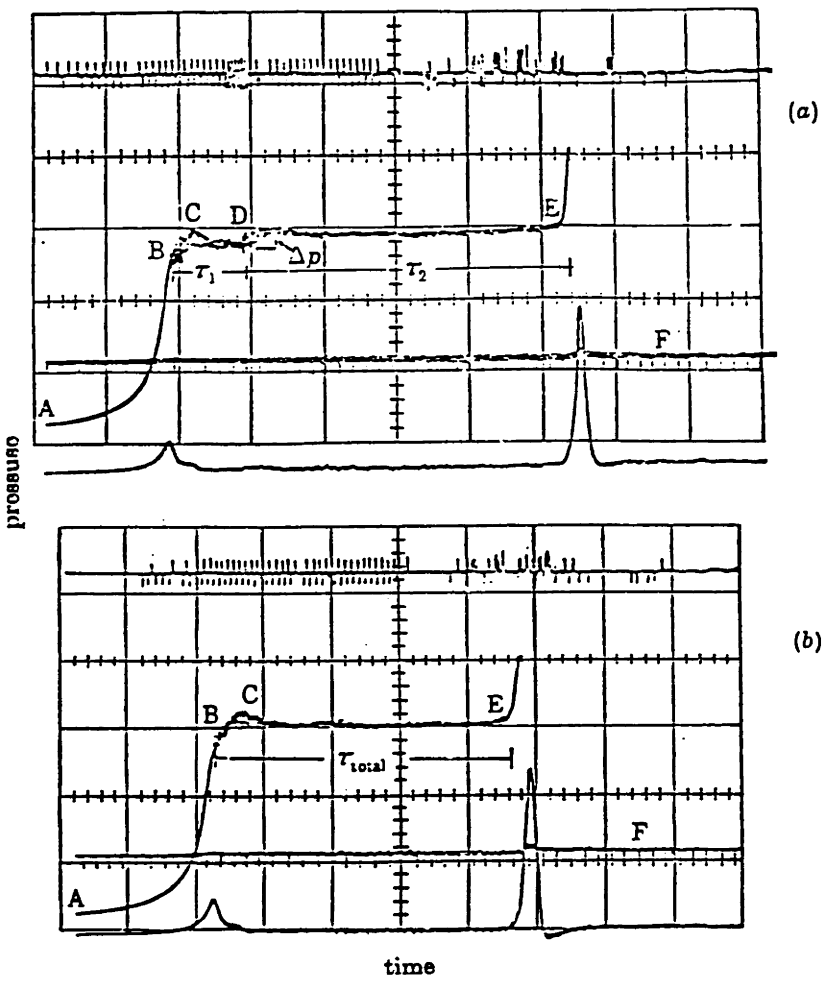

FIGURE 1. Typical oscilloscope records of the autoignition of a 0.9 stoichiometric mixture of iso-octane with air in a rapid-compression machine. (*a*) Two-stage ignition at a pressure and temperature of 1.86 MPa and 686 K; (*b*) single-stage ignition at a pressure and temperature of 2.12 MPa and 787 K. Trace ABCDE is the pressure record; the vertical scale corresponds to 690 kPa per large division. Trace F is the timing trace with markers at millisecond intervals. The total gas concentration at the end of compression is in both cases 3.3×10^{-4} mol cm^{-3}.

Figure 4.2 Pressure Traces for Two- and One-Stage Ignition

(from Halstead, et. al.[18])

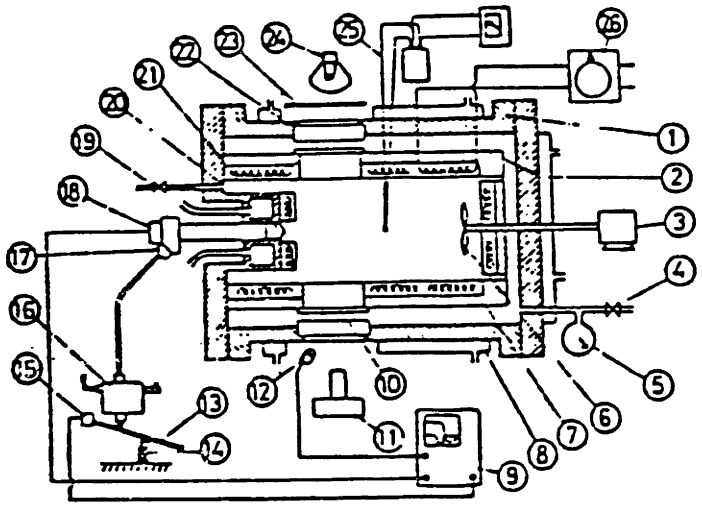

Key to Selected Components

1. Pressure vessel
2. Heating jacket
6. Fan
11. High-speed movie camera
12. Photodetector
16. Injection pump
17. Injection pressure transducer
18. Needle-lift sensor
24. Lamp

Figure 4.3 Schematic Diagram of the Combustion Bomb of Igura, Kadota, and Hiroyasu.

(from Ref. 28)

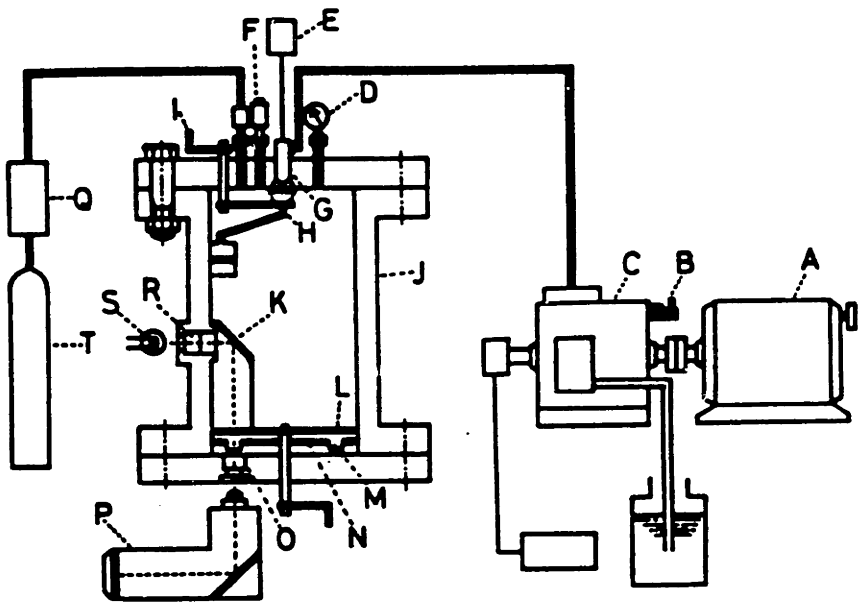

Key to Components

A- Motor
B- Control Rack
C- Injection Pump
D- Pressure Gauge
E- Pressure Pickup for Injection Pressure
F- Safety Valve
G- Nozzle
H- Spray Receptacle
I- Operating Lever
J- Pressure Vessel
K- Mirror
L- Slit Plate
M- Sampling Cell
N- Rotating Disk
O- Pyrex Glass
P- Camera
Q- Reducing Valve
R- Pyrex Glass
S- Lamp
T- Nitrogen Bottle

Figure 4.4 Schematic Diagram of Measuring Apparatus for Nonevaporating Sprays of Diesel Oil

(from Hiroyasu[49])

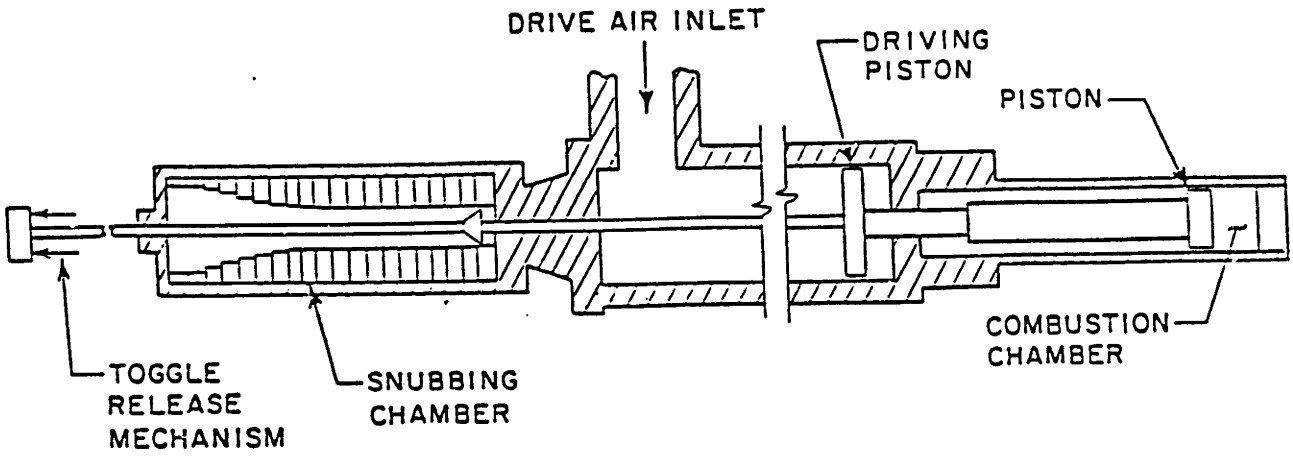

Current Specifications of the Rapid Compression Machine

Bore	10.16 (4.00 in.)
Stroke	44.7 (17.6 in.)
Clearance height	2.957 (1.164 in.)
Compression ratio	16.1:1
Crevice volume/clearance volume	< 0.4 %
Mean piston speed	10 - 15 m/s
Piston geometry	flat crown
Cylinder head geometry	flat
Injector	American Bosch UFIS
Nozzles	5 hole-type; evenly-spaced
Nozzle diameter	0.22 mm
Injection pressure	613.3 atm abs.

Figure 4.5 Schematic Diagram of the Rapid Compression Machine at the Massachusetts Institute of Technology

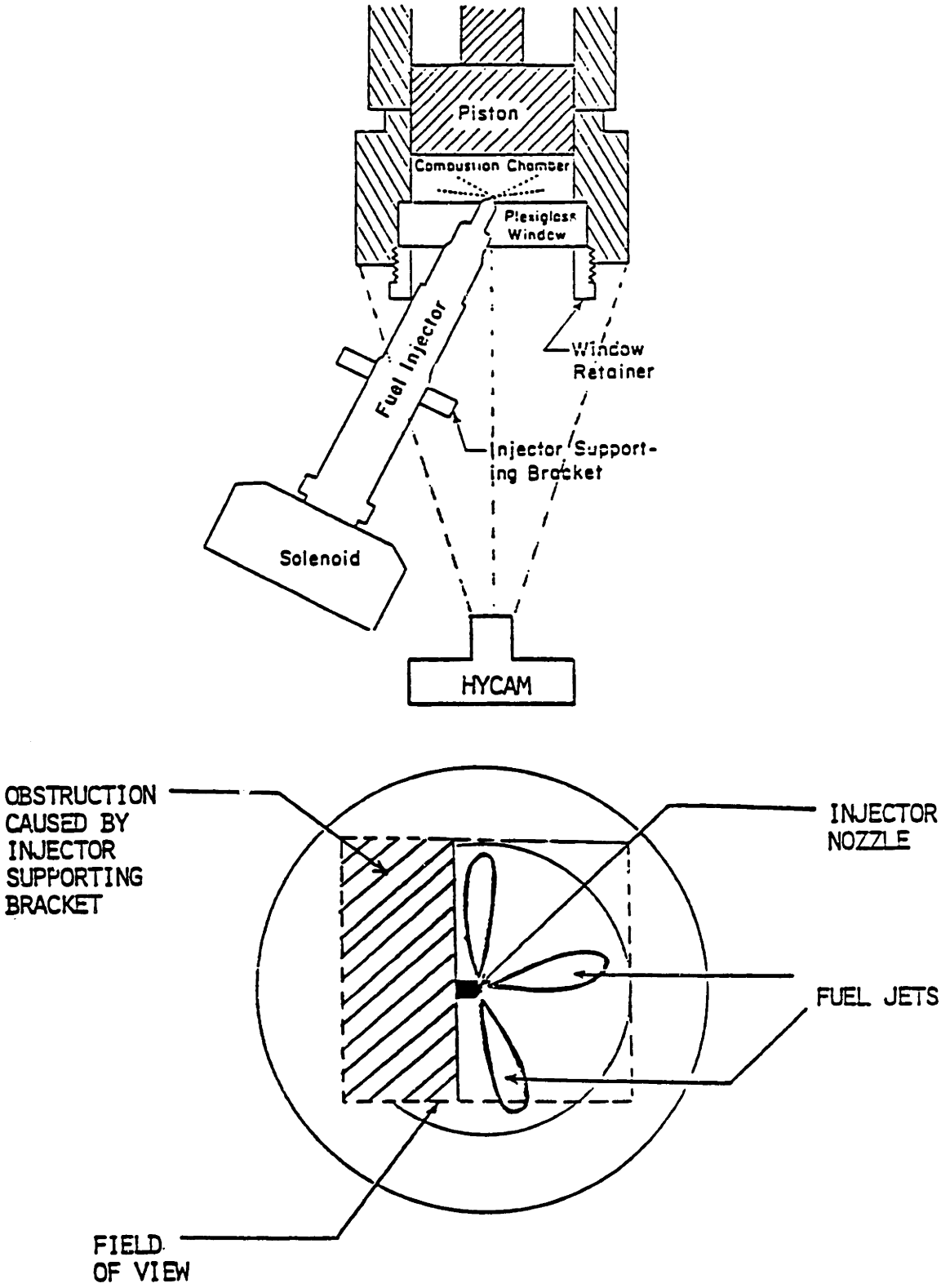

Figure 4.6 Field of View from the High-Speed Movie Camera

(from Colella[15])

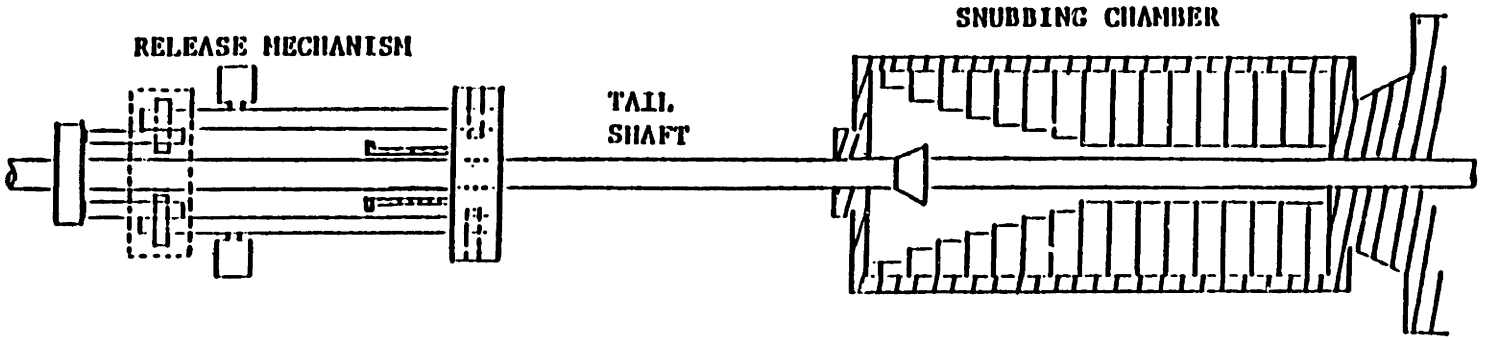

OPERATION OF RELEASE MECHANISM

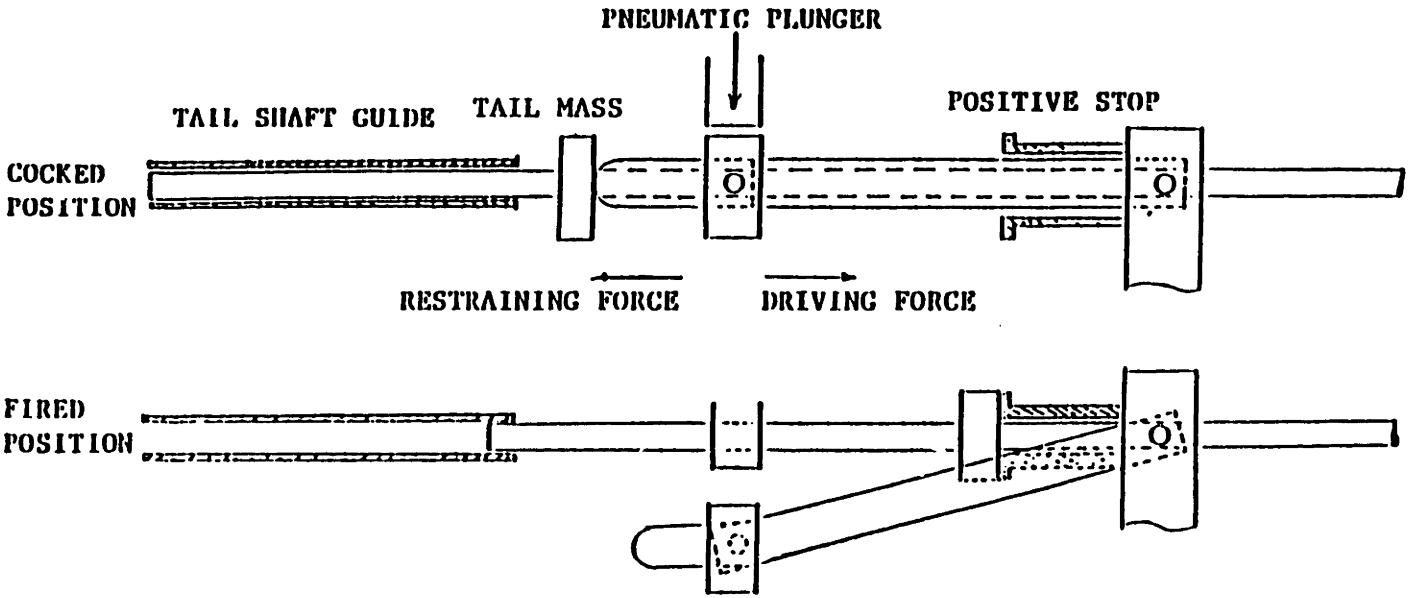

Figure 4.7 Release Mechanism of the RCM (Diagram from Colella[15])

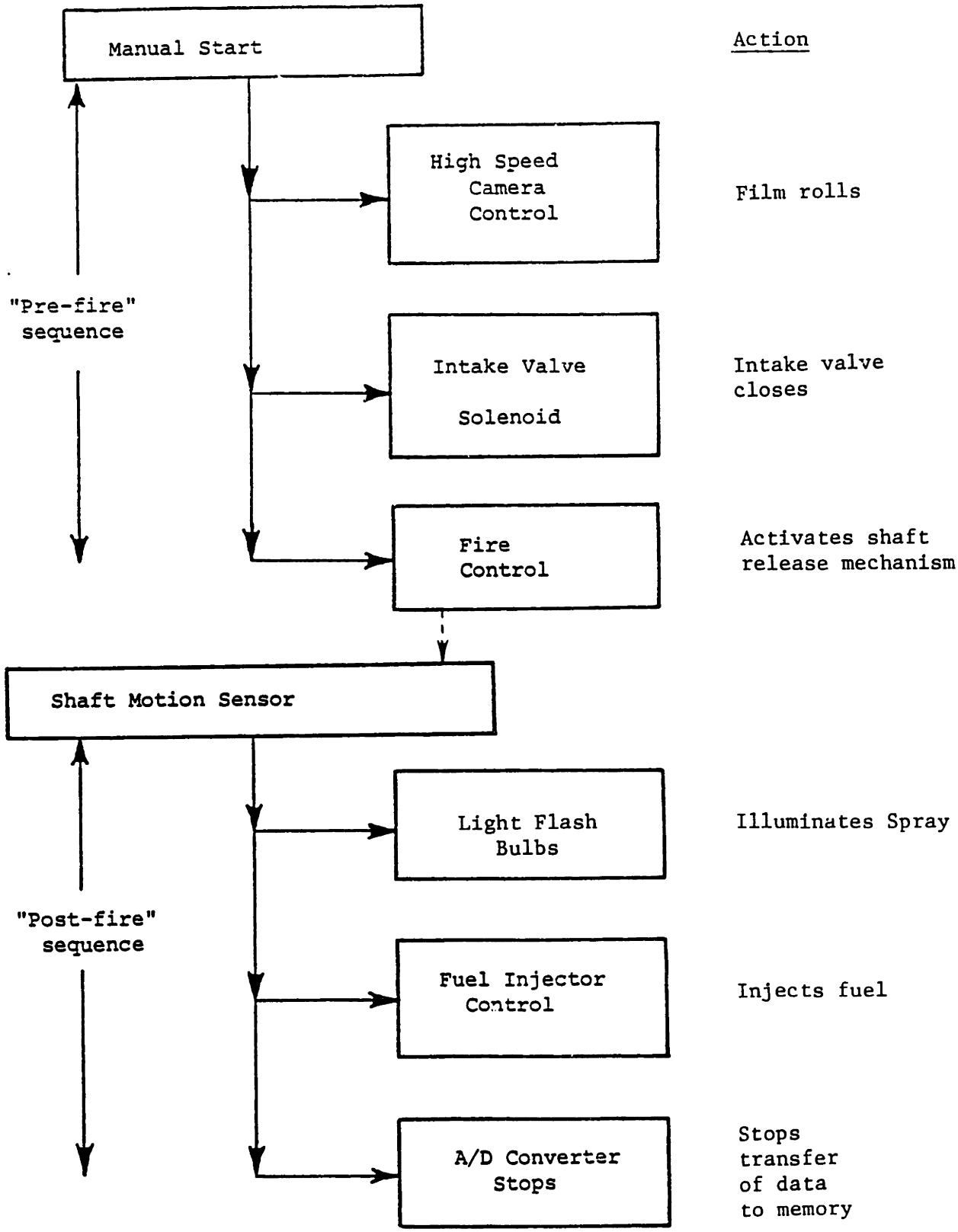

Figure 4.8 Control Sequence of the RCM

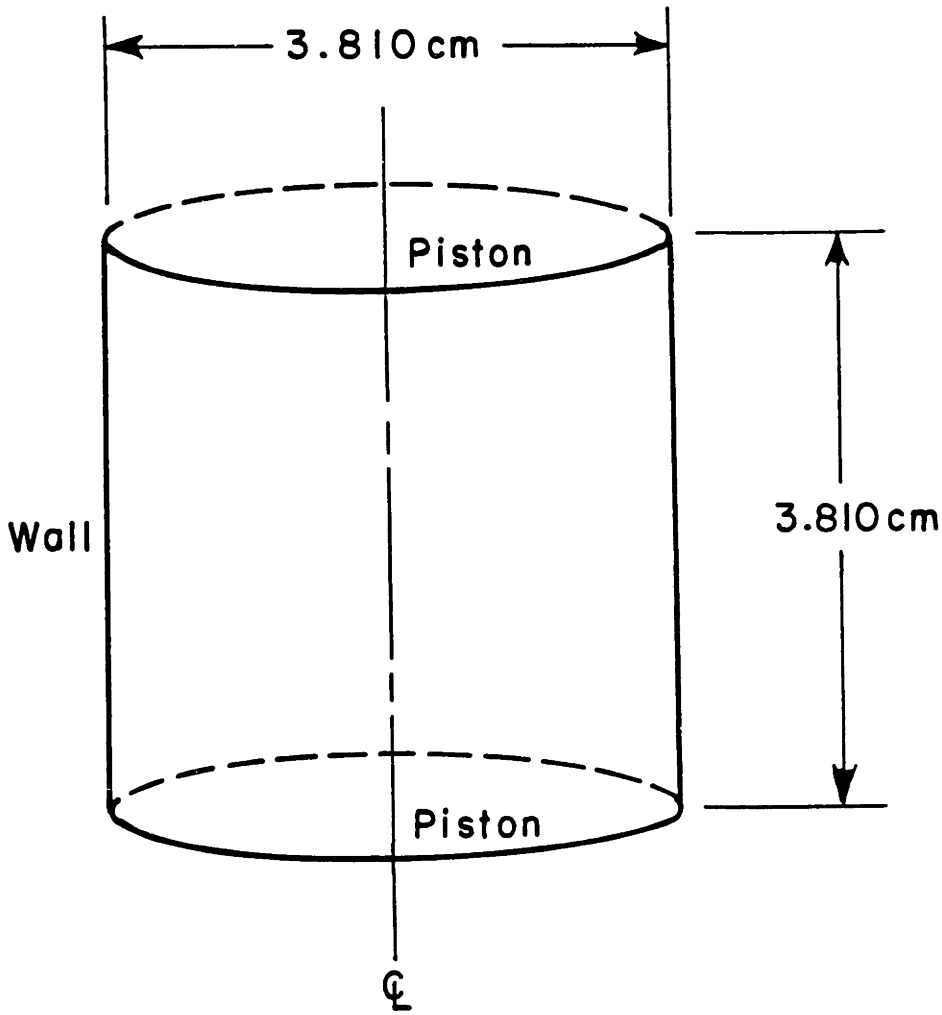

Figure 5.1 Axisymmetric Mesh Cell for Zero-Dimensional Simulation of the Shell Rapid Compression Machine

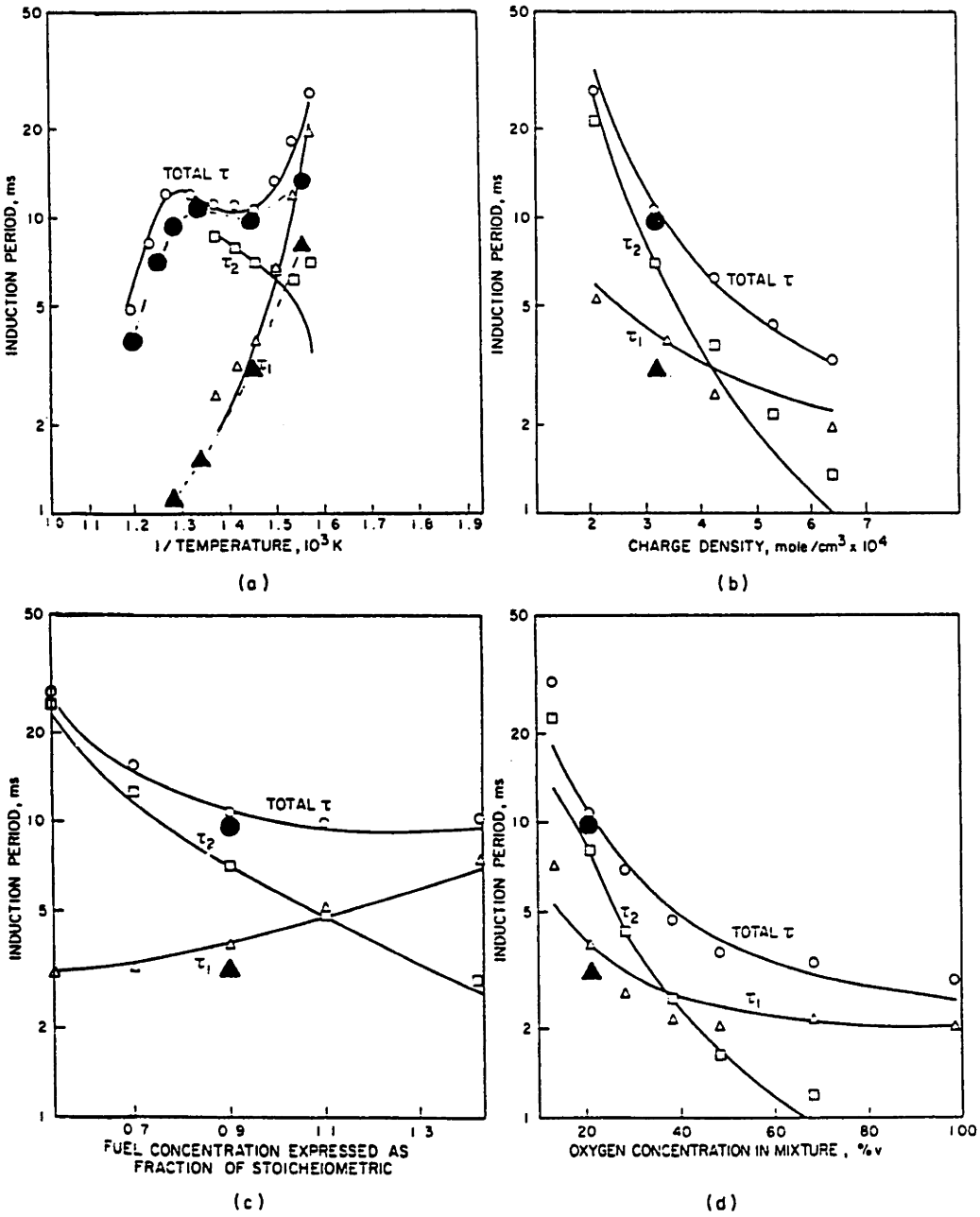

Comparison of experiment and model predictions for the autoignition of 90 RON Primary Reference Fuel: (a) effect of temperature; (b) effect of charge density; (c) effect of fuel concentration; (d) effect of oxygen concentration (variations are about a "base" mixture, 0.9 stoichiometric in air at a precompression pressure of 15 lb/in^2; end of compression temp. 690K, charge density=3.20 X 10^{-4} mole/cm^3; compression ratio=9.6:1; wall temp.=373K.

Present Calculation ● Total τ ▲ τ_1 (from Halstead, et. al.[30])

Figure 5.2 Zero-Dimensional Calculation of Autoignition Time Using The Modified 'KIVA' Program

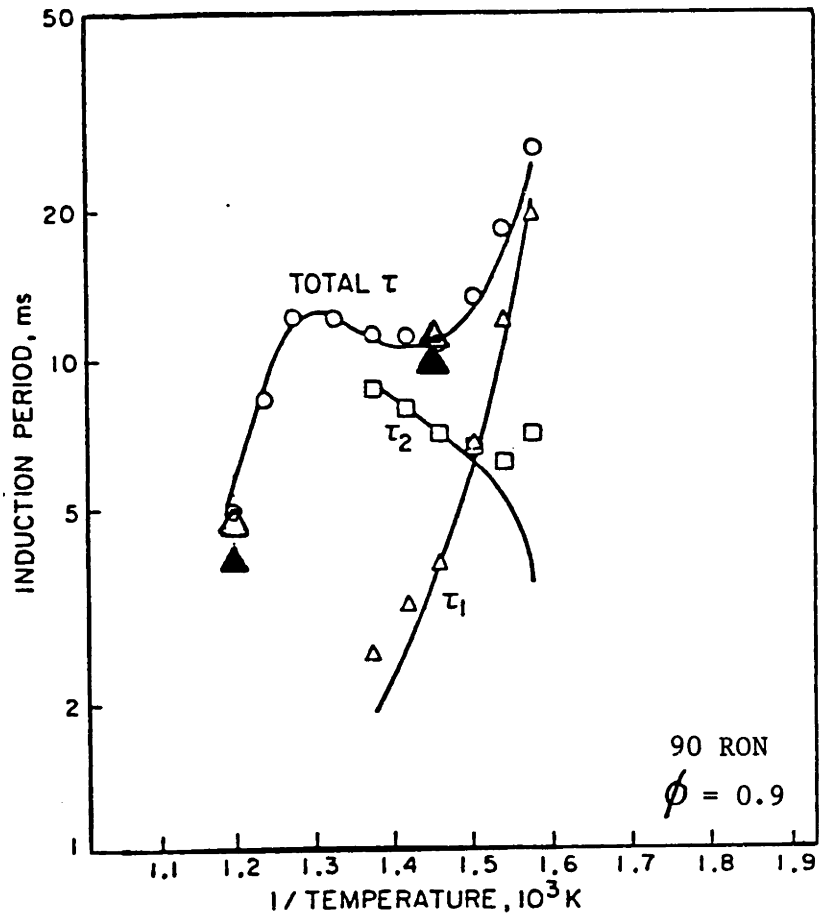

(from Halstead, et. al.[30])

Time Step: More Restrictive △ Present Calculation for Total τ
Less Restrictive ▲

Figure 5.3 Effect of Chemistry Sub-Timestep on Calculated Autoignition Time

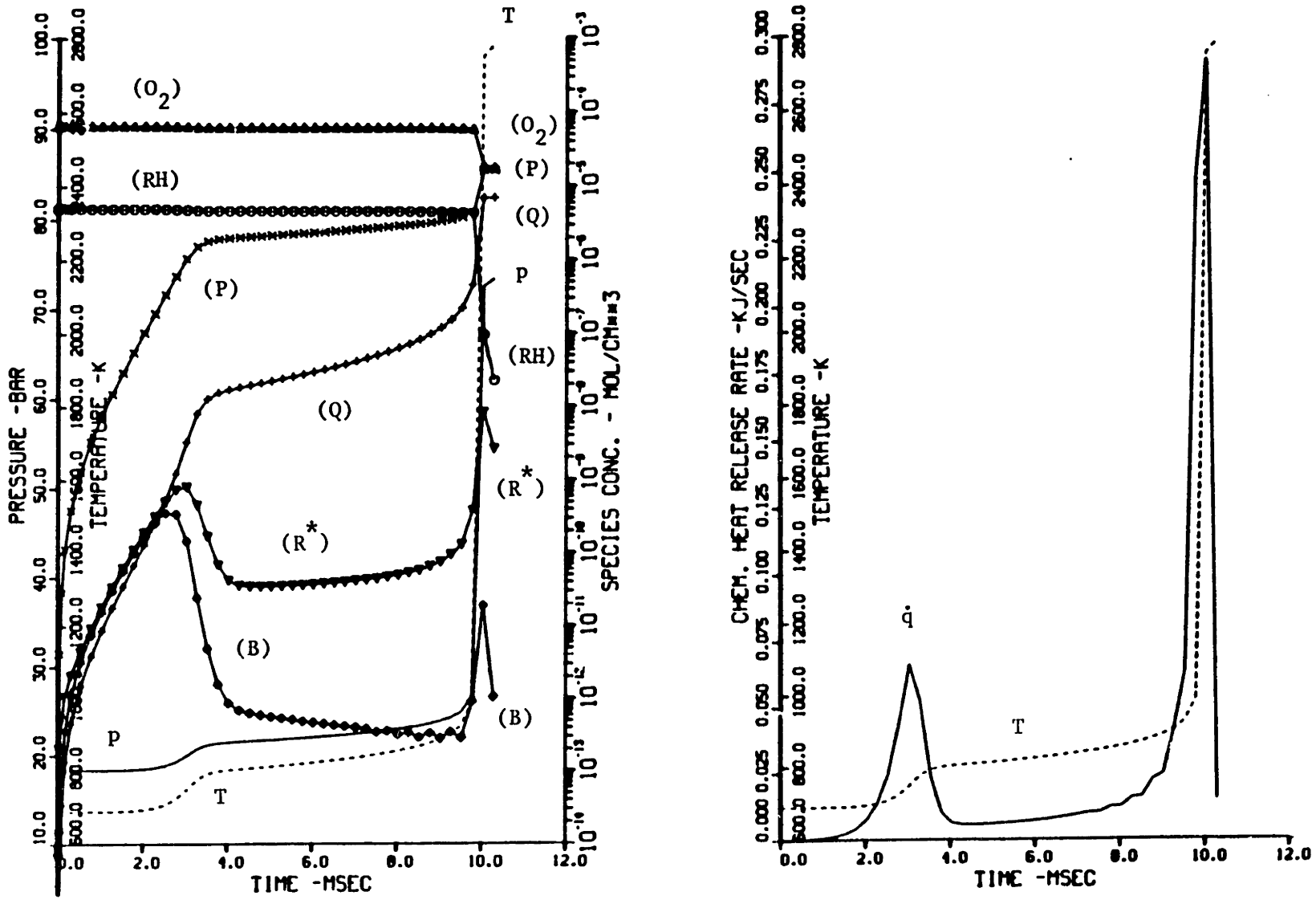

Figure 5.4 Two-Stage Ignition 90 RON; 690K; 3.2 X 10^{-4} mole/cm^3; ϕ =0.9

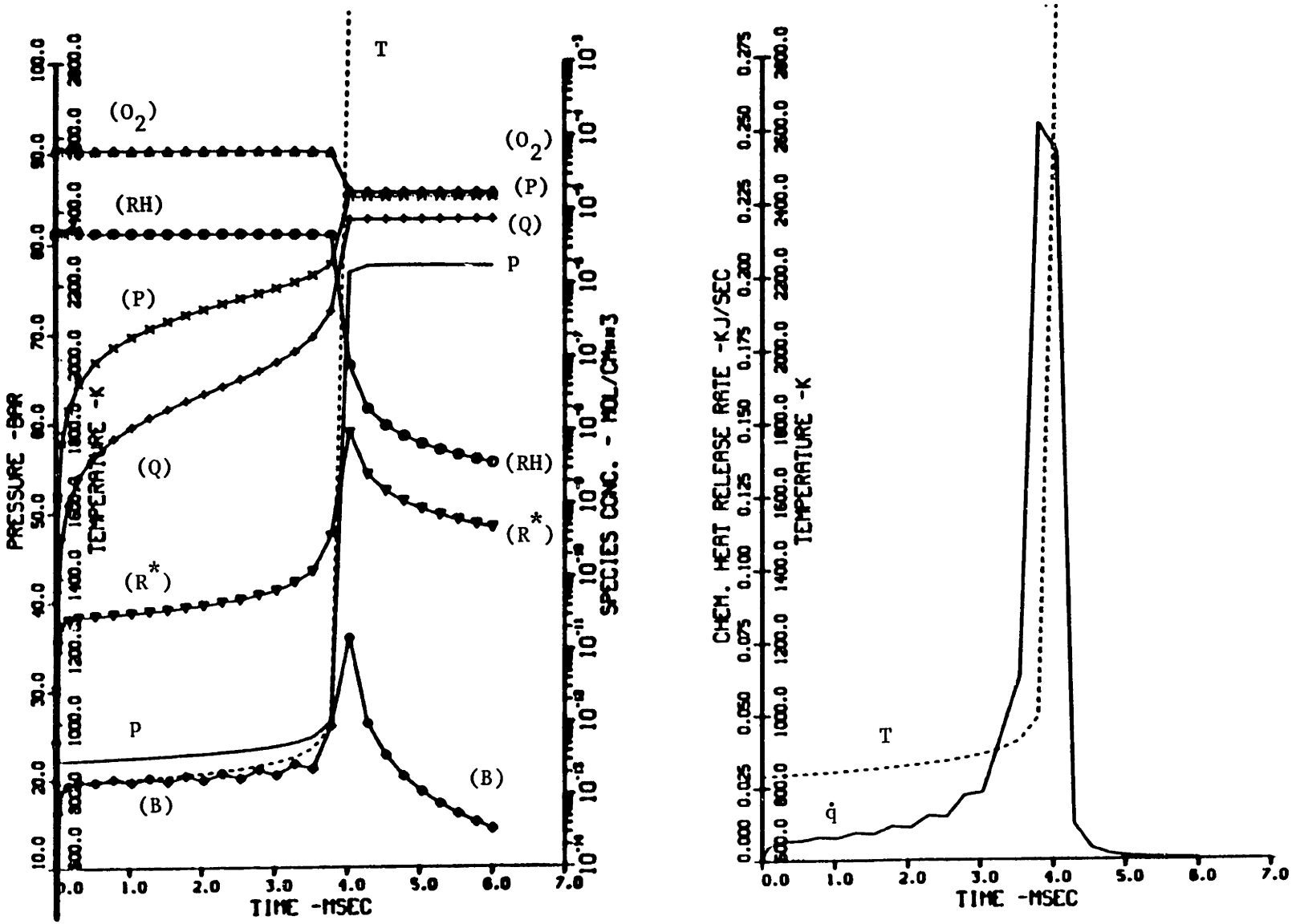

Figure 5.5 Single-Stage Ignition 90 RON; 833K; 3.2 X 10^{-4} mole/cm^3; ϕ =0.9

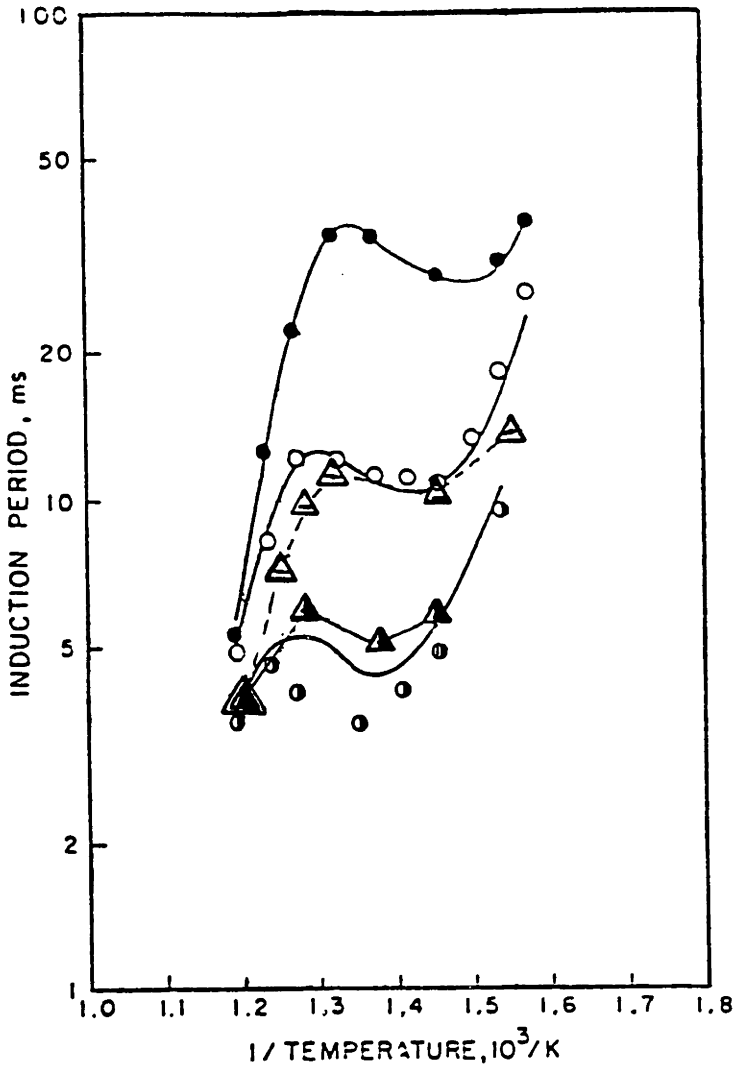

Fig. 4. Comparison of experiment and model predictions-the effect of temperature on total induction period for Primary reference fuels of different octane quality. (0.9 stoicheiometric mixtures, compression ratio 9.6:1, wall temperature = 373K).

from Halstead, et. al.[30] DATA: ● 100 RON, ○ 90 RON, ◑ 70 RON
CALCULATIONS: ———

Present Calculation: △ 90 RON, ▲ 70 RON

Figure 5.6 Zero-Dimensional Calculation of Autoignition Times for 70 and 90 RON Fuels

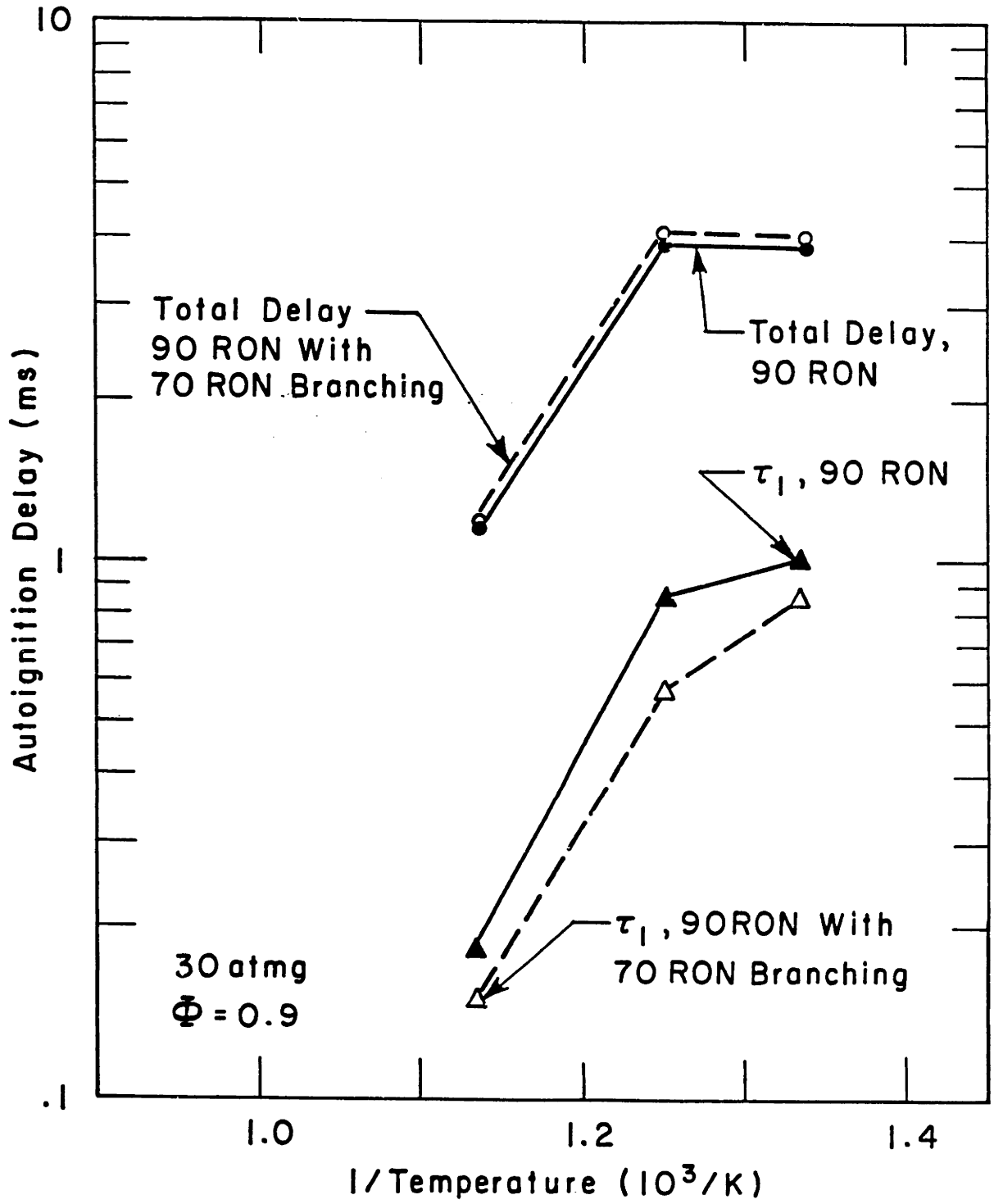

Figure 5.7 Effect of Variation of Branching Rate on Autoignition Delay

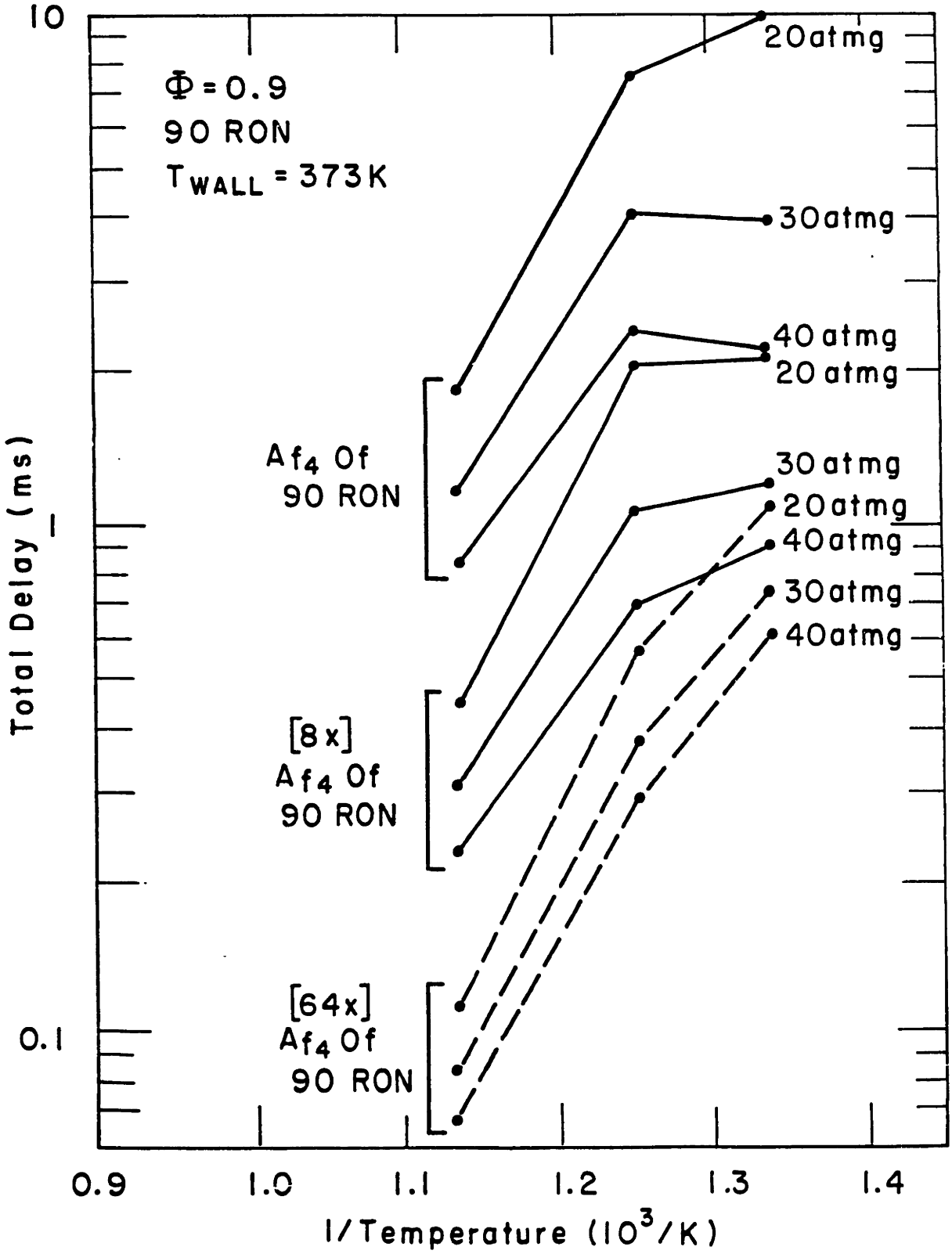

Figure 5.8 Effect of Variation of Q Formation Rate on Autoignition Delay

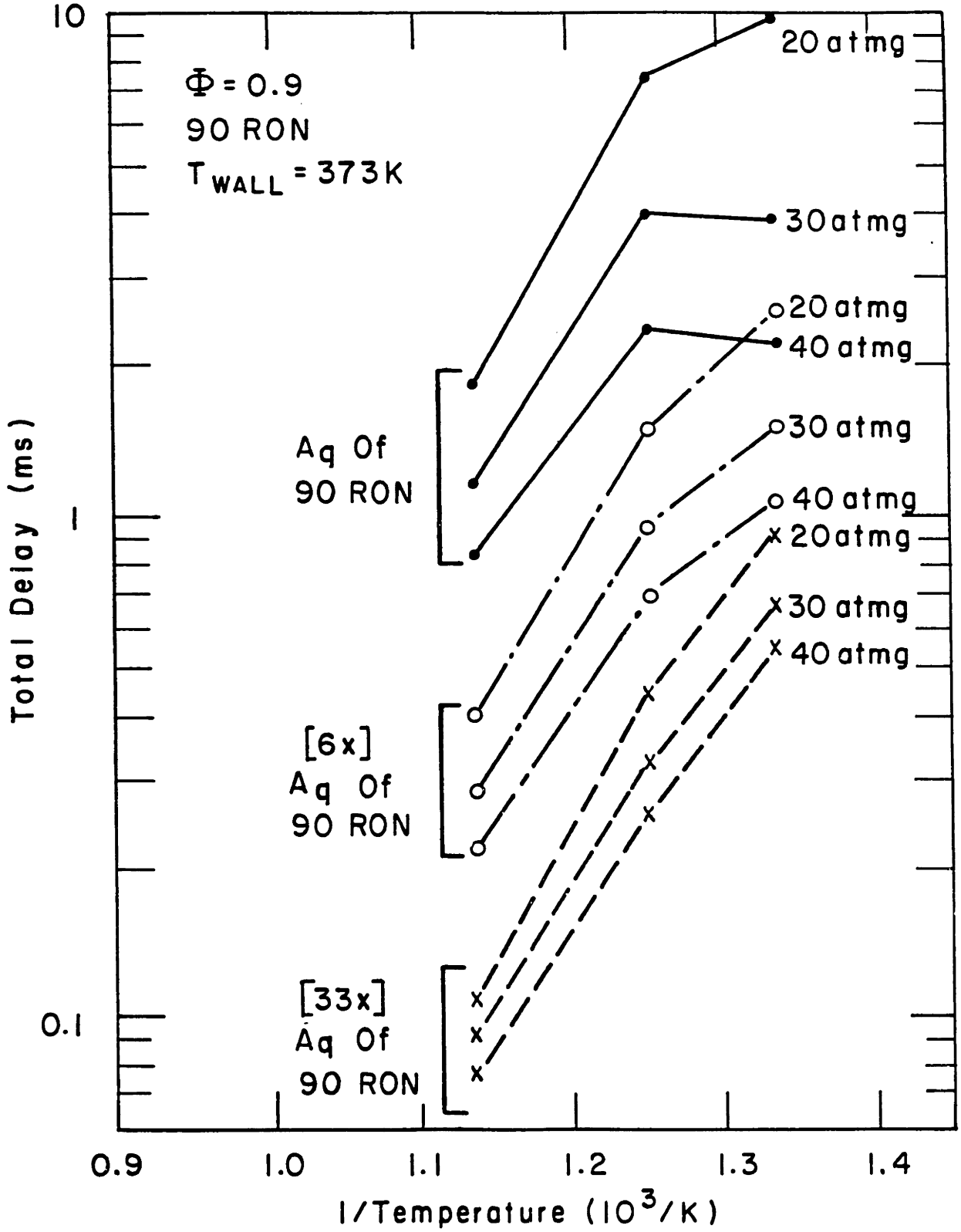

Figure 5.9 Effect of Variation of Initiation Rate on Autoignition Delay

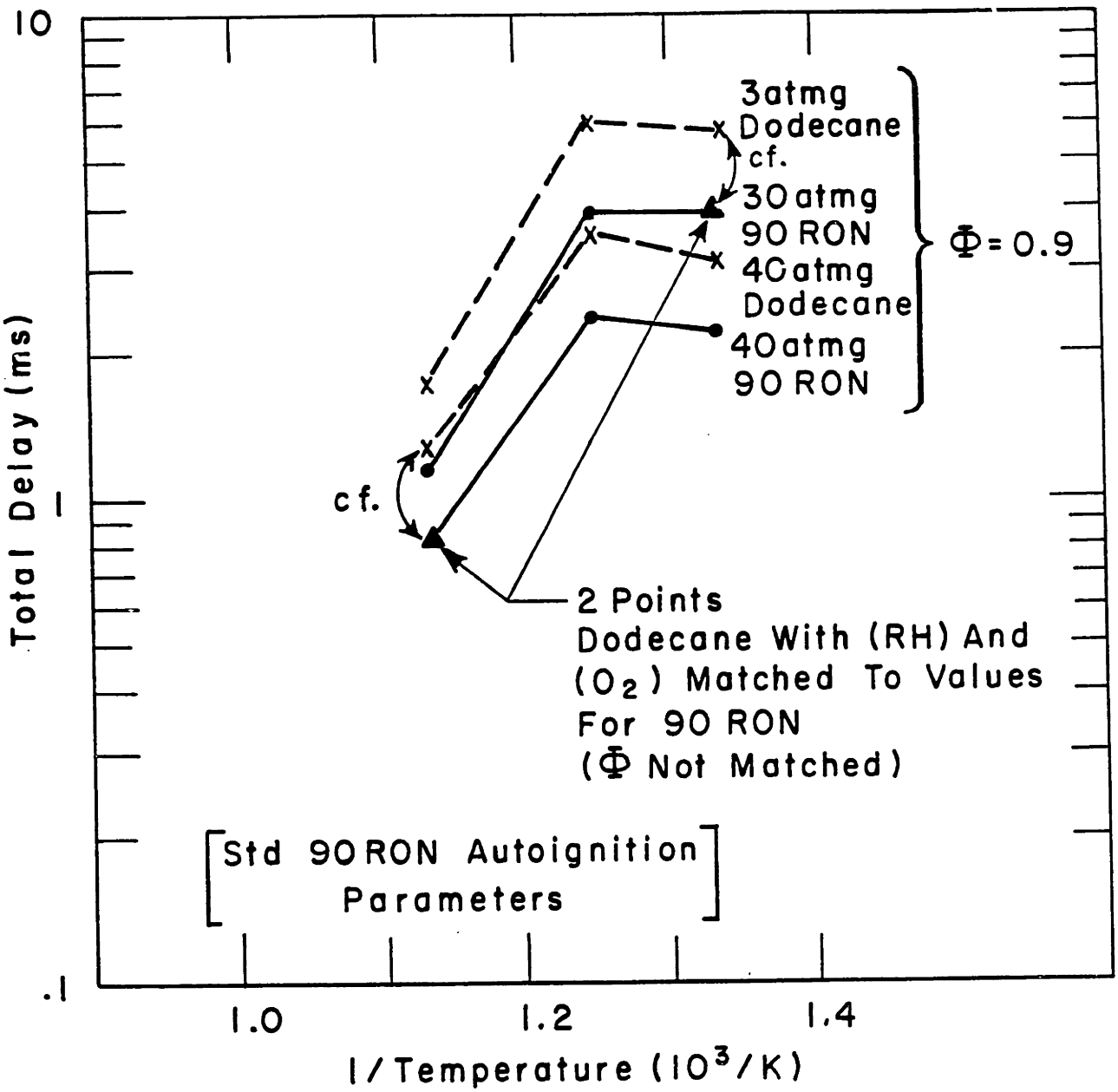

Figure 5.10 Effect of Fuel Properties on Ignition Delay for a Premixed Charge

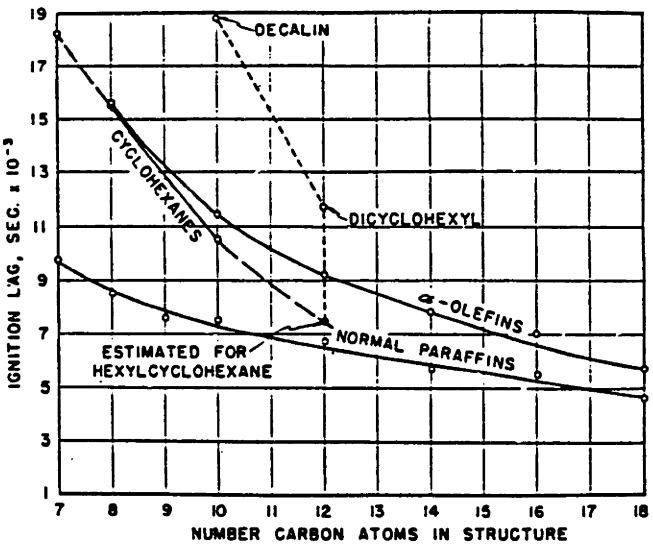

(a) Comparative Ignition Characteristics of Different Hydrocarbon Types

Bomb pressure, 300 pounds per square inch
Bomb temperature, 900° F.

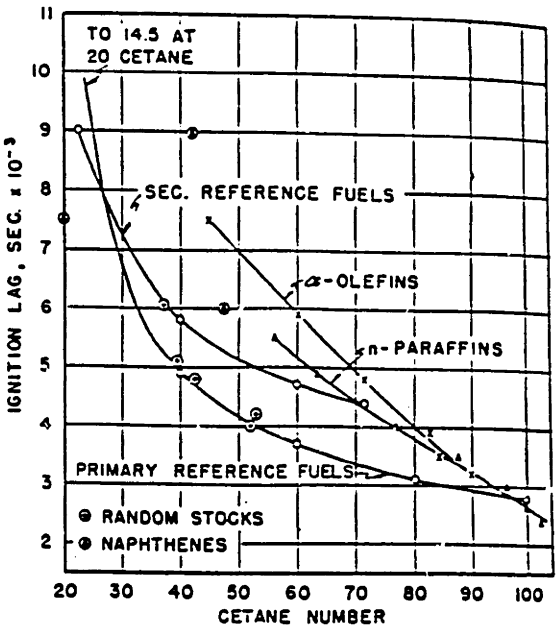

(b) Cetane Number–Ignition Lag Correlation for Various Fuel Types

Bomb pressure, 300 pounds per square inch
Bomb temperature, 1000° F.

(c) Correlation of Cetane Number with Molecular Structure

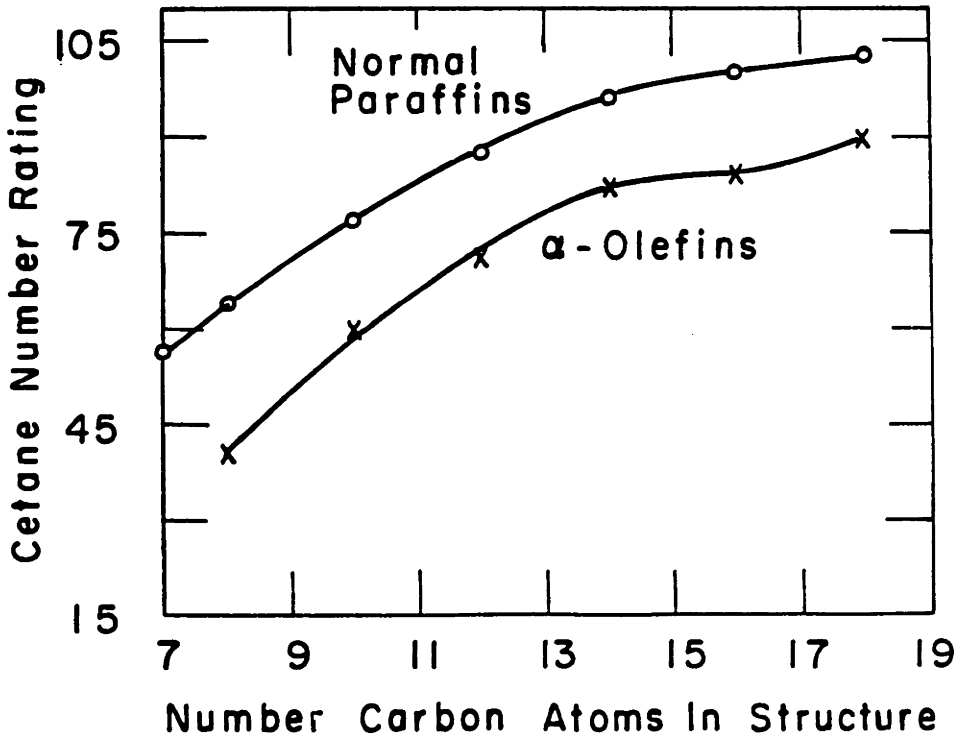

Figure 5.11 Ignition Data for Sprays of Various Fuels in a Combustion Bomb (from Hurn and Smith[26])

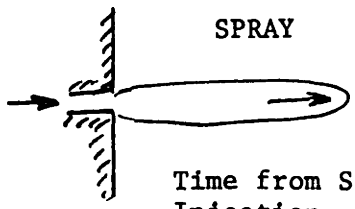

Time from Start of Injection

Ignition Delay = 3.6 ms

Fuel: Diesel Oil

Conditions: 850K
20 atmg

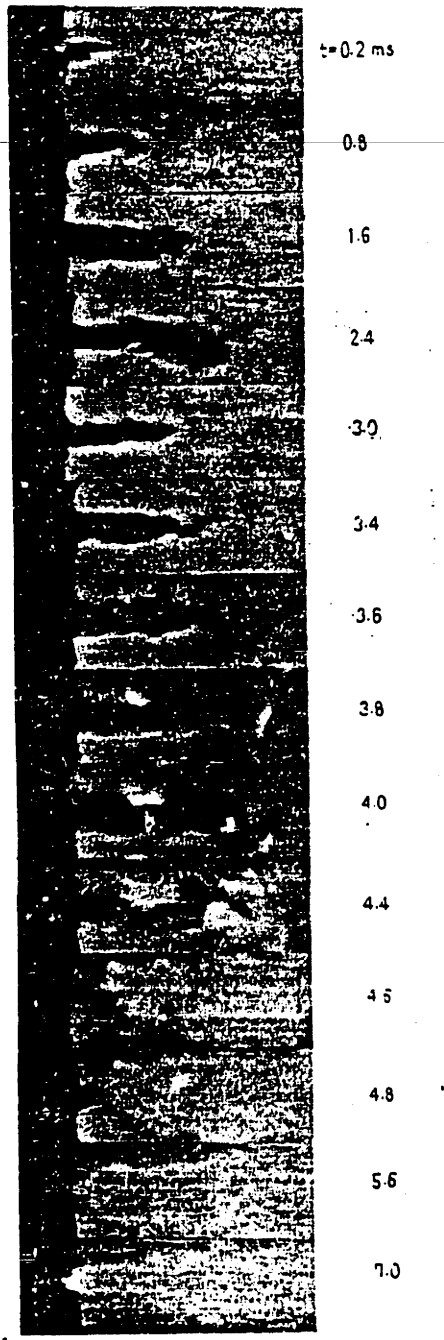

First Ignition Site Visible

2nd & 3rd Sites Visible

Engulfed

p=20 atg, T=580°C, DLS 301, 軽油, Q=0.13 cc/st.
V=0.89 m/s, p_o=100 kg/cm²

Figure 5.12 High-Speed Movie of an Autoigniting Fuel Jet

(from Hiroyasu[28])

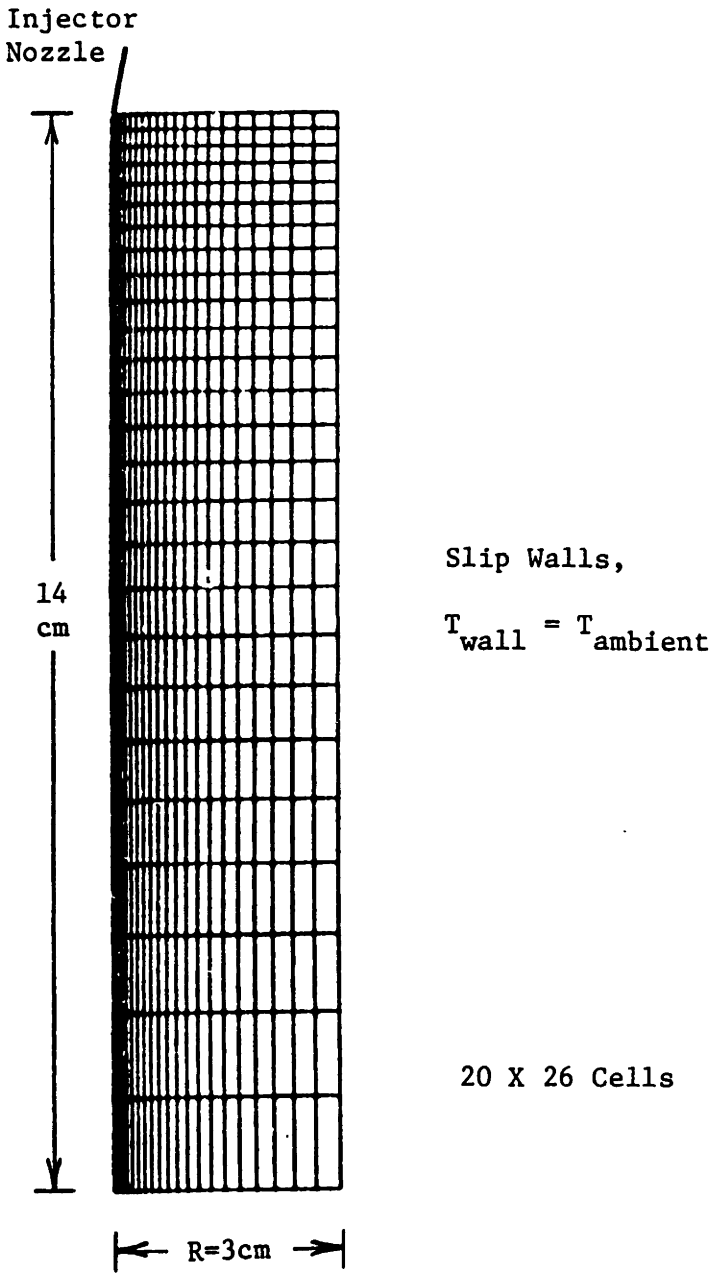

Figure 5.13 Grid for Spray Penetration Calculations

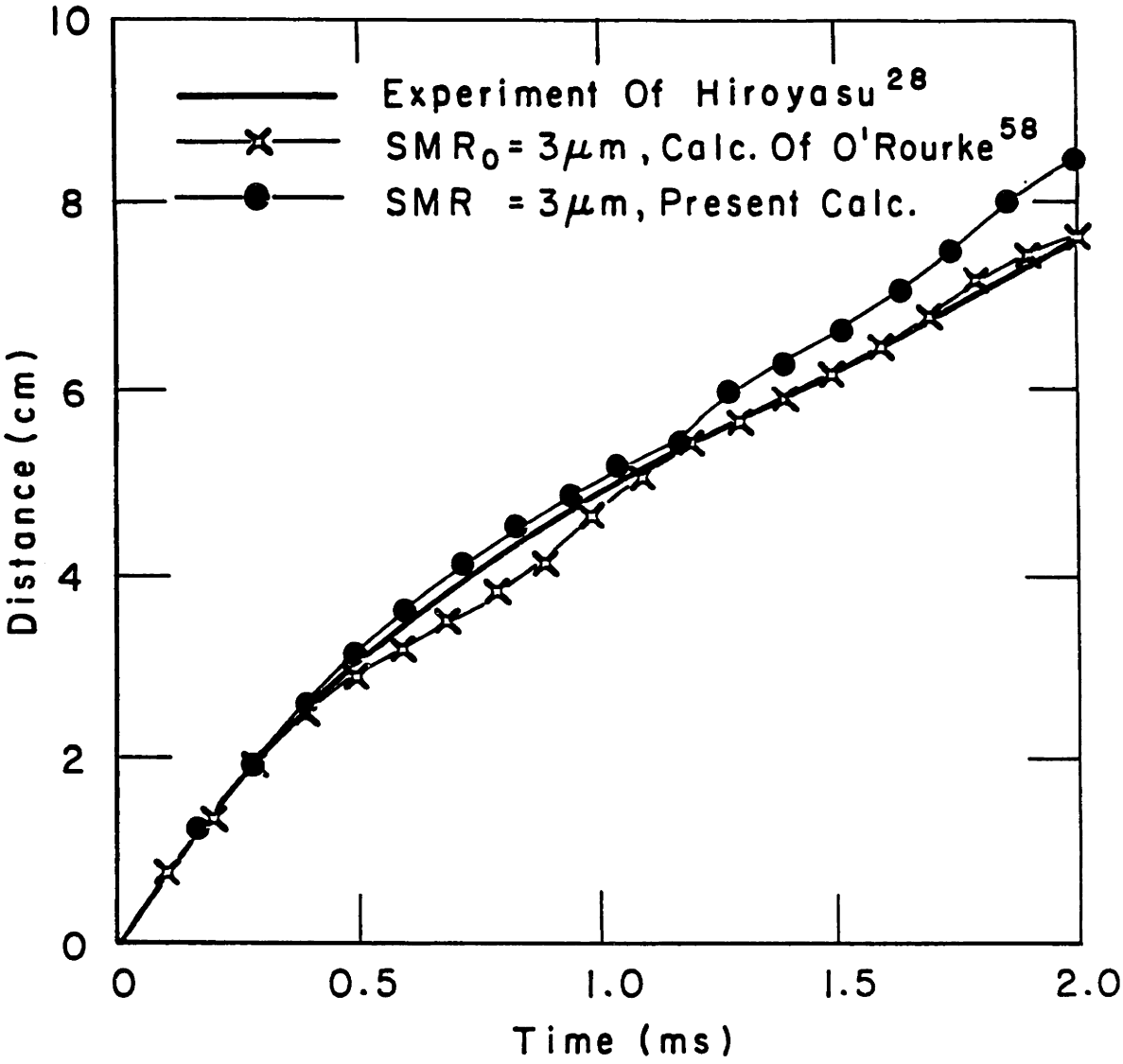

Figure 5.14 Spray Penetration Distance as a Function of Time for a Nonevaporating Spray

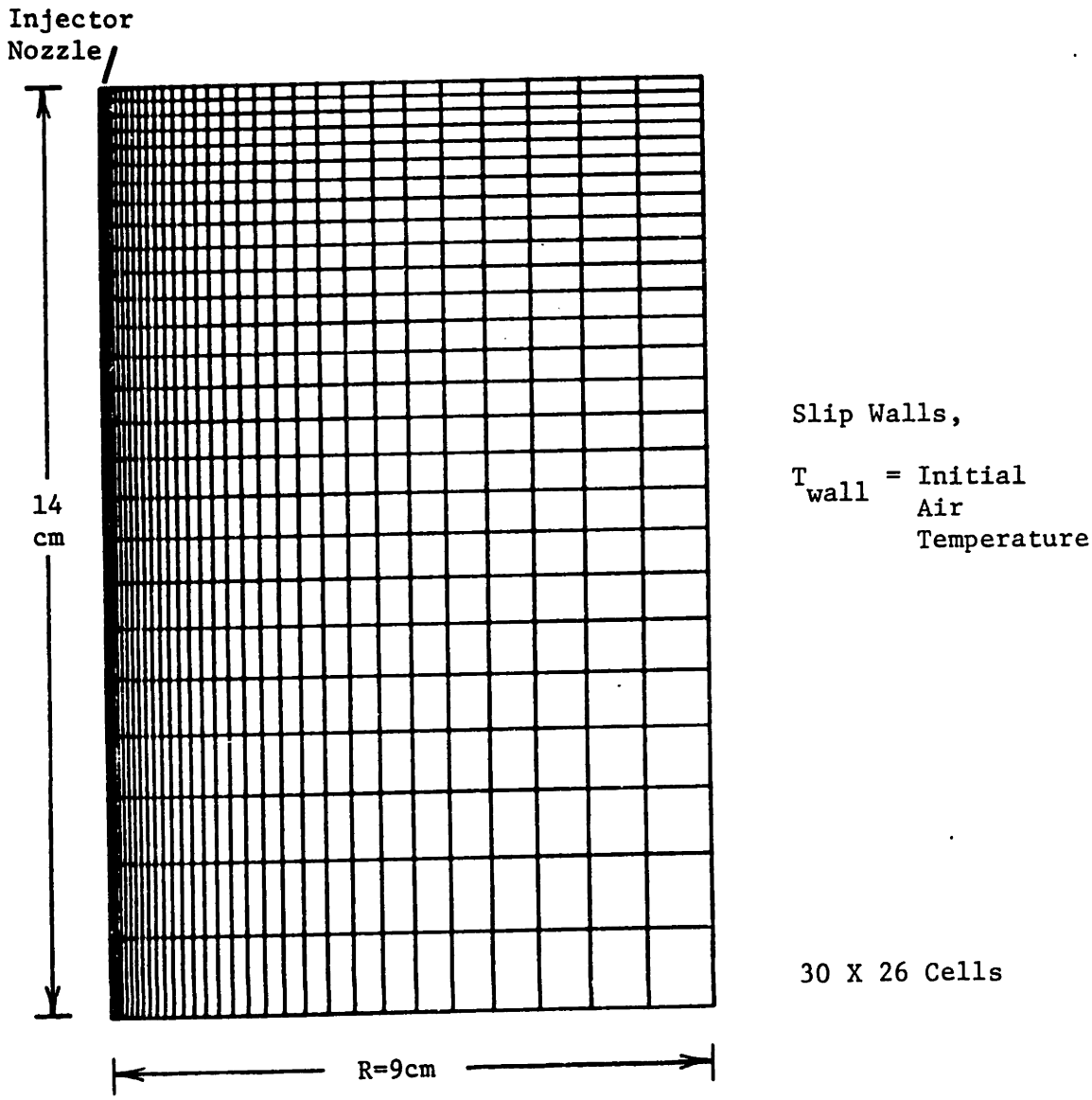

Figure 5.15 Grid for 2-D Autoignition Calculations

Figure 5.16 Format of Contour Plots

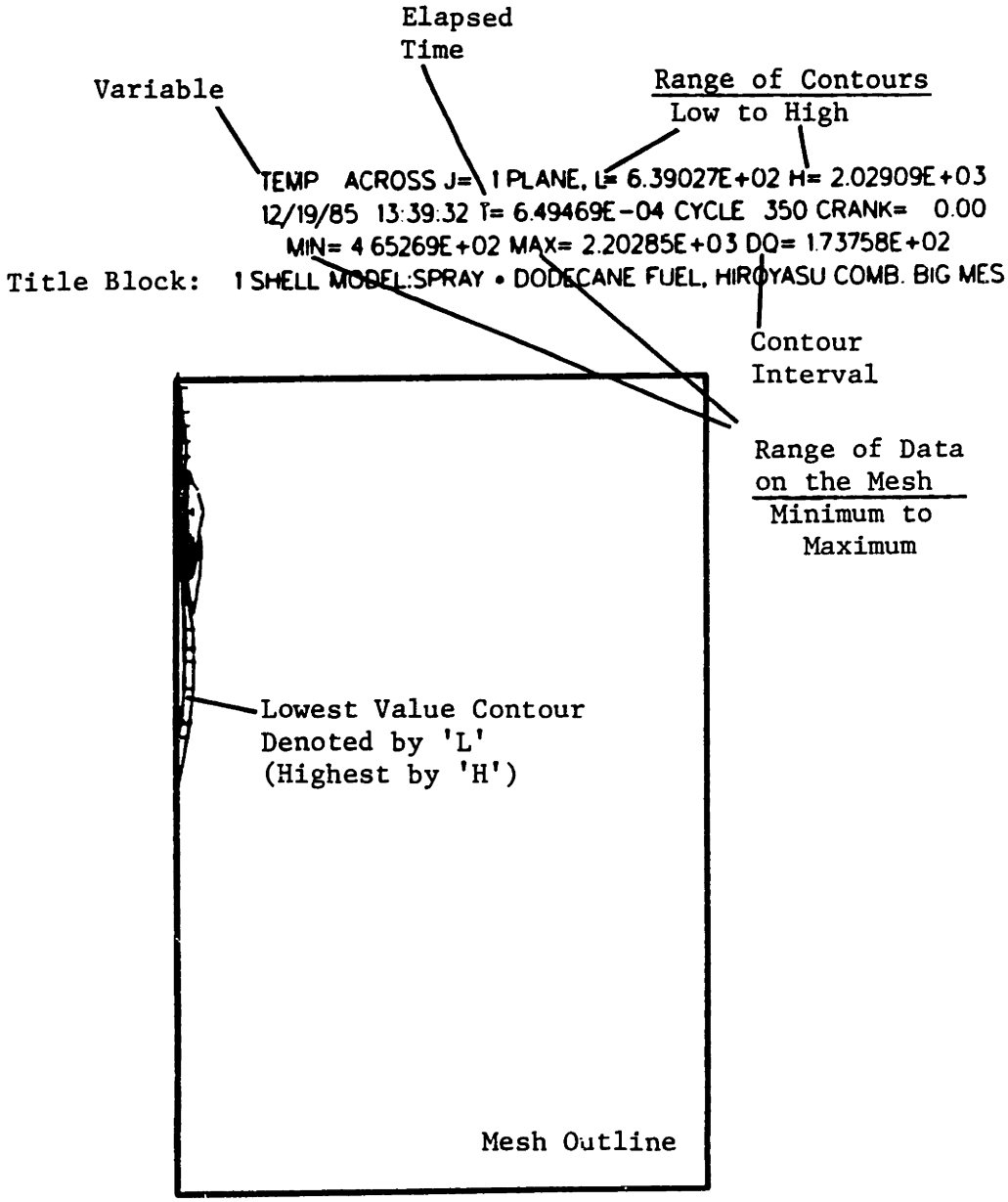

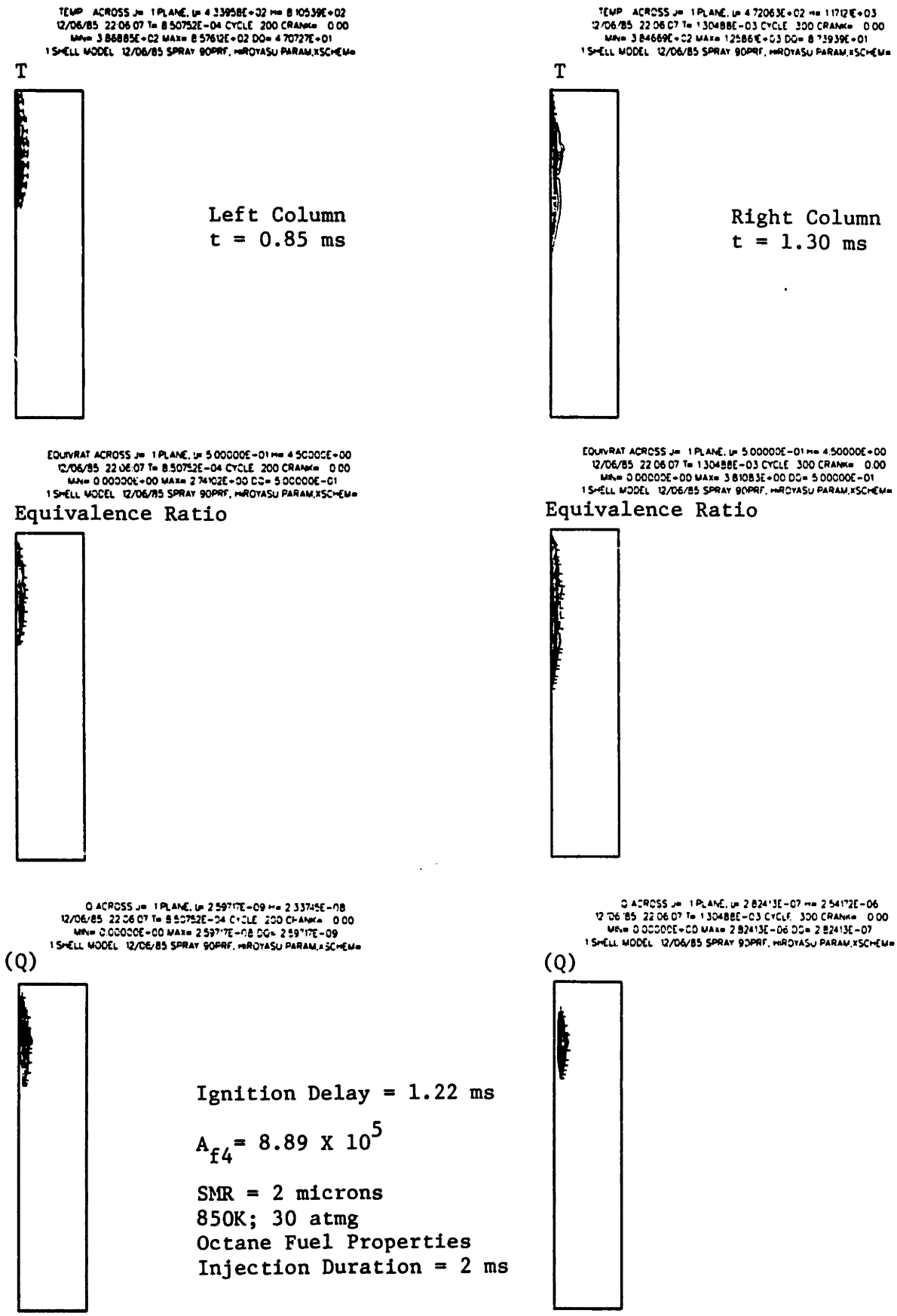

Figure 5.17 Autoignition of a Fuel Spray

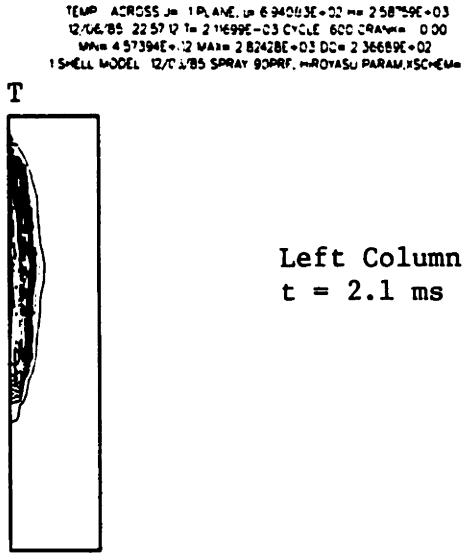

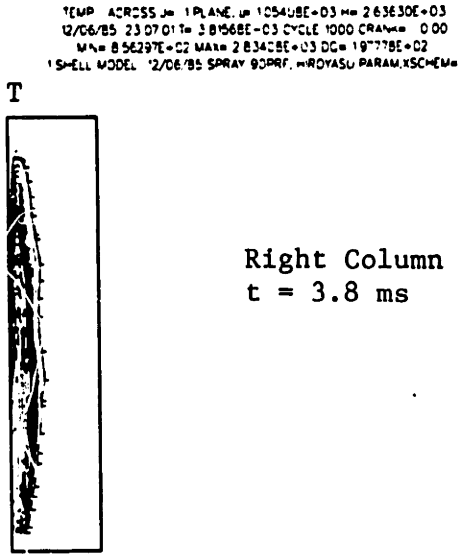

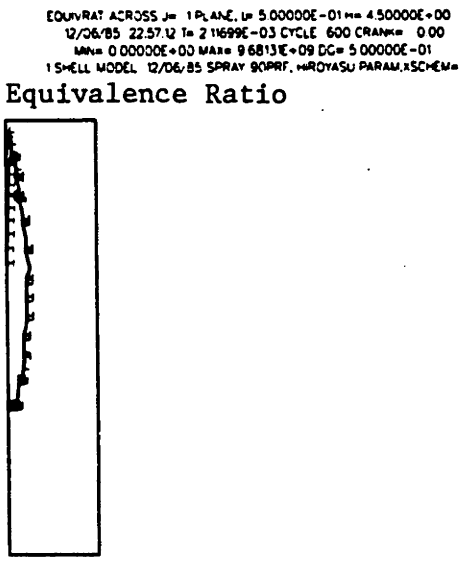

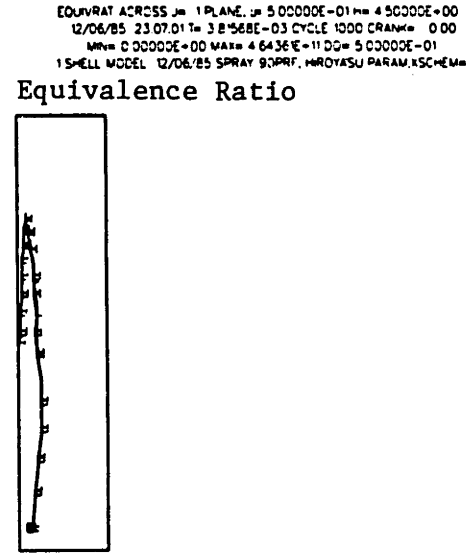

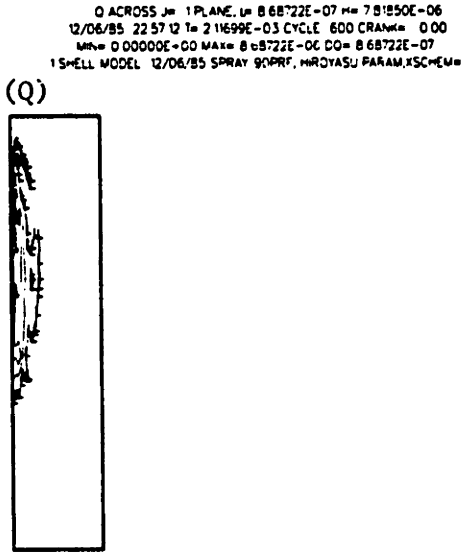

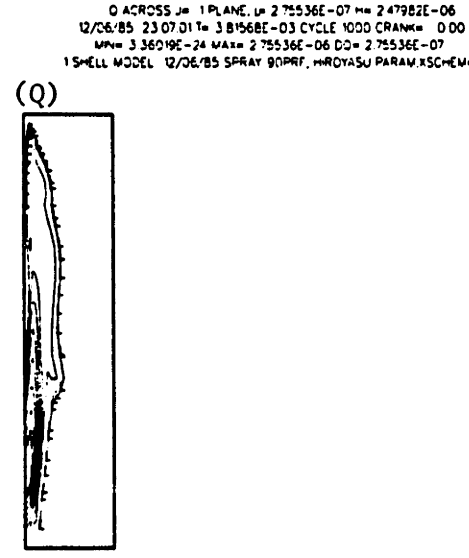

Figure 5.17 Autoignition of a Fuel Spray (Continued)

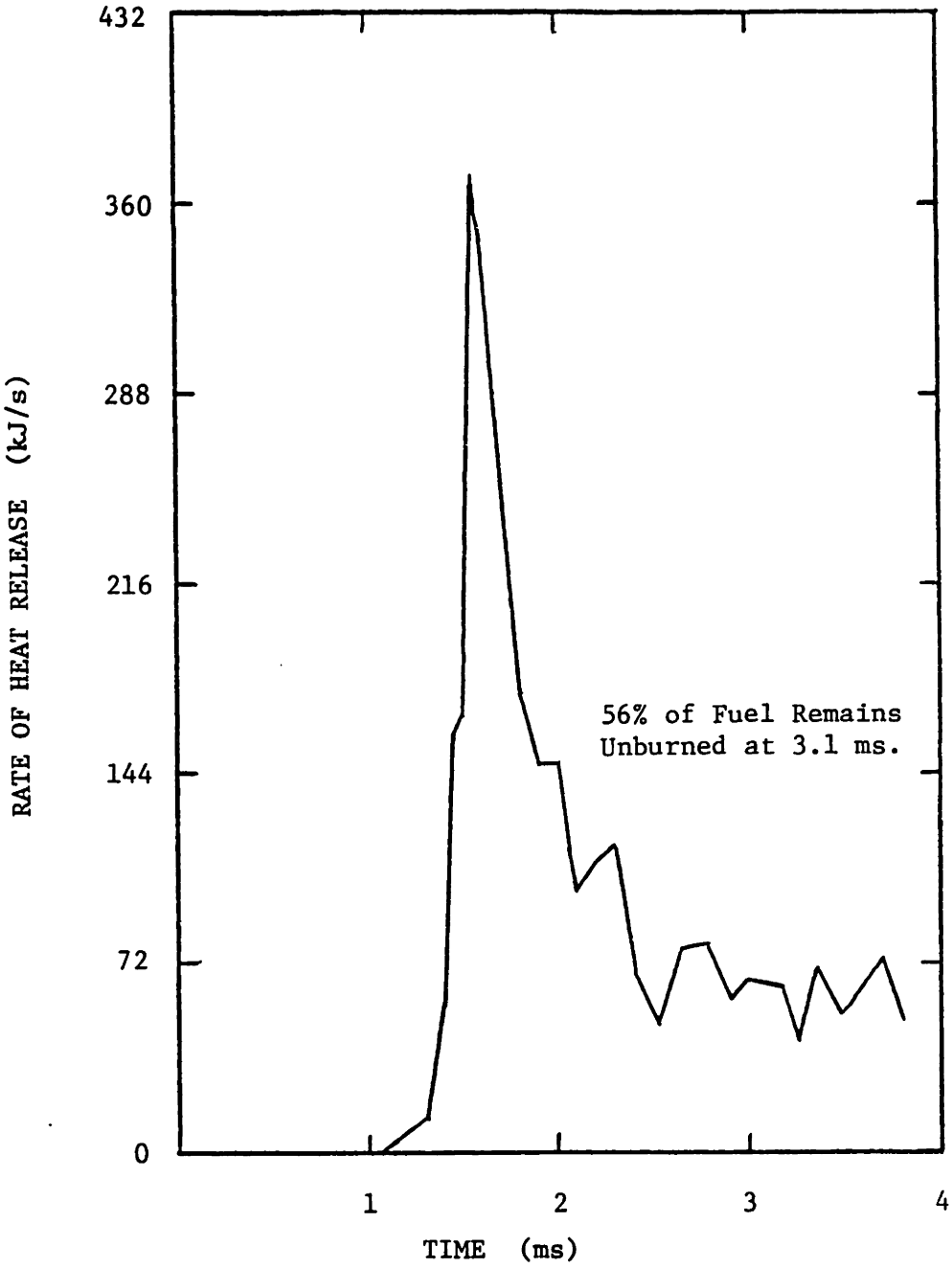

Ignition Delay = 1.22 ms

$A_{f4} = 8.89 \times 10^5$

SMR = 2 microns
850K; 30 atmg
Octane Fuel Properties
Injection Duration = 2 ms

Figure 5.18 Heat Release Profile of an Autoigniting Fuel Spray

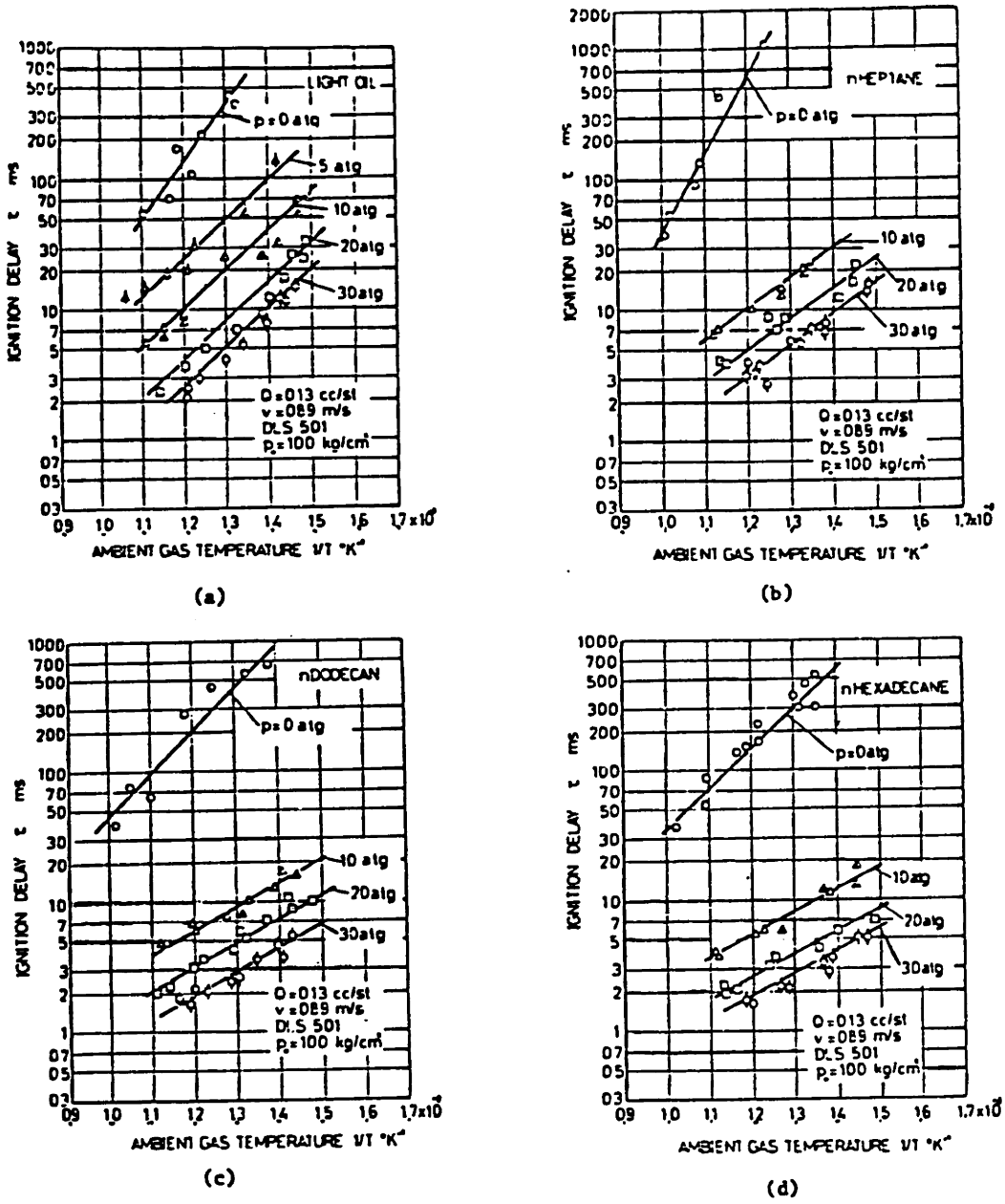

Figure 5.19 Autoignition Data of Hiroyasu[28] for Four Fuels
(a) Light Oil, (b) n-Heptane, (c) n-Dodecane, (d) n-Hexadecane

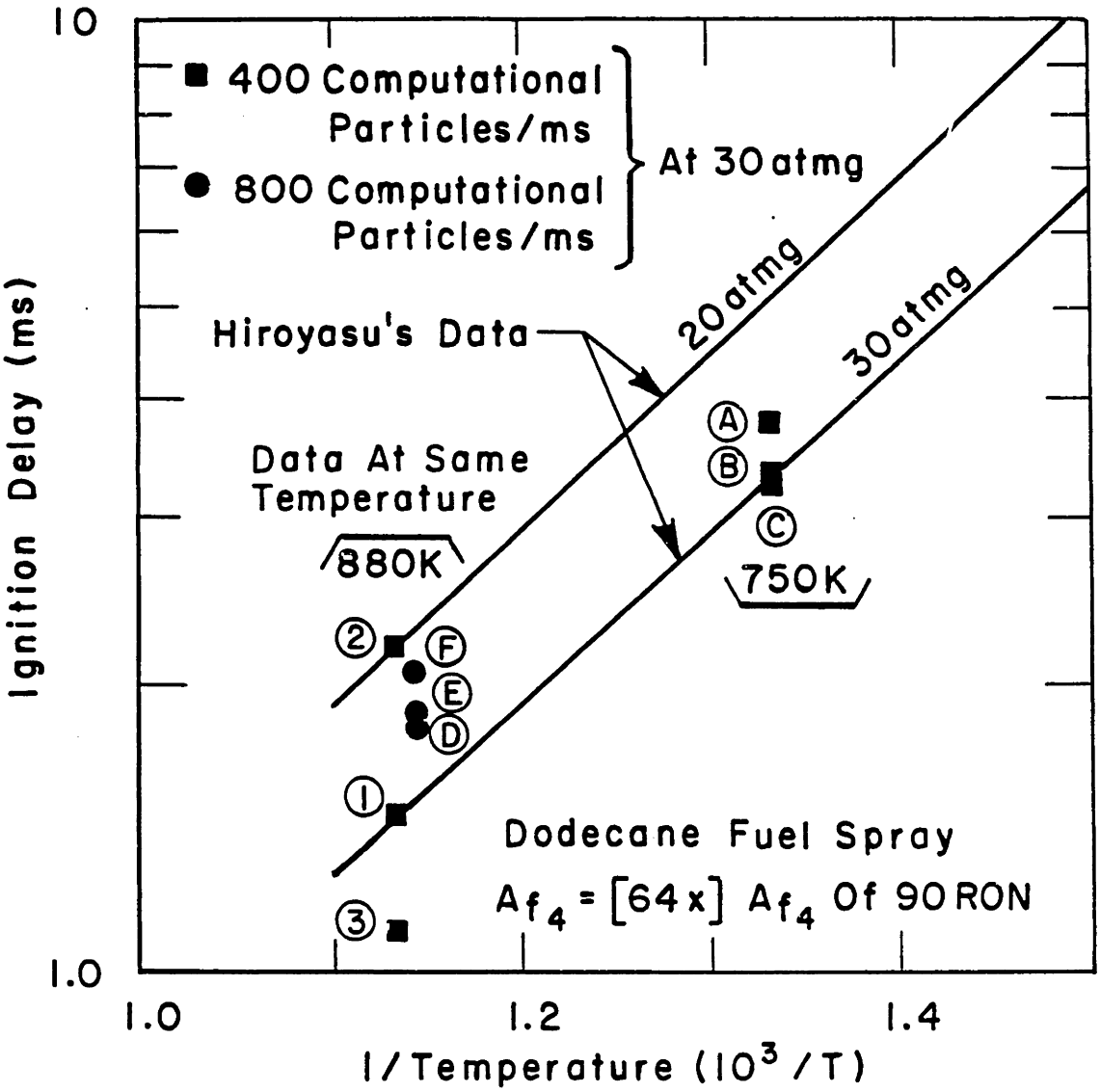

Figure 5.20 Effect of Changing the Random Number Sequence

Dodecane Fuel 750K; 30 atmg; $A_{f4} = 8.89 \times 10^5$

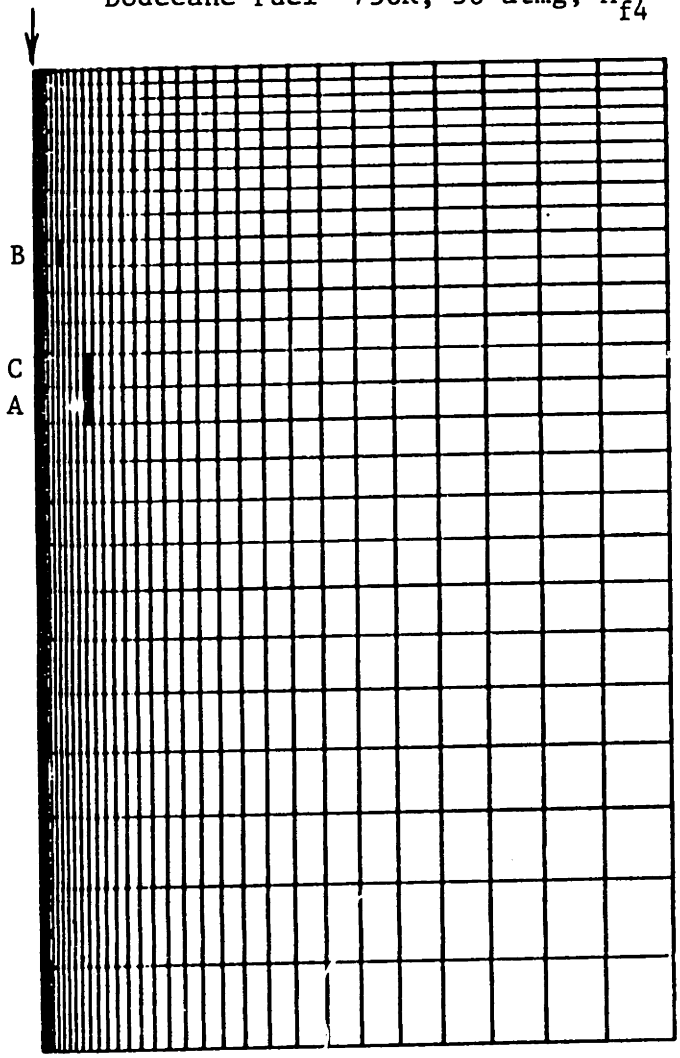

Site	(ms)	400 Particles/ms Injected
A	3.77	
B	3.28	$\bar{\tau}$ = 3.47 ms; $\sigma_\tau / \bar{\tau}$ = 7.5%
C	3.36	

Figure 5.21 Autoignition Sites for Different Random Number Sequences at 750K

Dodecane Fuel 880K; 30 atmg; $A_{f4} = 8.89 \times 10^5$

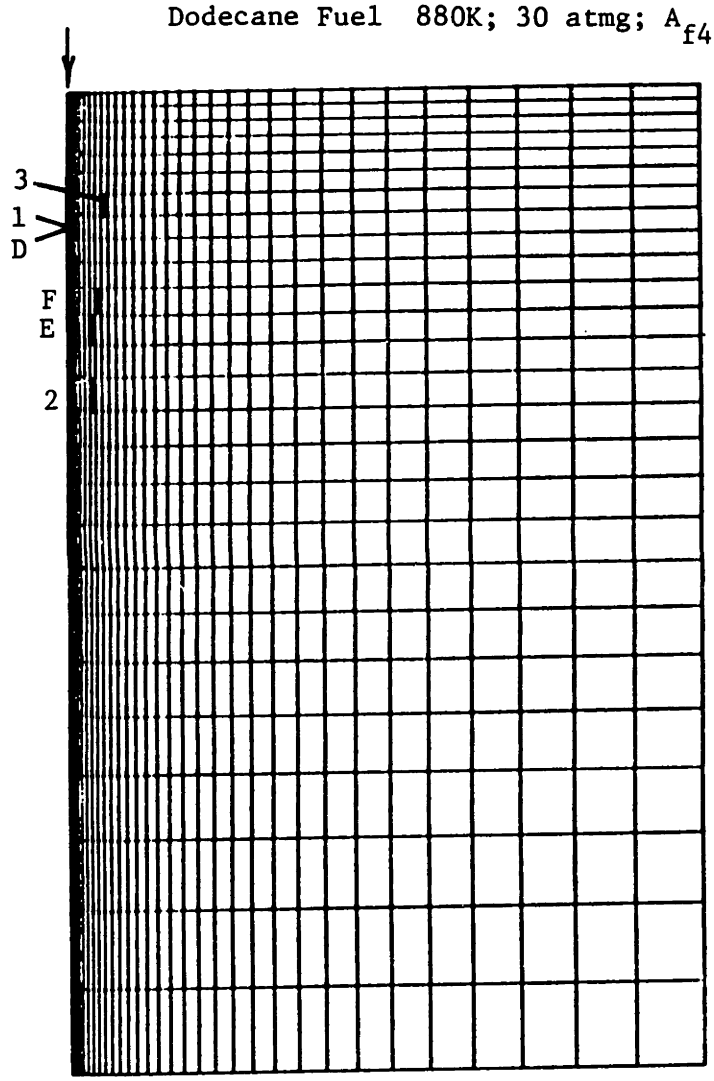

400 Particles/ms		800 Particles/ms	
Site	(ms)	Site	(ms)
1	1.47	D	1.79
2	2.21	E	1.85
3	1.11	F	2.06
$\bar{\tau} = 1.60$ ms		$\bar{\tau} = 1.90$ ms	
$\sigma_\tau/\bar{\tau} = 35\%$		$\sigma_\tau/\bar{\tau} = 7.5\%$	

Figure 5.22 Autoignition Sites for Different Random Number Sequences at 880K

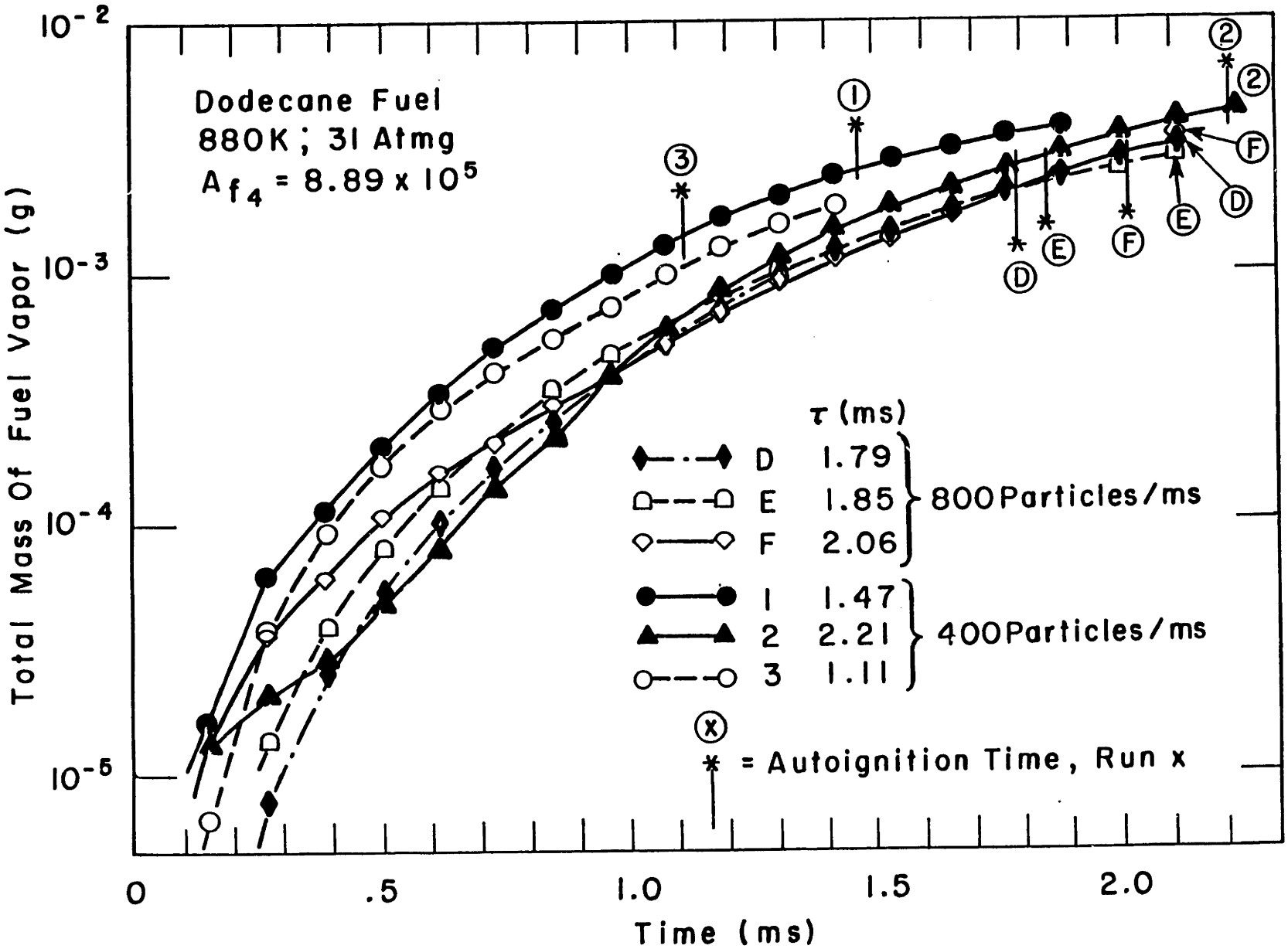

Figure 5.23 Time History of Total Fuel Vapor Mass for Different Random Number Sequences

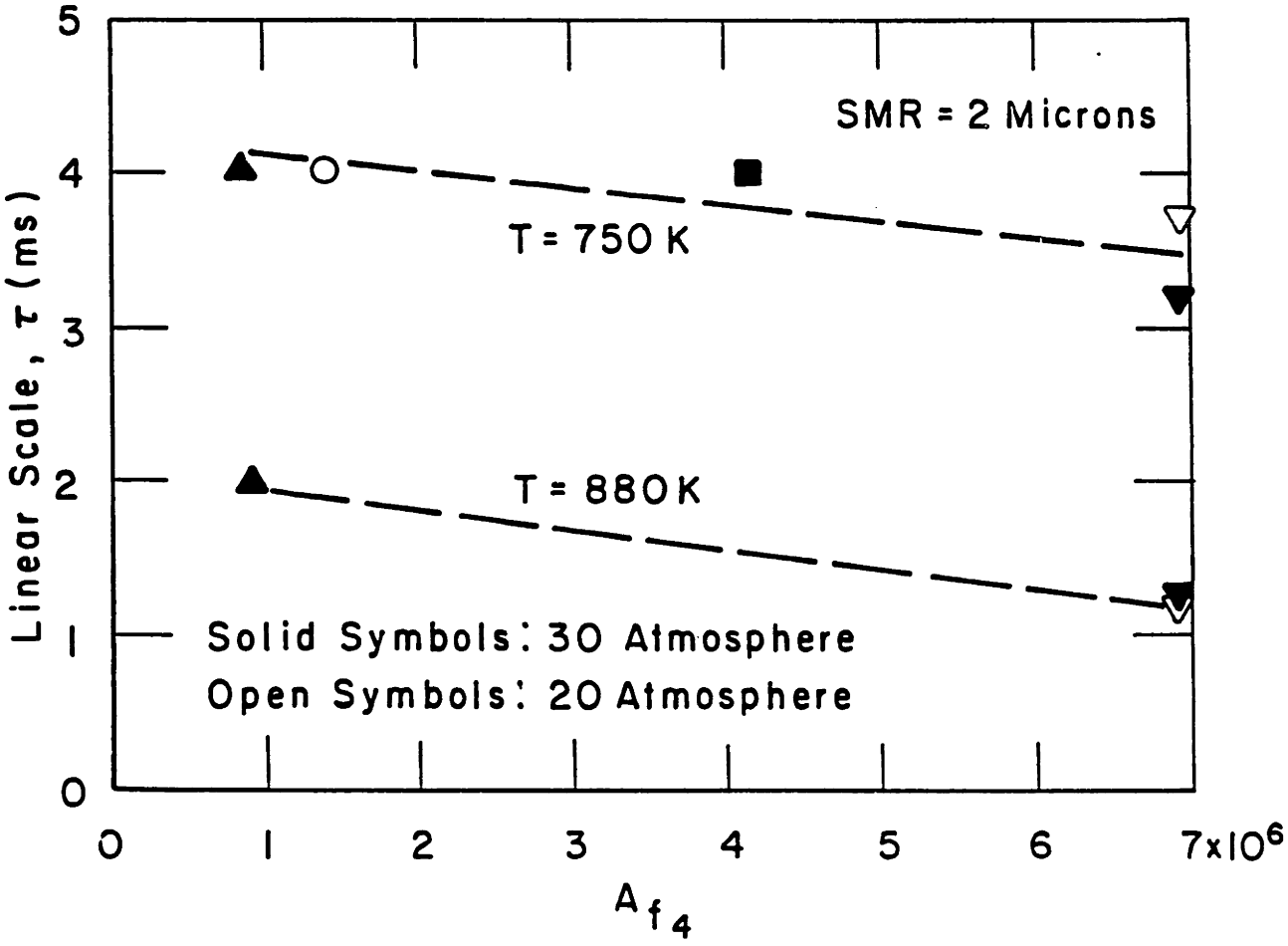

Figure 5.24(a) Effect of Parameter A_{f4} on the Ignition Delay of a Dodecane Spray
(See Fig. 5.24(b) for Symbols)

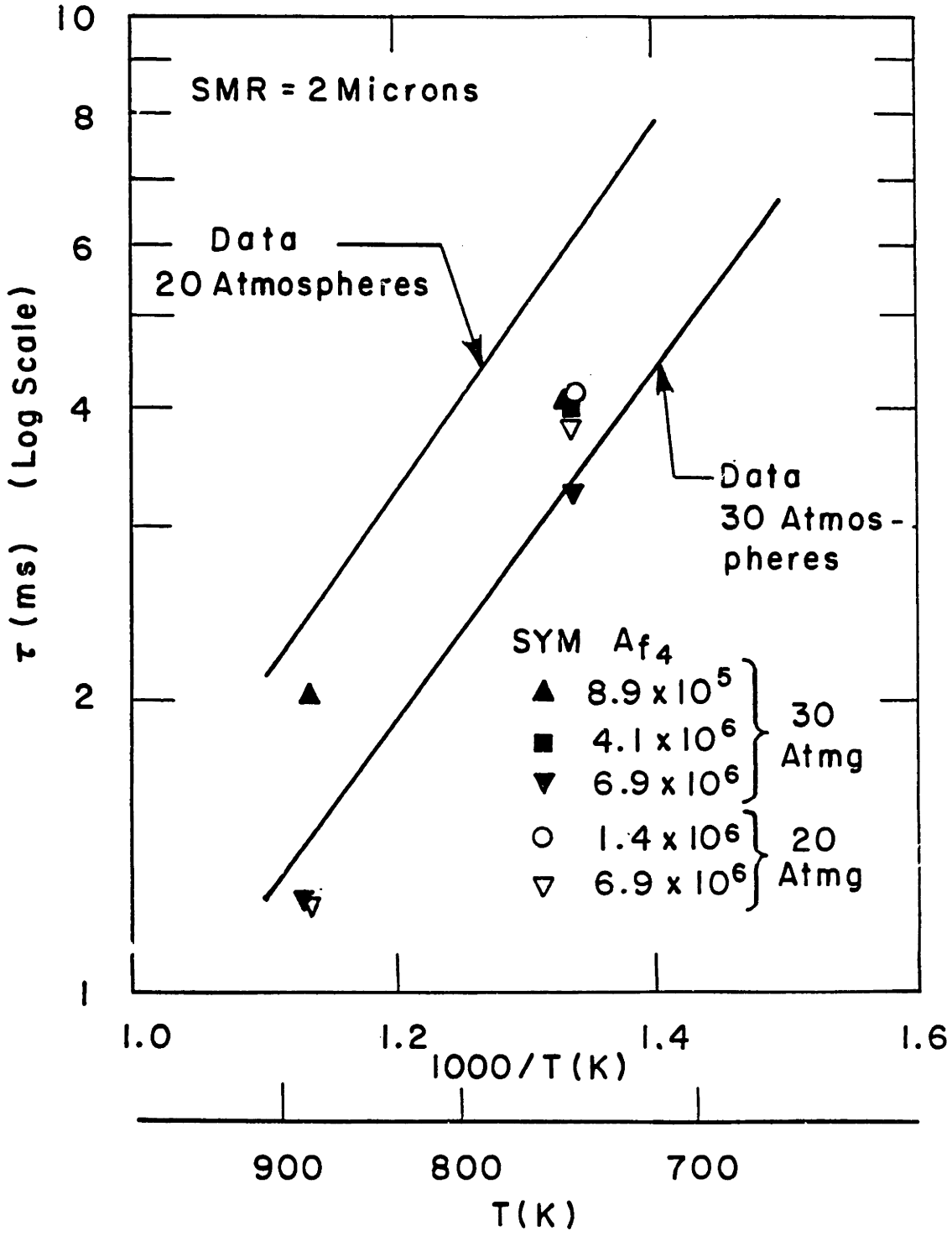

Figure 5.24(b) Effect of Parameter A_{f4} on the Ignition Delay of a Dodecane Spray: Comparison with Experimental Data

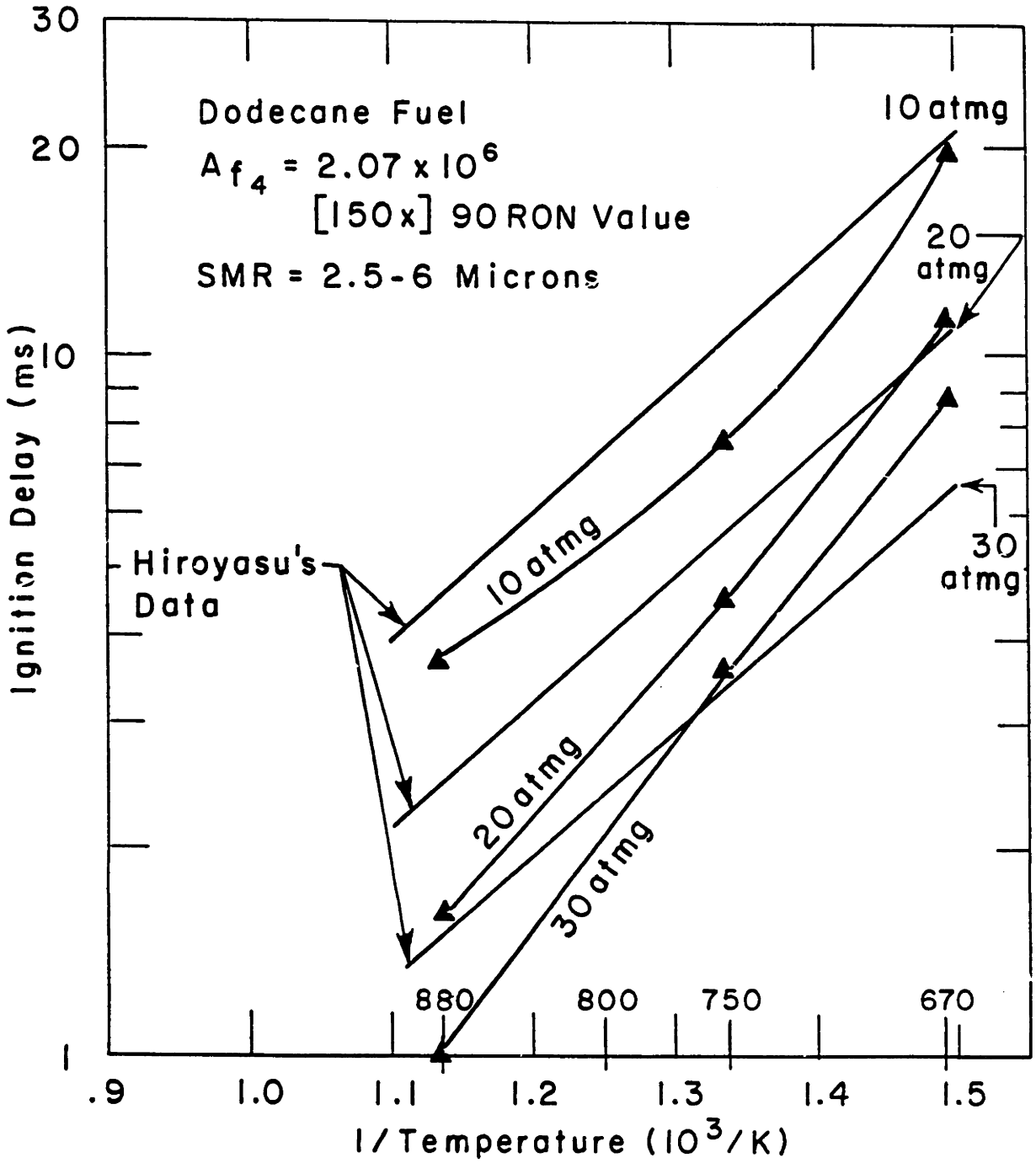

Figure 5.25 Calculated Dependence of Autoignition Delay on Temperature and Pressure

(a) t = 13.6 ms

(Q)

Q ACROSS J= 1 PLANE, I= 2.95370E-10 H= 2.65833E-0
12/18/85 03:47:41 T= 1.36164E-02 CYCLE 3500 CRANK= 0.(
MIN= 2.40326E-40 MAX= 2.95370E-09 DQ= 2.95370E-10
1 SHELL MODEL:SPRAY • DODECANE FUEL, HIROYASU COMB. BIG I

T

TEMP ACROSS J= 1 PLANE, I= 5.94353E+02 H= 6.67260E+(
12/18/85 03:47:41 T= 1.36164E-02 CYCLE 3500 CRANK= 0.(
MIN= 5.85240E+02 MAX= 6.76373E+02 DQ= 9.11331E+00
1 SHELL MODEL:SPRAY • DODECANE FUEL, HIROYASU COMB. BIG I

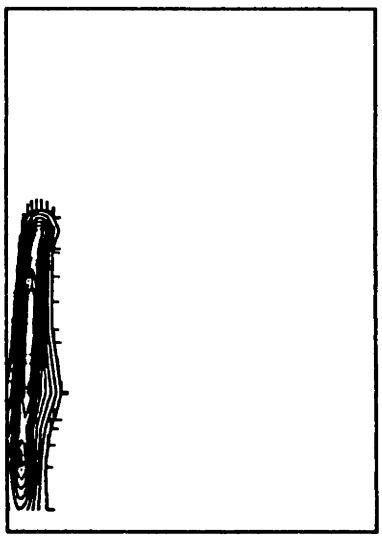

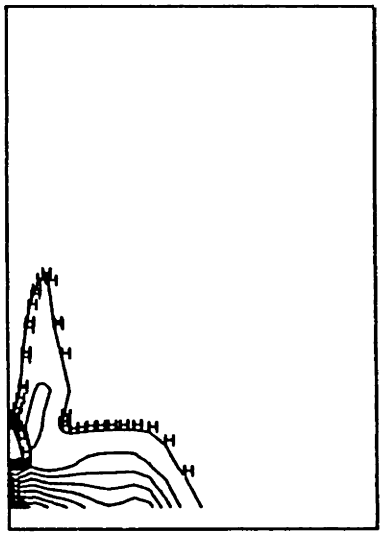

(b) t = 17.5 ms

(Q)

Q ACROSS J= 1 PLANE, I= 3.07725E-08 H= 2.78953E-(
12/18/85 04:45:37 T= 1.75200E-02 CYCLE 4500 CRANK= 0.
MIN= 0.00000E+00 MAX= 3.07725E-07 DQ= 3.07725E-08
1 SHELL MODEL:SPRAY • DODECANE FUEL, HIROYASU COMB. BIG

T

TEMP ACROSS J= 1 PLANE, I= 6.25259E+02 H= 8.12570E+(
12/18/85 04:45:37 T= 1.75200E-02 CYCLE 4500 CRANK= 0.
MIN= 6.01845E+02 MAX= 8.35984E+02 DQ= 2.34139E+01
1 SHELL MODEL:SPRAY • DODECANE FUEL, HIROYASU COMB. BIG

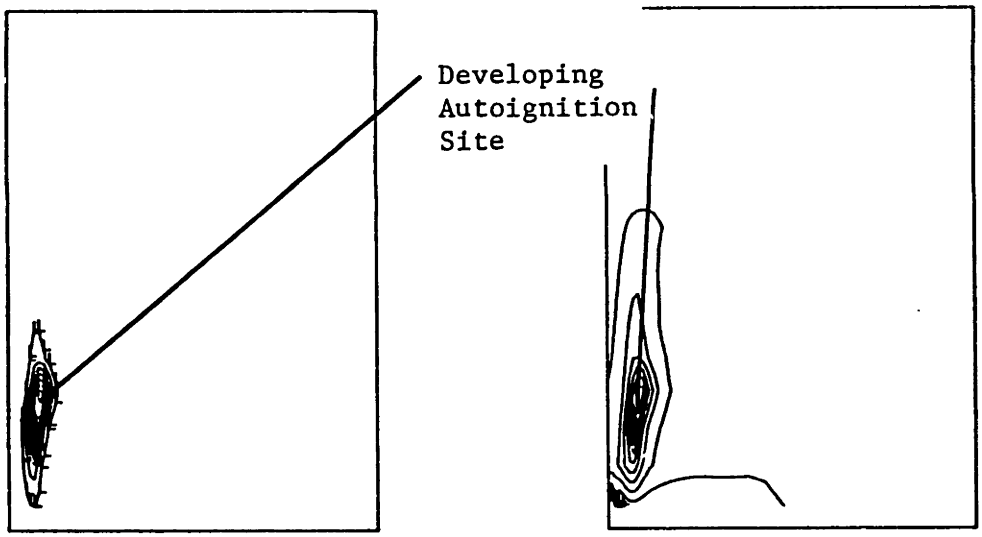

$A_{f4} = 2.07 \times 10^{6}$

Figure 5.26 Autoignition Calculation for Dodecane Spray
T = 670K; p = 10 atmg; τ = 19.6 ms

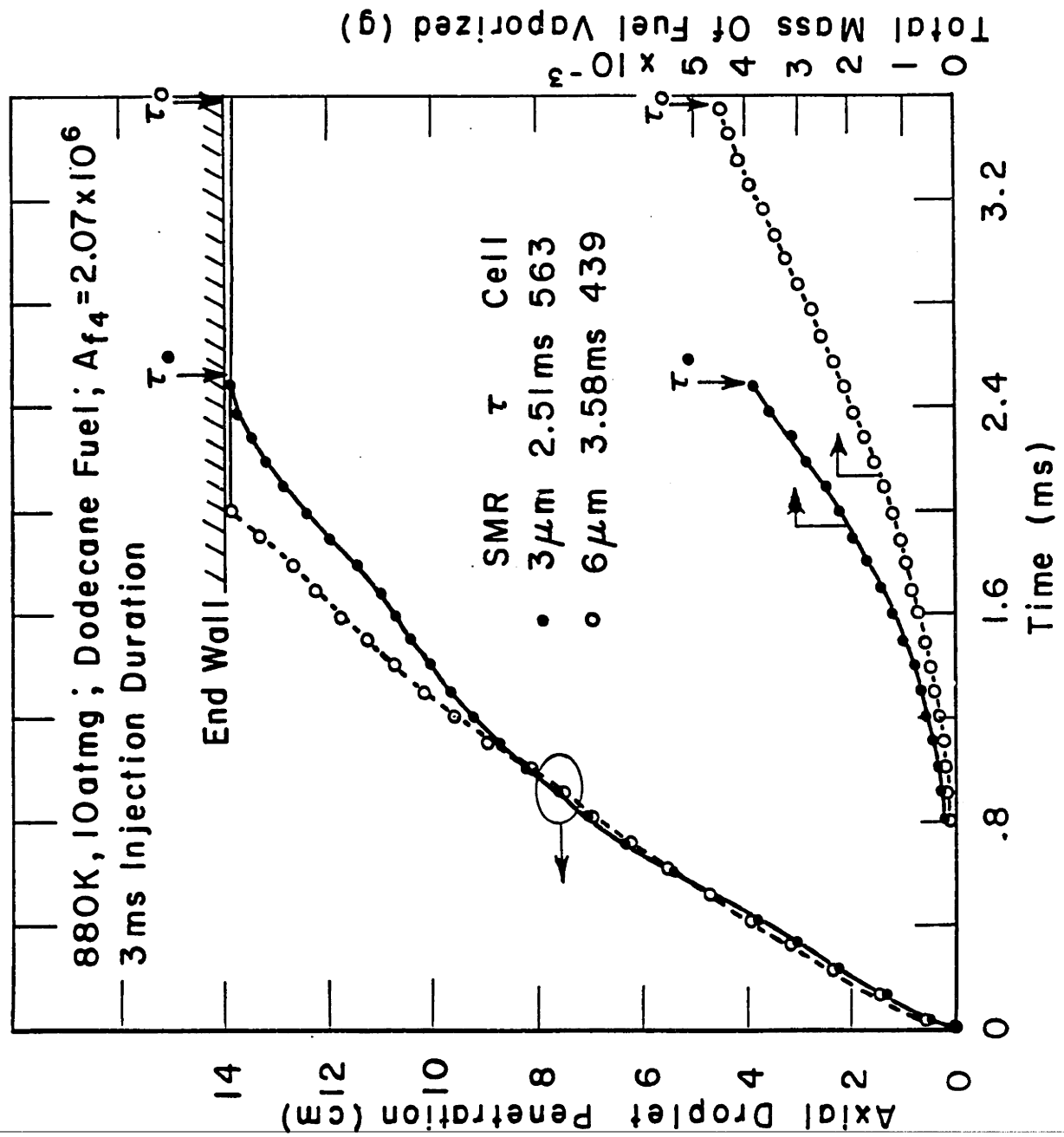

Figure 5.27 Effect of Halving the Sauter Mean Radius

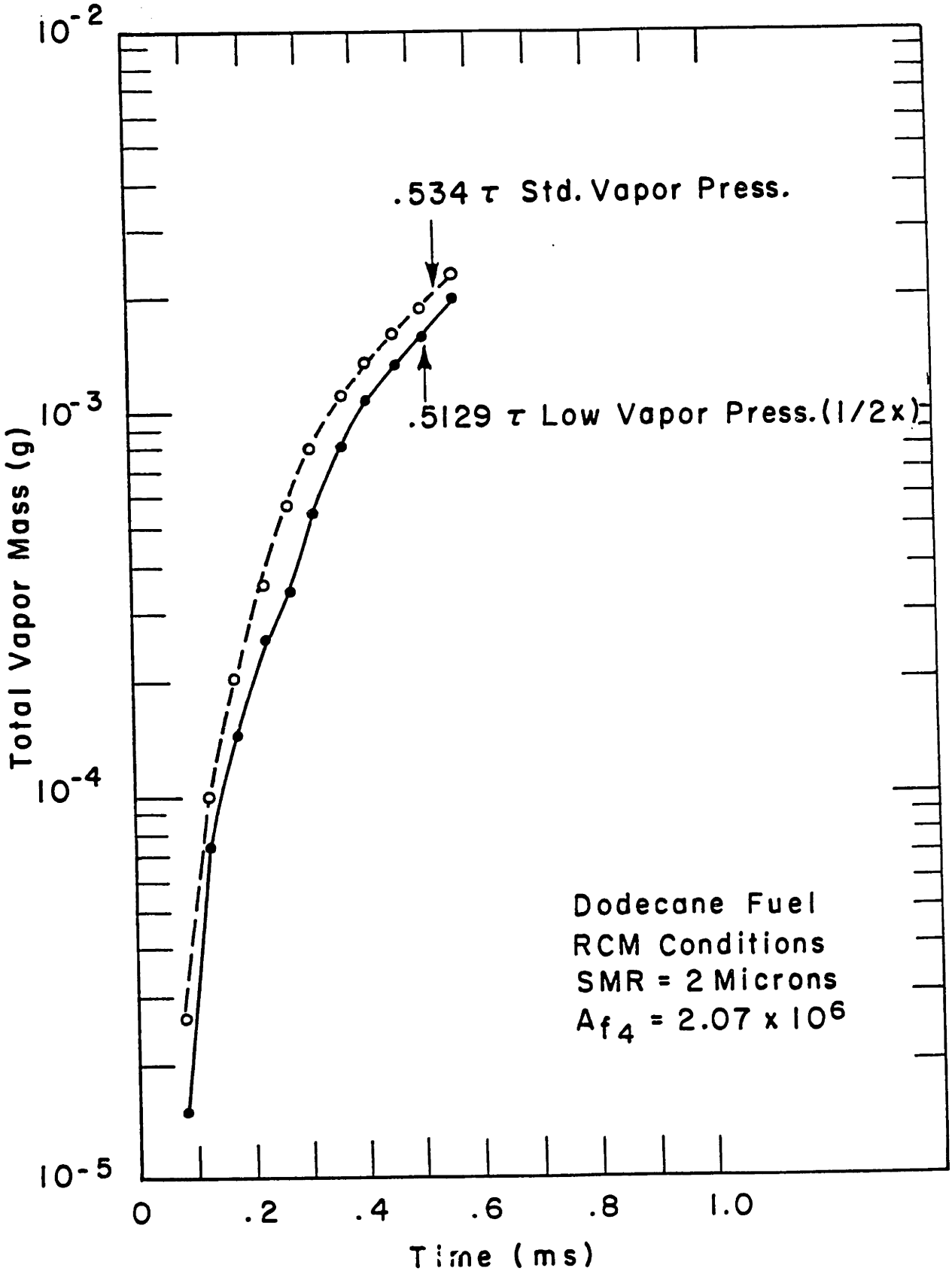

Figure 5.28 Effect of Decreased Fuel Vapor Pressure on τ and Vapor Mass

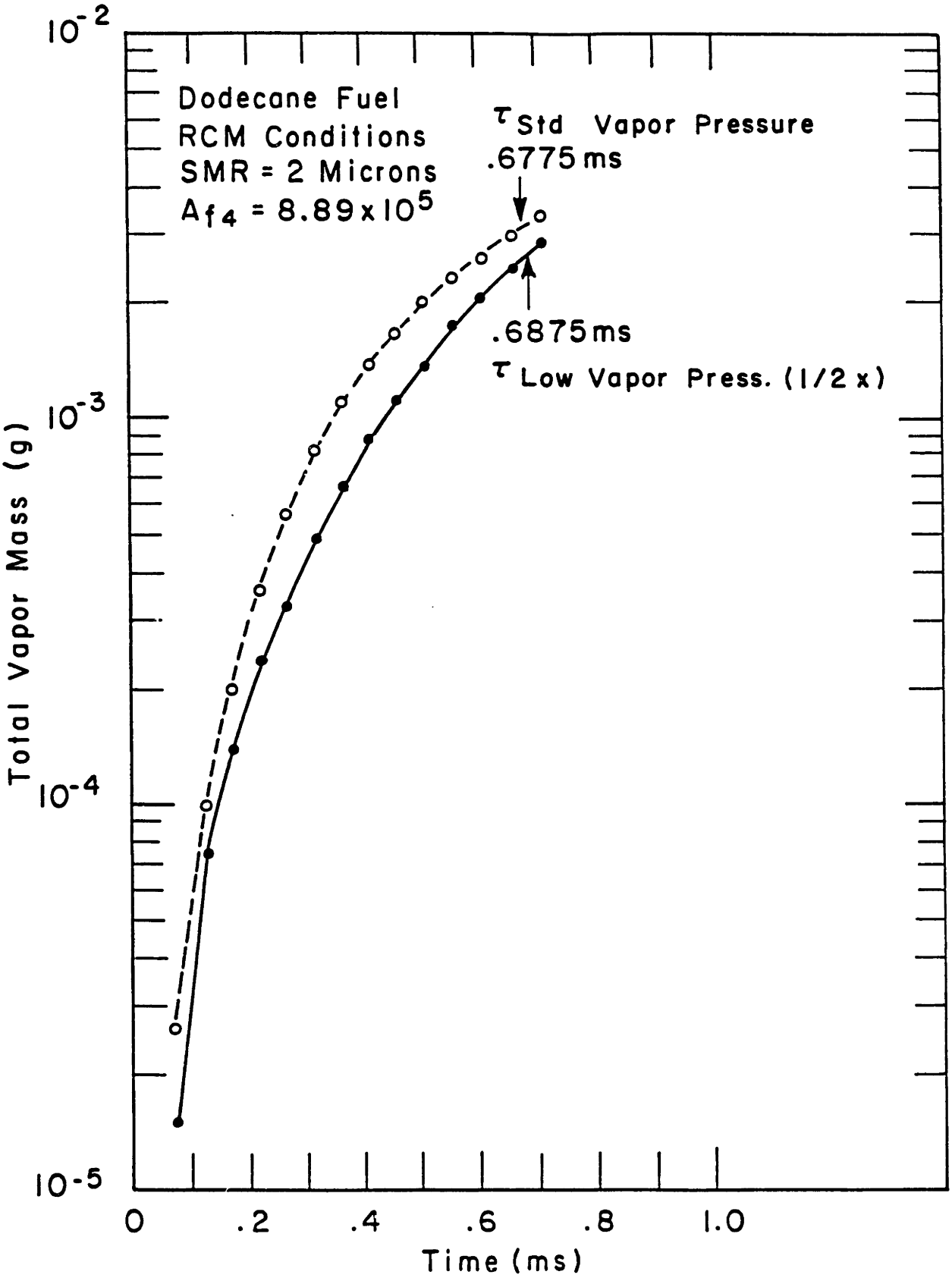

Figure 5.29 Effect of Decreased Fuel Vapor Pressure on τ and Vapor Mass

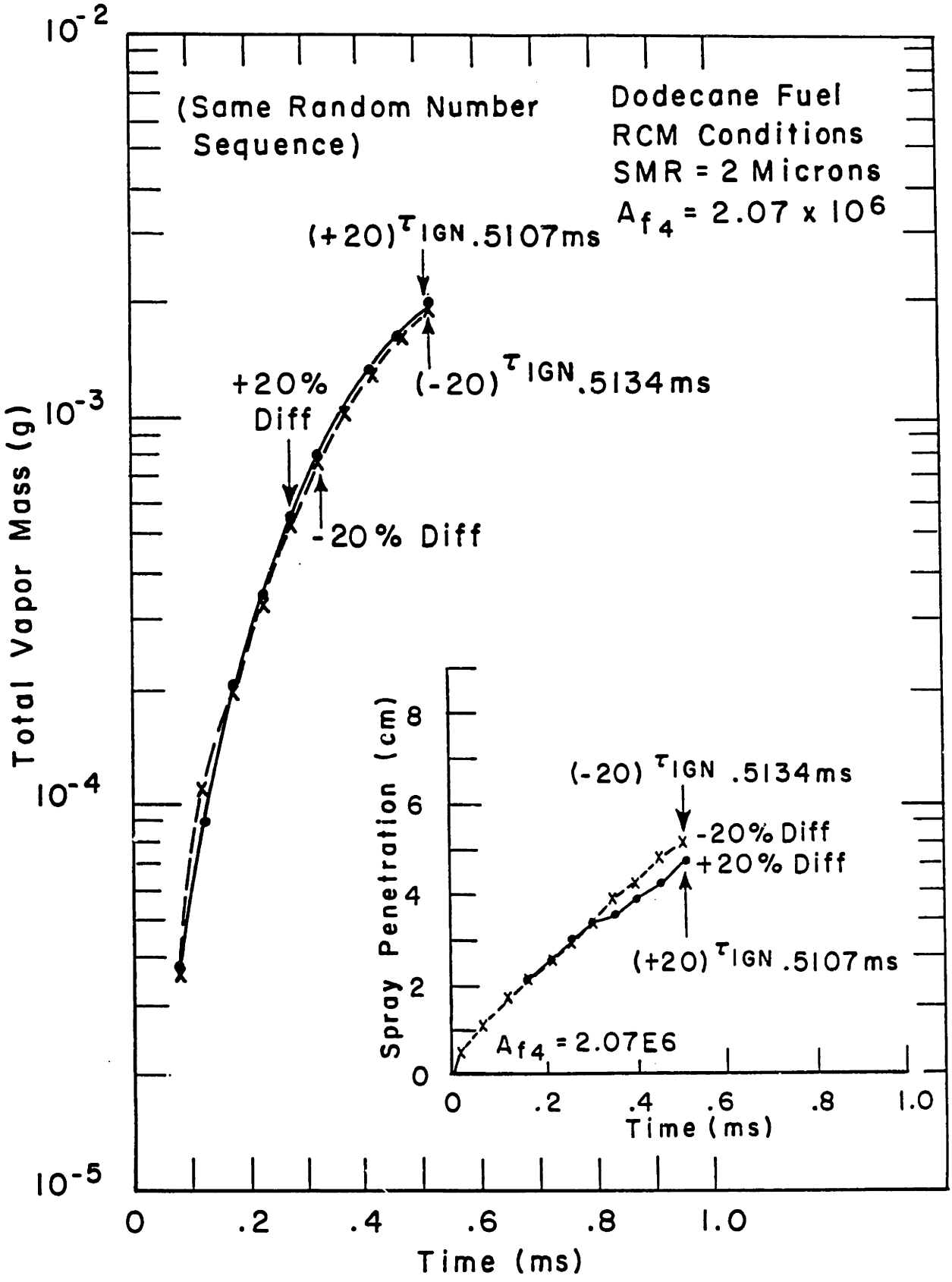

Figure 5.30 Effect of ±20% Variation in Diffusivity on τ, Vapor Mass, and Droplet Penetration

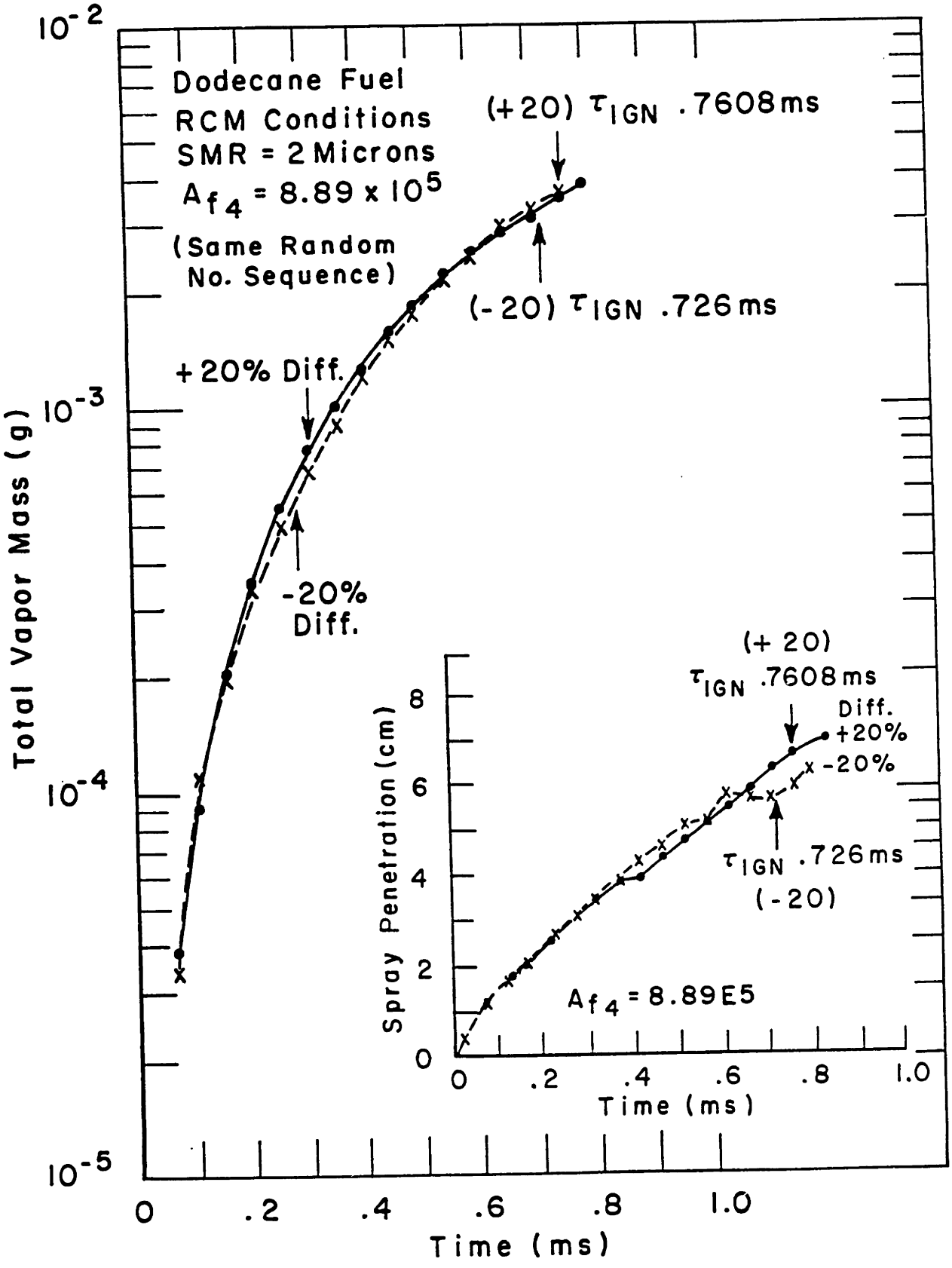

Figure 5.31 Effect of ±20% Variation in Diffusivity on τ, Vapor Mass, and Droplet Penetration

Rapid Compression Machine Conditions
880K; 38 atm abs.

$A_{f4} = 2.21 \times 10^5$ $\tau = 1.12$ ms

T (Q) Equivalence Ratio ϕ

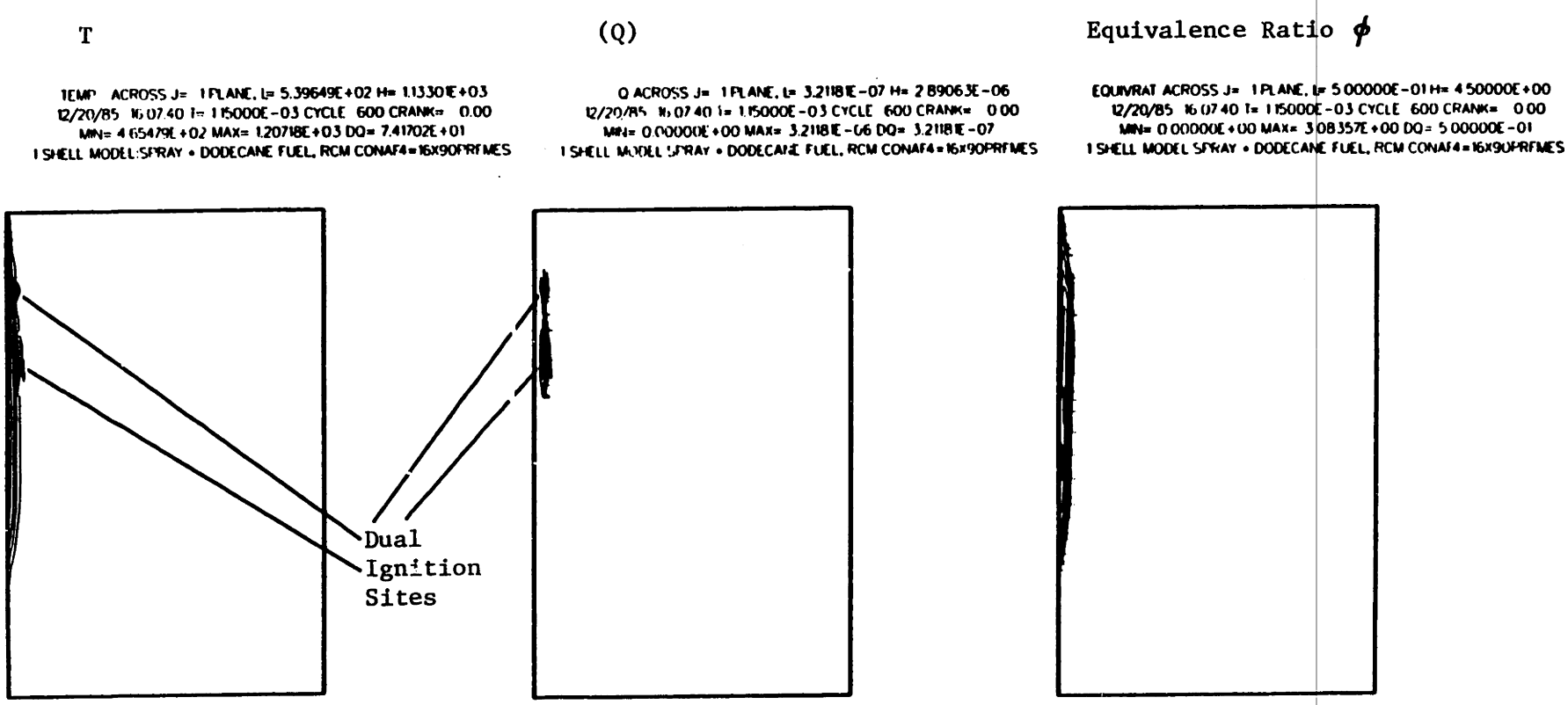

Figure 5.32 Apparent Dual Ignition Sites

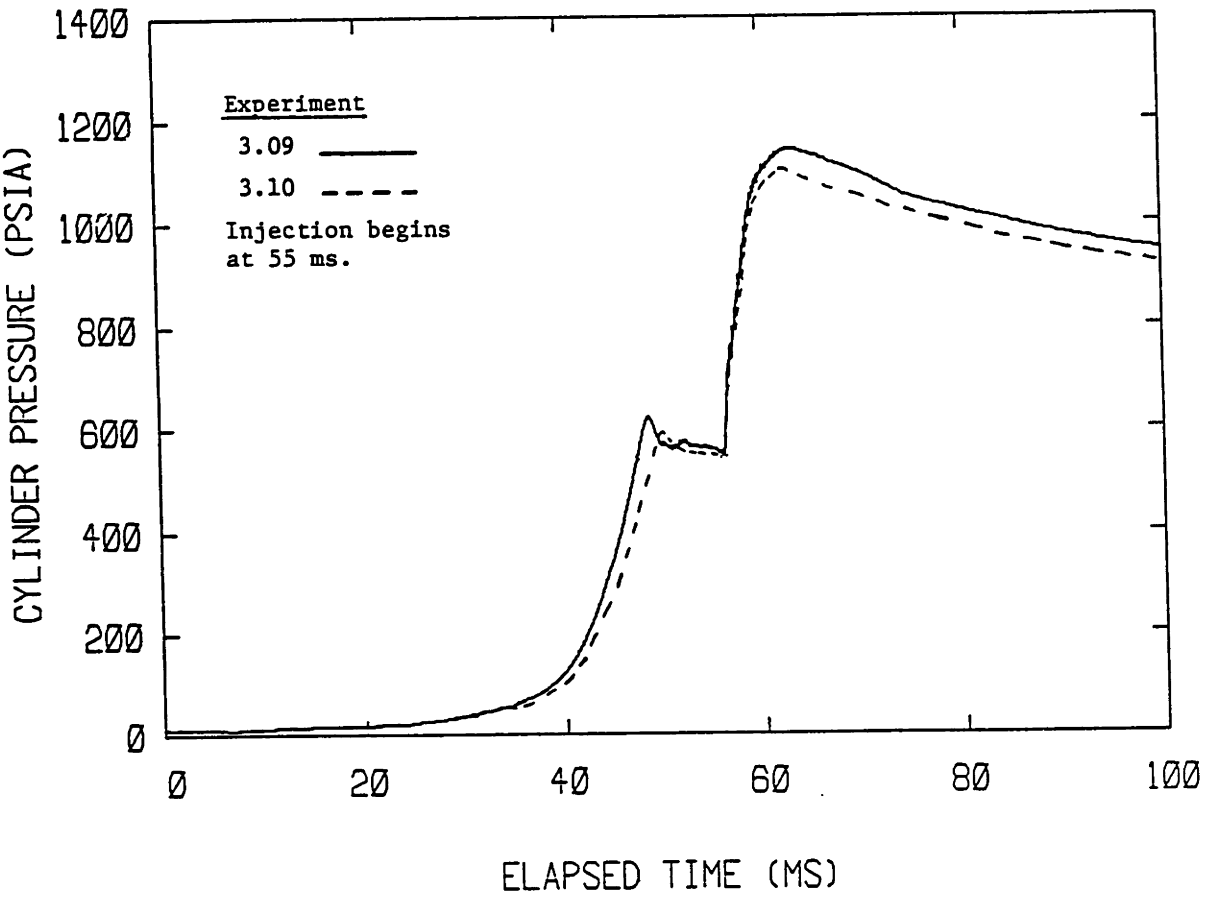

Figure 5.33 Pressure Traces for RCM Experiments 3.09 and 3.10

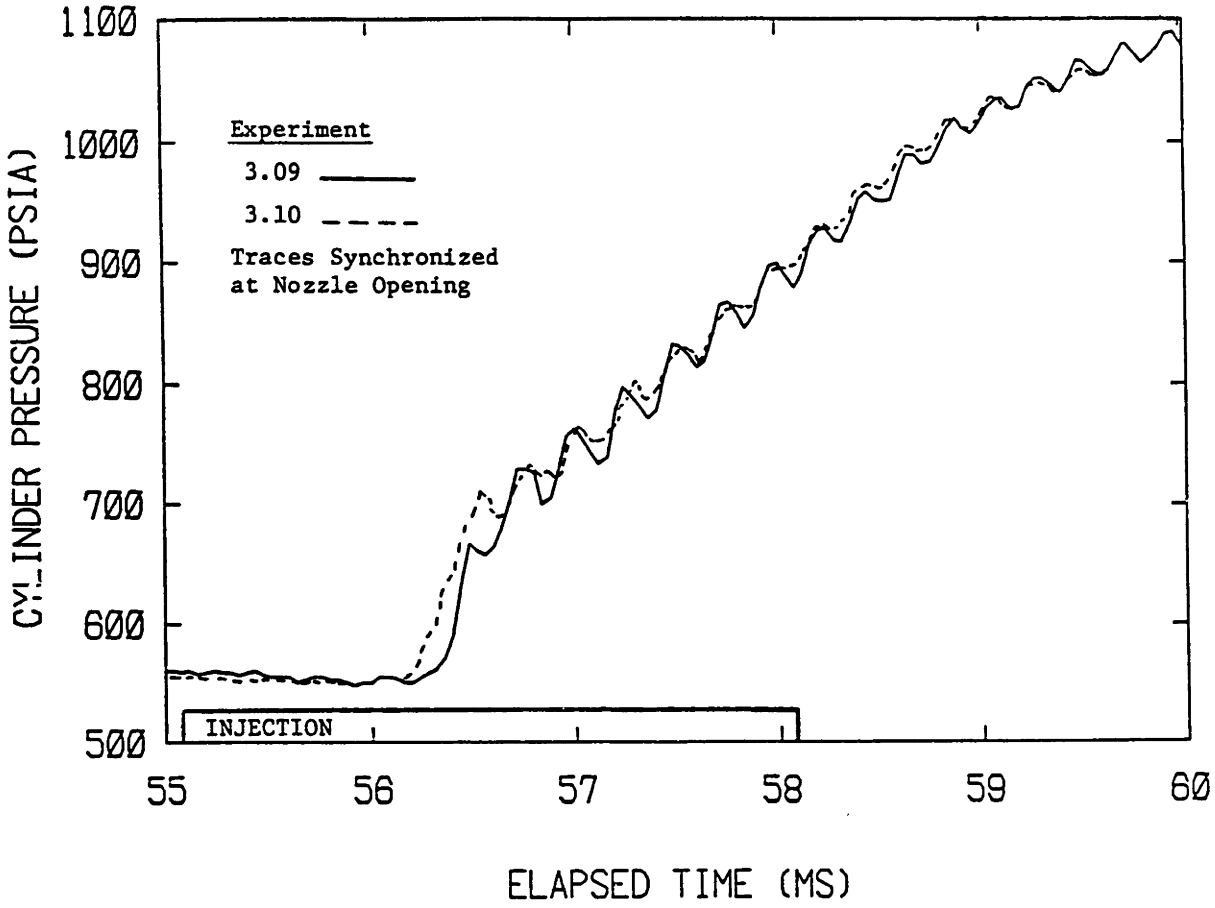

Figure 5.34 Pressure Rise at Ignition for RCM Experiments 3.09 and 3.10

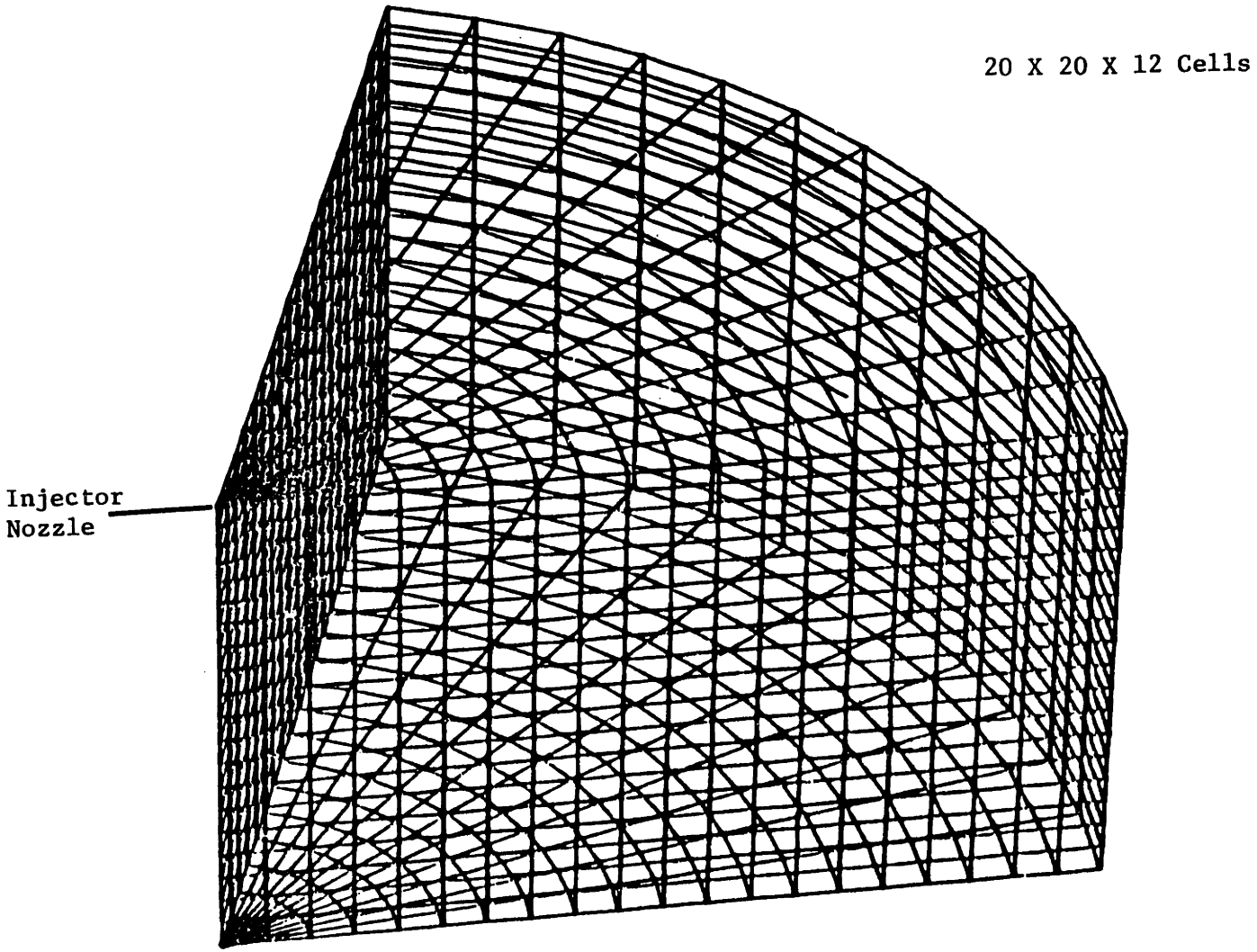

Figure 5.35 Grid for 3-D Computations

KIVA 12-17-85 17:57:13 SECT 59. 121685 DODECANE ANUD=6.9 TETRADEC AO=.75 BD=1. NON-WHEELFLOW SWIRL
T= 0.000000E+00 CYCLE 0 CRANK= 0.00 DEG ATDC

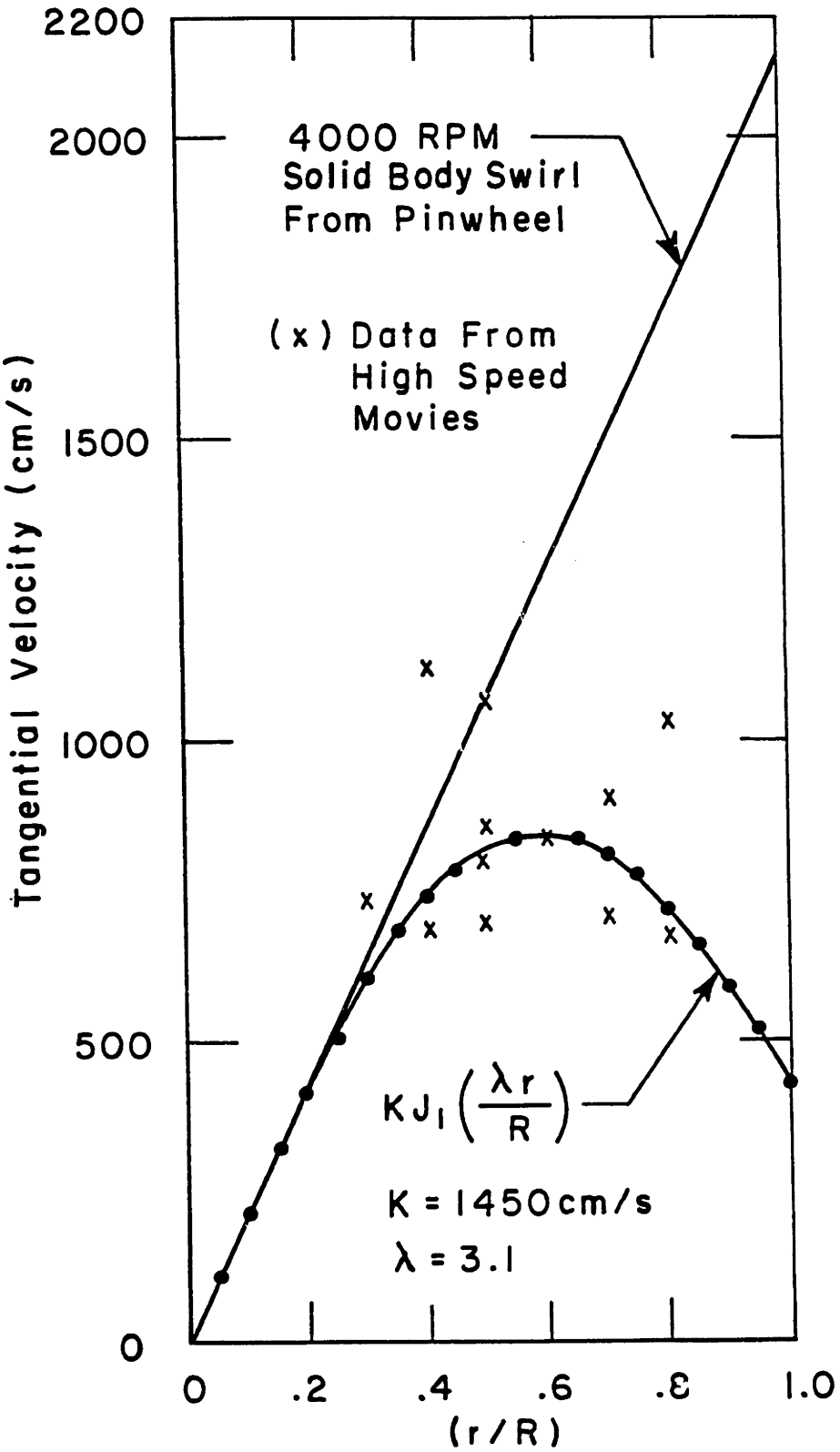

Figure 5.36 Swirl Profiles for the Rapid Compression Machine (Data at the same radius correspond to different azimuthal locations)

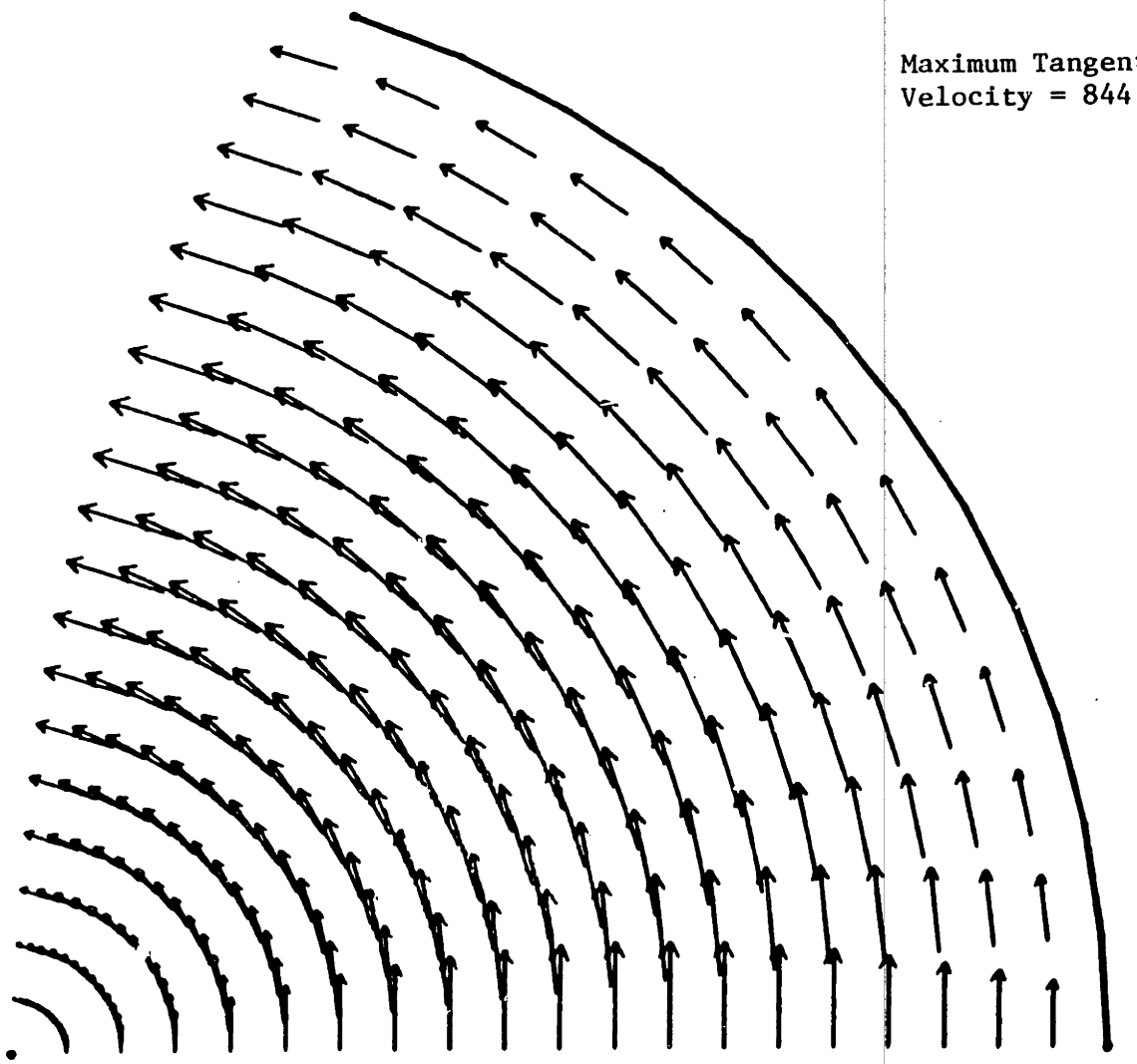

Figure 5.37 Initial Swirl for 3-D Calculations

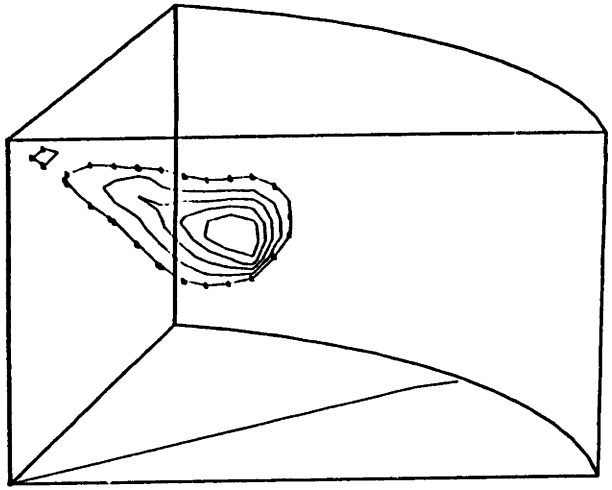

Equivalence Ratio

t = 0.3 ms

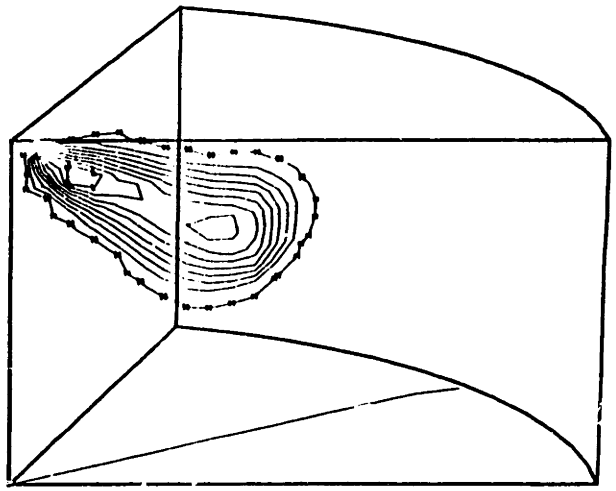

T

Ignition Delay = 0.44 ms

$A_{f4} = 2.07 \times 10^6$

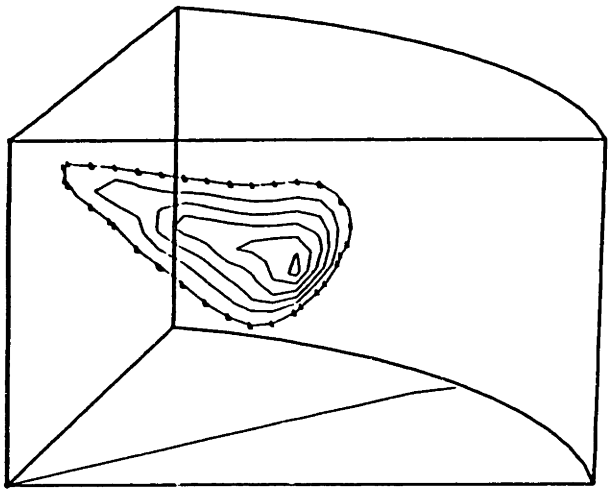

Equivalence Ratio

t = 0.54 ms

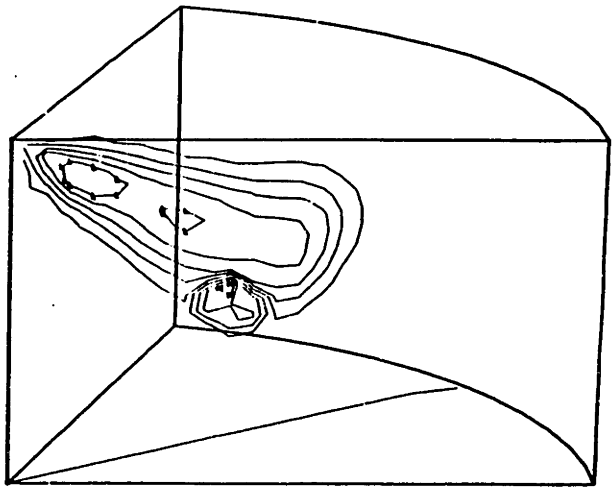

T

Figure 5.38 3-D Computation: Run A

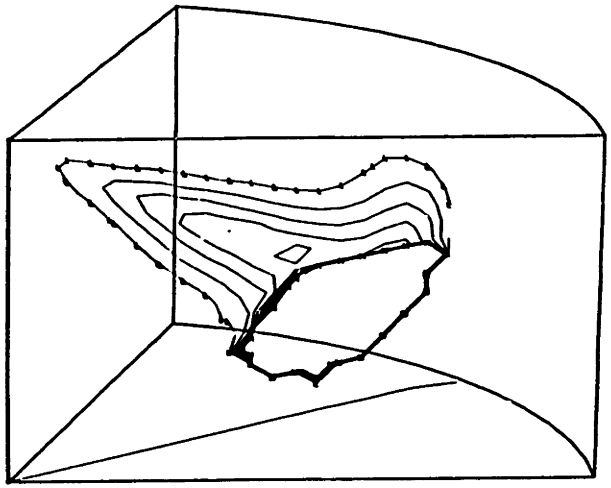

Equivalence Ratio

t = 1.0 ms

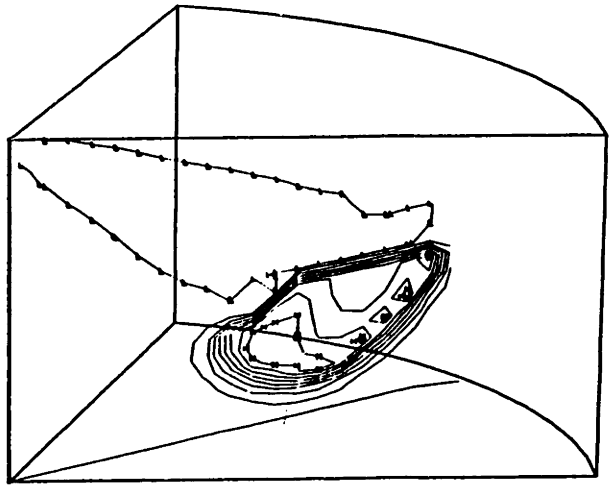

T

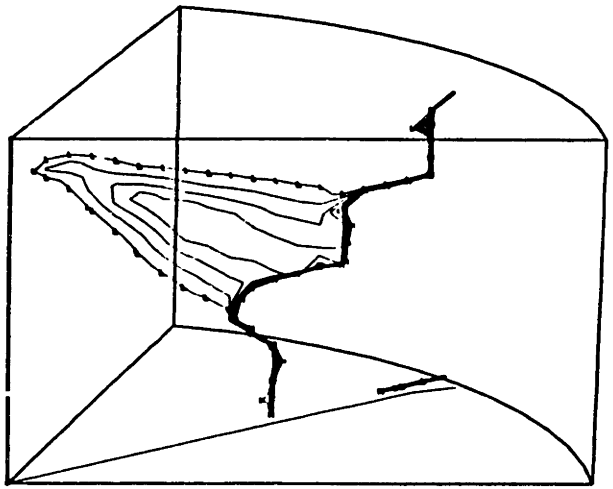

Equivalence Ratio

t = 2.0 ms

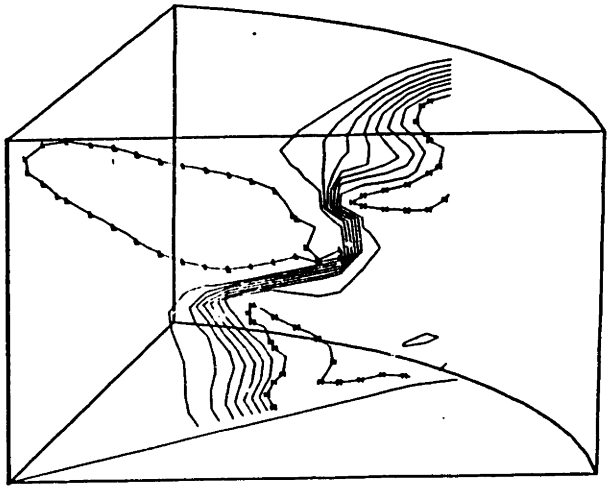

T

Figure 5.38 3-D Computation: Run A (Continued)

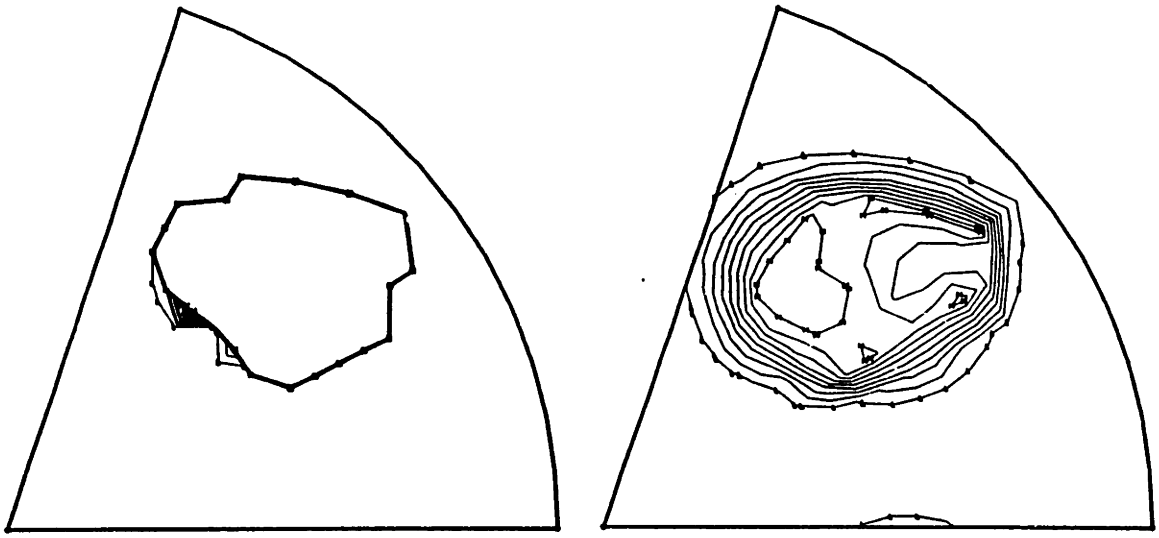

Equivalence Ratio T

t = 1.0 ms

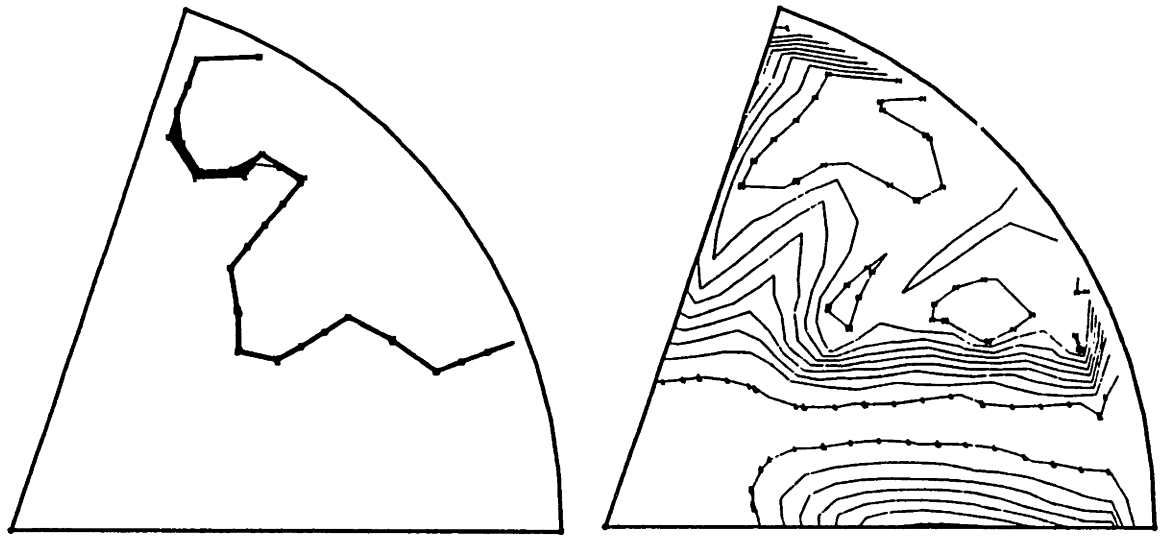

Equivalence Ratio T

t = 2.0 ms

Figure 5.39 3-D Computation: Run A

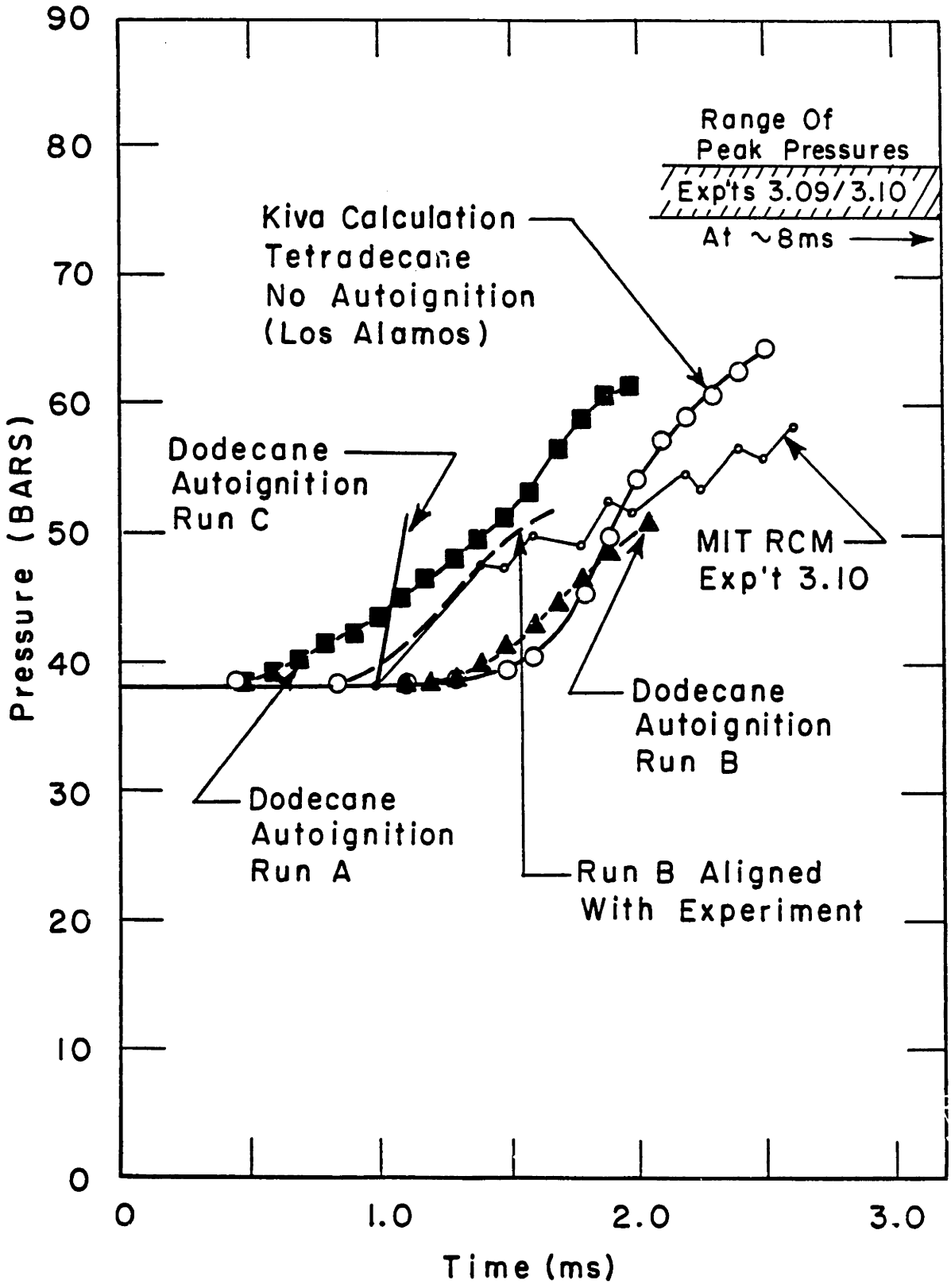

Figure 5.40 Pressure Traces from 3-D Calculations

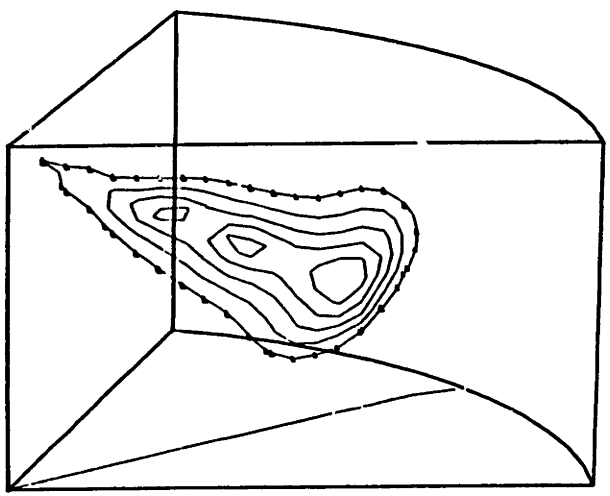

Equivalence Ratio

t = 0.92 ms

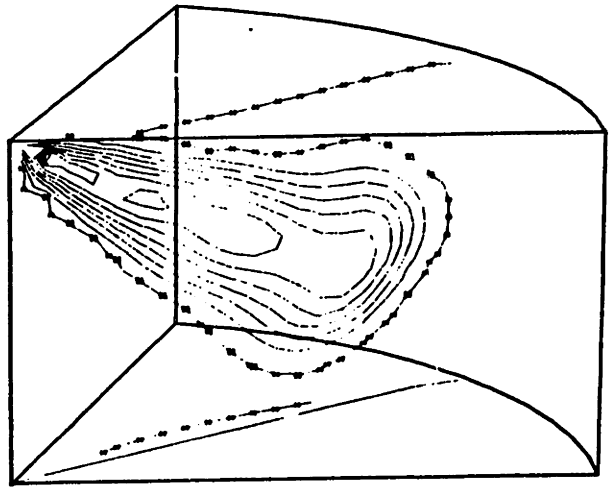

T

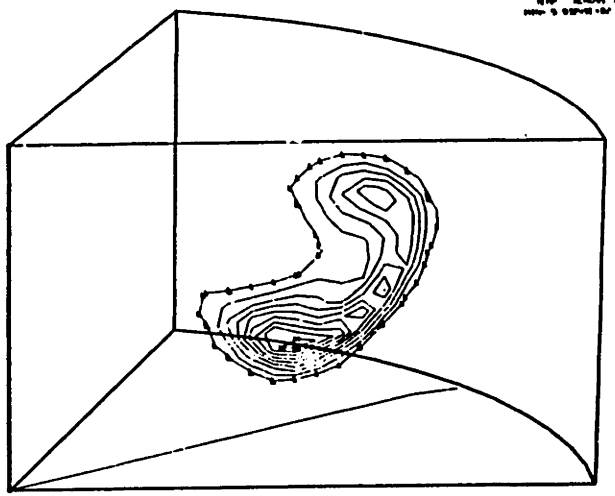

(Q)

Ignition Delay = 1.02 ms

A_{f4} = 2.21 X 10^5

Figure 5.41 3-D Computation: Run C

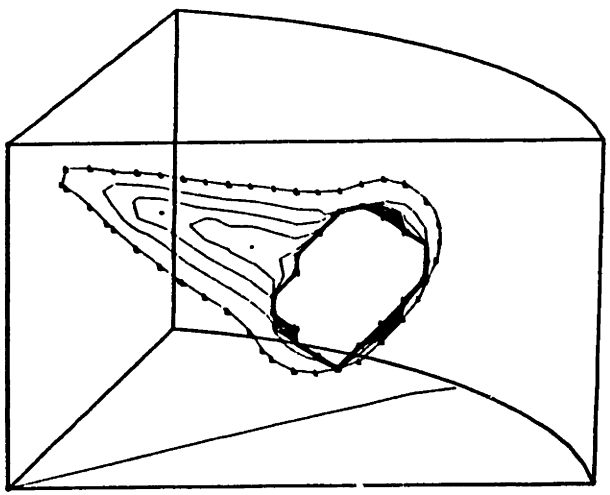

Equivalence Ratio

t = 1.05 ms

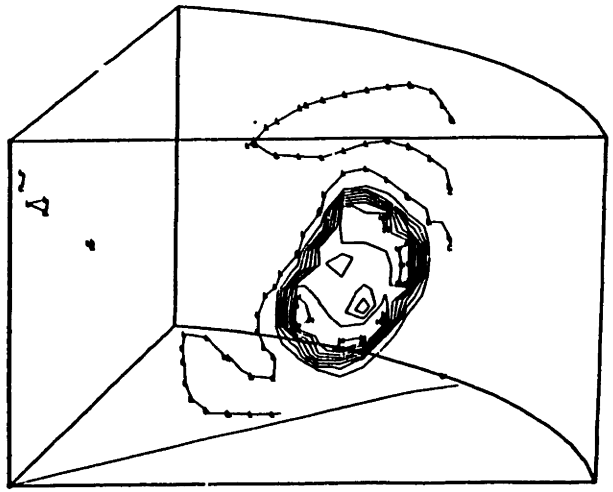

T

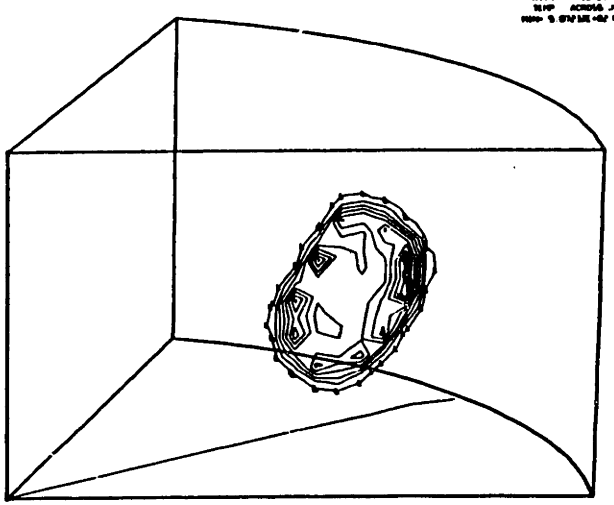

(Q)

Figure 5.41 3-D Computation: Run C (Continued)

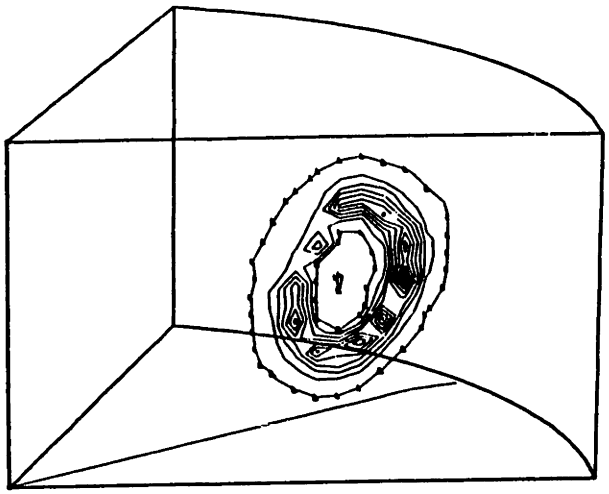

p

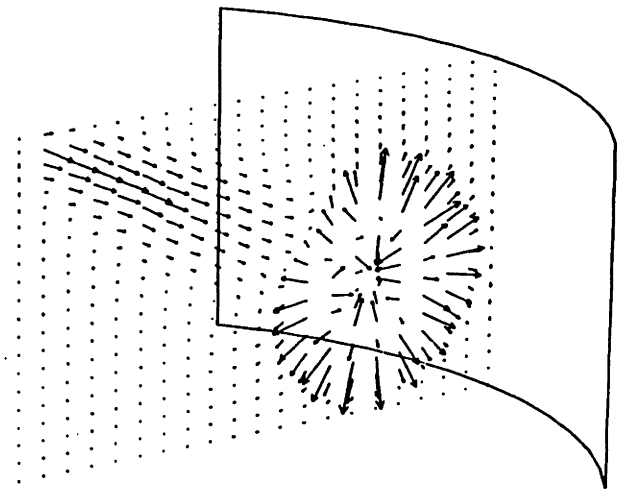

Velocity Vectors

t = 1.05 ms

Figure 5.41 3-D Computation: Run C (Continued)

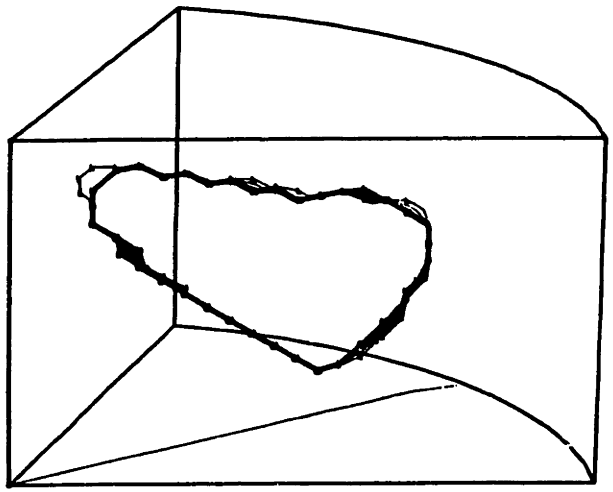

Equivalence Ratio

t = 1.08 ms

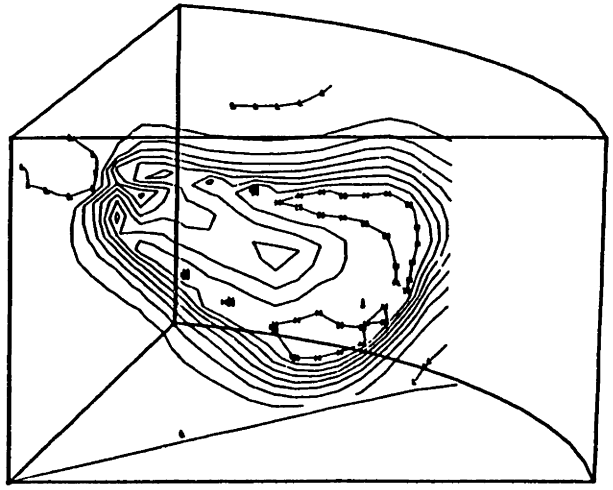

T

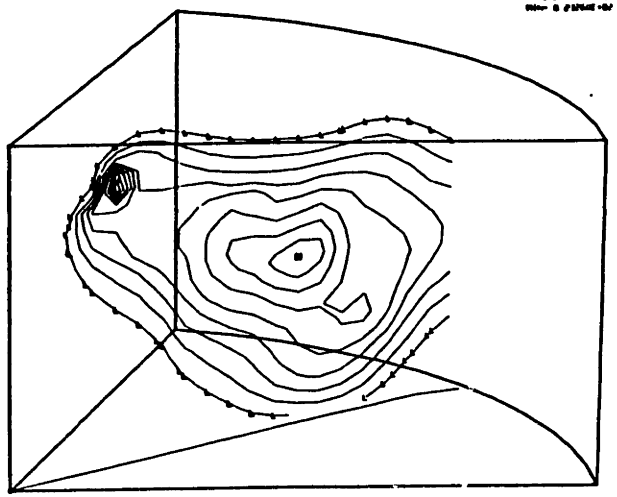

(Q)

Figure 5.41 3-D Computation: Run C (Continued)

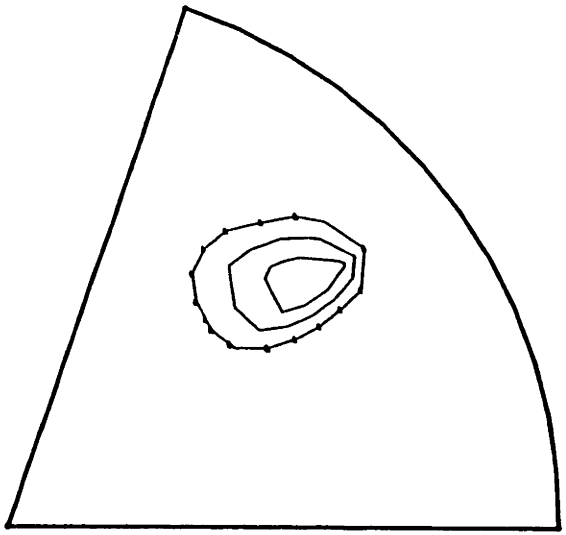

Equivalence Ratio

t = 0.92 ms

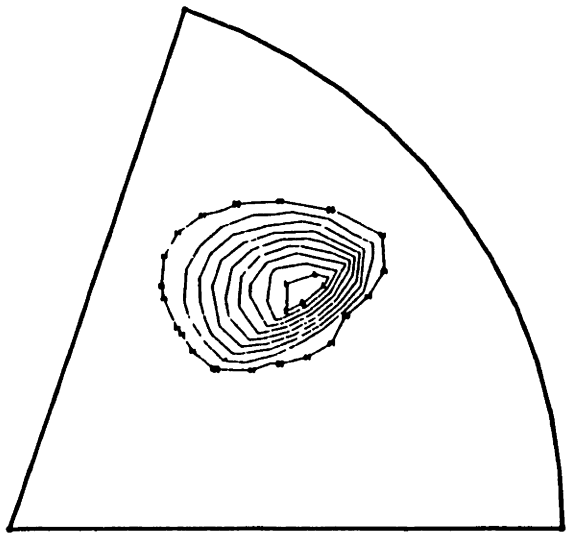

T

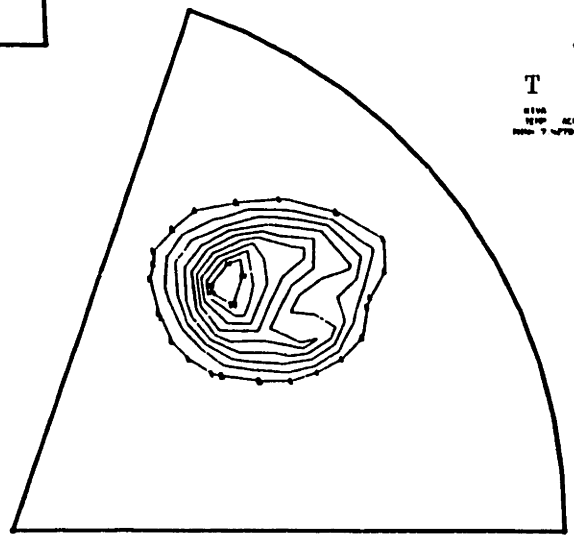

(Q)

Ignition Delay = 1.02 ms

Figure 5.42 3-D Computation: Run C

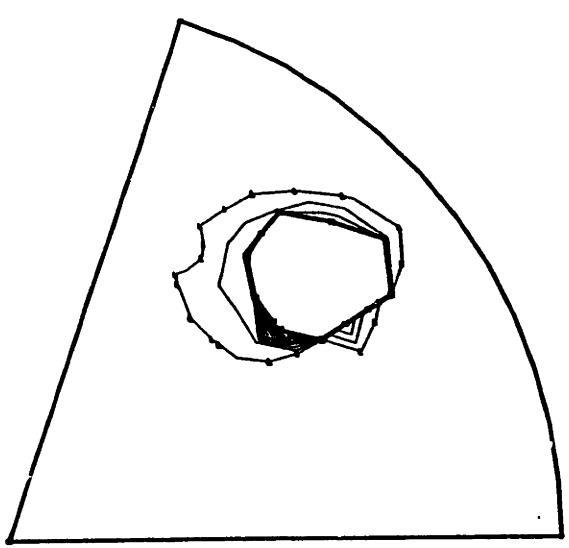

Equivalence Ratio

t = 1.05 ms

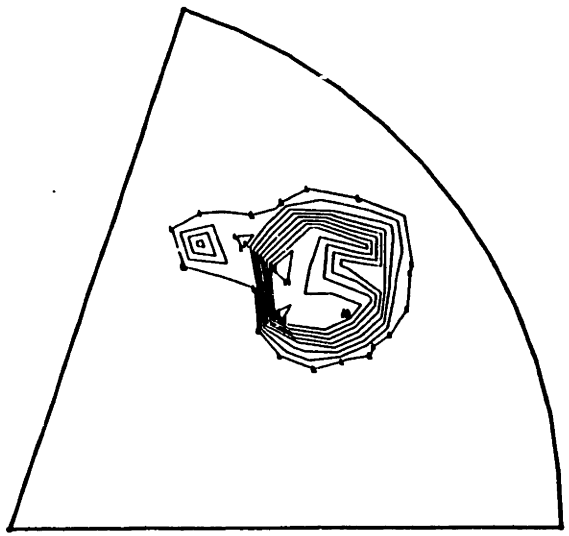

T

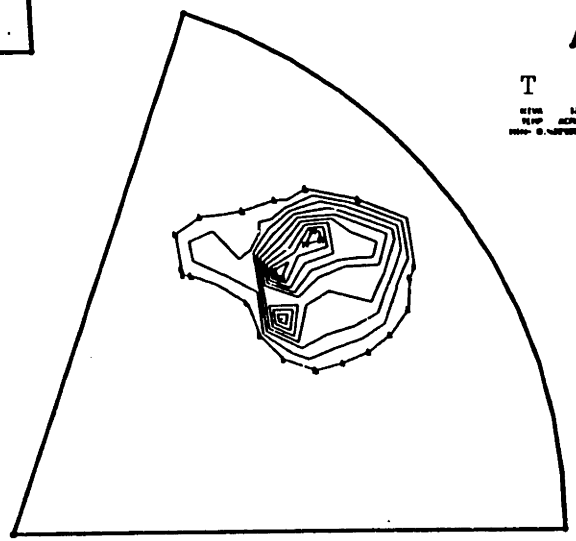

(Q)

Figure 5.42 3-D Computation: Run C (Continued)

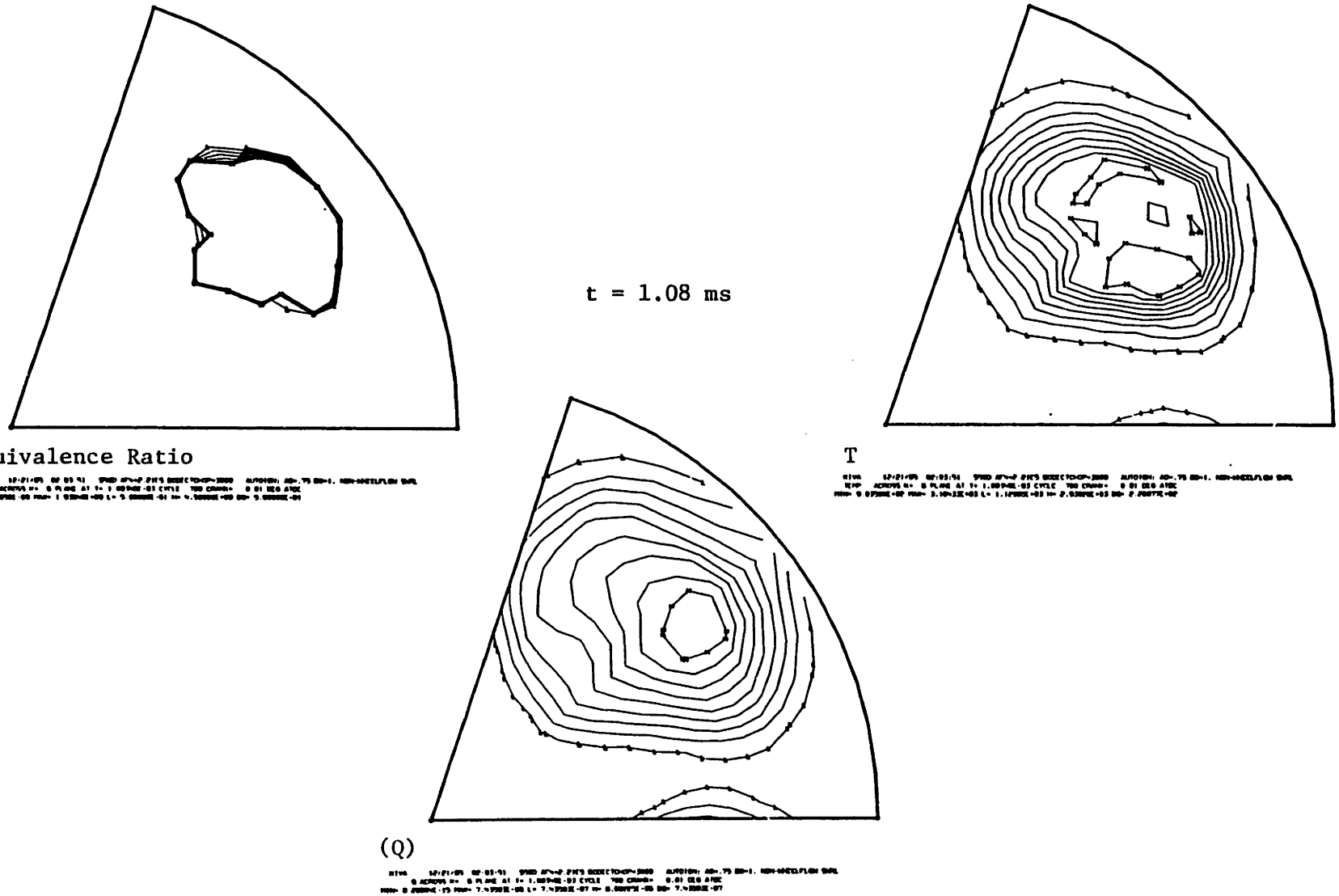

Figure 5.42 3-D Computation: Run C (Continued)

APPENDIX A

KIVA Program Updates for Autoignition

A.1 The Shell Autoignition Model Installed in Subroutine CHEM

```
IDENT SHELSUE
/.        SHELL AUTOIGNITION MODEL CHEMISTRY
/.          ALL EXTRA PARAMETERS AND SPECIAL RATE FORMULATION ARE
/.          CONTAINED HERE.
/.
/.            MAT 10/28/85
/.      DODECANE MASS RATIOS INSTALLED 12/13:  AFO4 MUST BE SET
/.          CURRENT PARAMETERS FOR 90 RON ISOOCTANE/HEPTANE MIX
/.&&&&&&&&&&&&&&&&&&&&&&&&&&&&&&&&&&&&&&&&&&&&&&&&&&&&&&&&&&&&&&&&&&&&
/.    THIS VERSION INCORPORATES-----
/.          ALTERNATE (B) TEST FOR SUBCYCLING
/.          TURNOFF OF AUTOIGNITION EQUATIONS WHEN HIGH TEMP REACHED.
/.
/.++++++++++++++++++++++++++++++++++++++++++++++++++++++++++++++++++++++++++
/.      CHEMICAL (KINETICS) SUBCYCLING UPDATE
/.
/.      ROUTINE ADDS A CHEMICAL SUBCYCLING AEILITY TO
/.       SUBROUTINE CHEM FOR SOLVING THE AUTOIGNITION MODEL OF
/.       HALSTEAD ET AL  (SHELL MODEL).  THE SUBCYCLE TIME IS
/.       ADJUSTED DYNAMICALLY FOR EACH CELL AS A FUNCTION OF THE LOCAL
/.       POPULATION CHANGE OF [B], THE BRANCHING AGENT.
/.        IF [B] IS LOW, NO SUB-CYCLING IS PERFORMED.
/.       IF [RH] OR [O2] ARE LOW, CHEMISTRY IS SKIPPED.
/.       IF TEMP IS HIGH AND [O] IS LOW, AUTOIGNITION IS SKIPPED.
/.       MAIN HEAT RELEASE IS SKIPPED NLESS T>TFREEZ
/.
/.
/.--------------------------------------------------------------------
I.CHEM.5
      COMMON/CHUBS/ICSLOG,ICSLC
I.CHEM.6
                STORE SPECIAL RATE PARAMETERS FOR SHELL MODEL
       NOTE ALL ACTIV. ENERGIES ARE SCALED TO ACTIV. TEMPS ....
                ALL HEATING VALUES ARE ERGS/MOLE.
      DATA X1,X3,X4 / 1.0, 0., -1./,Y1,Y3,Y4 /0., 0., 0.35/
      DATA FUELN,FUELM,FUELQ,COF,CO2F,PSTOIC,CRATIO,OFUEL
     1 ,RMN2 /12.0, 13.0,1.88764,0.61846,0.304620, 1.11385,0.67,
     2         3.9363E12            ,3.60714 /
      DATA AFO1, EF1, AFO2, EF2, AFO3, EF3, AFO4, EF4 /
     1 7.3E-4, -7.55E3,180., -3.53E3, 1.47, 5.04E3, 2.07E6,1.51E4/
      DATA TFREEZ,RTFREZ,TINHIB,COINH
     1      /950., 1.052631E-3, 900., 1.0E-7/
      DATA AP1,EP1,AP2,EP2,AP3,EP3 /
     1     1.0E12, 0., 1.0E11, 7.56E3, 1.0E13, 428./
      DATA IGLOG/0/,ICSLOG/0/,IGLOGO/0/,IGLOG2/0/
      DATA TCHOP / 1000./
I.CHEM.7
      DATA XSCHEM /1.00/, ICSLIM/200/
I.CHEM.10
      ICSLOG=0
I.CHEM.16
      IF(TEMP(I4).LT.TCUT) GO TO 80
      SISTOC=SIE(I4)
      IF (SPD(I4,7)*RMW(7).LE.1.E-15) GO TO 9000
        DO NOT SUBCYCLE IF CELL TOO HOT FOR AUTOIGNITON EQUATIONS
      IF (TEMP(I4).GT.TCHOP) GO TO 9000
      RTIJK= 1./TEMP(I4)
      IF (TEMP(I4).GT.TFREEZ) RTIJK=RTFREZ
      TKBEST=CF(4)*EXP(-EF(4)*RTIJK)
   TOTAL NET B RATE CONSIDERED TO SET SUBCYCLING
      CONB= SPD(I4,7)*RMW(7)
      CONR= SPD(I4,6)*RMW(6)
      CONQ= SPD(I4,8)*RMW(8)
      CONRH= SPD(I4,1)*RMW(1)
      CONOX= SPD(I4,2)*RMW(2)
      P1K= AP1*EXP(-EP1*RTIJK)
      P2K= AP2*EXP(-EP2*RTIJK)
      P3K= AP3*EXP(-EP3*RTIJK)
      PTK= 1./(1./(CONOX*P1K)+ 1./P2K + 1./(CONRH*P3K))
      FO1=AFO1*EXP(-EF1*RTIJK)
      FO2=AFO2*EXP(-EF2*RTIJK)
      F1L= FO1*(CONOX**X1)*(CONRH**Y1)
      F2P= FO2*PTK
      TKBEST= ABS((-TKBEST*CONB+F1L*PTK*CONR+F2P*CONR*CONQ)/ CONB )
      ICS=IFIX(DT*TKBEST/XSCHEM)
      IF (ICS.LT.1) ICS=1
      IF (ICS.GT.ICSLIM) ICS=ICSLIM
      DTC=DT/(FLOAT(ICS))
      GO TO 9010
 9000 ICS=1
```

```
      DTC=DT
 9010 CONTINUE
       IF (ICS.GT.ICSLOG) ICSLC=I4
      IF (ICS.GT.ICSLOG) ICSLOG=ICS

      %%%%%%SET EXPONENTS AND STOICH. COEF. FOR SHELL....
              DO NOT MOVE THESE TO A DATA STATEMENT AS THEY ARE
              OVERWRITTEN IN RINPUT %%%%%%%%%%
      FBM(4,2)=CO2F
      FBM(9,2)=COF
      FBMAM(4,2)=CO2F
      FBMAM(9,2)=COF
      FBM(3,5)=RMN2
      FBM(3,6)= 2.-RMN2
      FBMAM(3,5)=RMN2
      FBMAM(3,6)= 2.-RMN2
 %%%%%%%%%%%%%%%%%%%%%%%%%%%%%%%%%%%%%%%%%%%%%%%%%%%%%%%%%%%%%%%%%%%%%%%%
      DO 75 IC=1,ICS
      2ND STAGE IGNITION DETECTOR
      IF((TEMP(I4).GT.1000.).AND.(IGLOGO.EQ.0)) GO TO 7002
      GO TO 7003
 7002 WRITE(59,7012) T+(IC-1)*DTC,I4
      IGLOGO=1
 7003 IF((TEMP(I4).GT.1100.).AND.(IGLOG.EQ.0)) GO TO 7000
      GO TO 7004
 7000 WRITE(59,7010)  T + (IC-1)*DTC , I4
 7010 FORMAT(5X,'1100 DEGREE K IGNITION AT T=',E10.4,' AT CELL ',I5)
      IGLOG=1
 7004 IF((TEMP(I4).GT.2000.).AND.(IGLOG2.EQ.0)) GO TO 7006
      GO TO 7020
 7006 WRITE(59,7014) T+(IC-1)*DTC,I4
      IGLOG2=1
 7020 CONTINUE
 7012  FORMAT(5X,'1000 DEGREE K IGNITION AT T=',E10.4,' AT CELL ',I5)
 7014  FORMAT(5X,'2000 DEGREE K IGNITION AT T=',E10.4,' AT CELL ',I5)
D,CHEM.18
I,CHEM.19

       FREEZE REACTION RATES OF KNOCK MODEL TO 950K IF TEMP HIGHER.
           (NOTE PREXPONENTIAL TEMP FACTOR NOT FROZEN, BUT NEVER USED.)
       IF (TIJK.GT.TFREEZ) RTIJK= RTFREZ
       CONO=SPD(I4,8)*RMW(8)
         INHIBIT KNOCK MODEL IF T HIGH AND (O) LOW
        IF ((TIJK.GT.TINHIB).AND.(CONO.LT.COINH)) GO TO 900
         SHUT DOWN AUTOIGNITION EQUATIONS IF CELL ALREADY HOT
       IF (TIJK.GT.TCHOP) GO TO 900
       CONOX=SPD(I4,2)*RMW(2)
       CONRH=SPD(I4,1)*RMW(1)
     JUMP OUT OF LOOP IF NO FUEL OR O2 AVAILABLE
       IF(CONRH.LT.1.E-10) GO TO 76
       IF (CONOX.LT.1.E-10) GO TO 76
       FO1=AFO1*EXP(-EF1*RTIJK)
       FO2=AFO2*EXP(-EF2*RTIJK)
       FO3=AFO3*EXP(-EF3*RTIJK)
       FO4=AFO4*EXP(-EF4*RTIJK)
       P1K=AP1*EXP(-EP1*RTIJK)
       P2K=AP2*EXP(-EP2*RTIJK)
       P3K=AP3*EXP(-EP3*RTIJK)
       F1L=FO1*(CONOX**X1)*(CONRH**Y1)
       F3L=FO3*(CONOX**X3)*(CONRH**Y3)
       F4L=FO4*(CONOX**X4)*(CONRH**Y4)

        PTK=1./(1./(CONOX*P1K) + 1./P2K + 1./(CONRH*P3K))
    ABOVE FORM FOR PTK IS CORRECTED VERSION 11/ 27/ 85
       F1P=F1L*PTK
       F2P=FO2*PTK
       F3P=F3L*PTK
       F4P=F4L*PTK
       SPECIAL TEMP/CONC. DEPENDENT STOICHIOMETRY FACTORS
       EQLL= (F1L*MW(7)+F4L*MW(8))/(MW(1)/FUELM+PSTOIC*MW(2))
       ASP1= (EQLL+1.)/FUELM
       ASP2= (EQLL+1.)*PSTOIC
       SET STOICH. FACTORS IN PROPAGATION EQUATION NRK=2
       FAM(1,2) = ASP1
       FAM(2,2) = ASP2
       FBM(7,2) = F1L
       FBM(8,2) = F4L
       FBMAM(1,2) = -ASP1
       FBMAM(2,2) = -ASP2
       FBMAM(7,2) = F1L
```

```
      FBMAM(8,2) = F4L
D.CHEM.20
      DO 70 IR=1,NRK-1
/,    REMOVE UNUSED BACK REACTION OVERHEAD
D.CHEM.40,CHEM.44
/,    REMOVE UNUSED BACK REACTION OVERHEAD
I.CHEM.52
      IF (IR.EQ.2) KF= PTK
      IF (IR.EQ.3) KF=F2P
      IF (IR.EQ.5) KF=F3P
D.CHEM.73
      DOMEGA(IR)=ROM*DTC*(CTOP-CBOT)/((ROM+DTC*CBOT)*(FLBM-FLAM))
D.CHEM.77
           HEAT RELEASE ONLY ON PROPAGATION STEP SCALED BY
                REACTANT CONSUMPTION.
      DECHEM = 0.
      IF (IR.EQ.2) DECHEM=OFUEL*(EOLL+1.)*DOMEGA(2)/RO(I4)
D.CHEM.78
D.CHEM.80
I.CHEM.81
900   CONTINUE

**********MAIN HEAT RELEASE TURNED ON!!--TO TURN OFF, INSTALL NEXT LINE.
      GO TO 970

*************************************************************************
          DISALLOW HEAT RELEASE REACTION IF . LT.TINHIB [NEW]
      IF (TIJK.LT.TINHIB) GO TO 970
           MAIN HEAT RELEASE IR=NRK, LAST KINETIC EQN
      IR=NRK
                  RESET TEMP TO UNFREEZE IF PREVIOUSLY FROZEN
      RTIJK= 1./TIJK
      RP=1.
      PP=1.
      NE=NELEM(IR)
      DO 920 KK=1,NE
      ISP=CM(KK,IR)
      ROM=SPD(I4,ISP)*RMW(ISP)
      IF (AM(ISP,IR).EQ.0) GO TO 910
      IF (ROM.LE.0.) RP=0.
      IF (ROM.GT.0.) RP=RP*ROM**AE(ISP,IR)
910   IF (BM(ISP,IR).EQ.0) GO TO 920
      IF (ROM.LE.0.) PP=0.
      IF (ROM.GT.0.) PP=PP*ROM**BE(ISP,IR)
920   CONTINUE
      KB=0.
      KF=0.
      TEB=1.
      TEF=1.
      EKB=1.
      EKF=1.
      IF (CB(IR).LE.0.) GO TO 930
   BACKWARD REACTION COEF
      IF (EB(IR).NE.0.) EKB=EXP(-EB(IR)*RTIJK)
      IF (ZETAB(IR).NE.0.) TEB=TIJK**ZETAB(IR)
      KB=CB(IR)*TEB*EKB
930   IF (CF(IR).LE.0.) GO TO 940
   FORWARD REACTION COEF
      IF (EF(IR).NE.0.) EKF=EXP(-EF(IR)*RTIJK)
      IF (ZETAF(IR).NE.0.) TEF=TIJK**ZETAF(IR)
      KF=CF(IR)*TEF*EKF
   NONSTANDARD RATE COEFS GO HERE
      FIND REF SPECIES
940   OMEG=KF*RP-KB*PP
      RMIN=0.
      IF (OMEG.EQ.0.) GO TO 970
      DO 950 KK=1,NE
      ISP=CM(KK,IR)
      IF (SPD(I4,ISP).LE.0.) GO TO 950
      ROM=OMEG*FBMAM(ISP,IR)*MW(ISP)/SPD(I4,ISP)
      IF (ROM.GE.0.) GO TO 950
      IF (ROM.LT.RMIN) IREF=ISP
      RMIN=AMIN1(RMIN,ROM)
950   CONTINUE
      ROM=SPD(I4,IREF)*RMW(IREF)
      FLAM=FAM(IREF,IR)
      FLBM=FBM(IREF,IR)
      CTOP=FLAM*KB*PP+FLBM*KF*RP
      CBOT=FLAM*KF*RP+FLBM*KB*PP
```

```
      DOMEGA(IR)=ROM*DTC*(CTOP-CBOT)/((ROM+DTC*CBOT)*(FLBM-FLAM))
      DO 960 ISP=1,NSP
      SPD(I4,ISP)=SPD(I4,ISP)+MW(ISP)*FBMAM(ISP,IR)*DOMEGA(IR)
960    CONTINUE
     DECHEM=OR(NRK)*DOMEGA(IR)/RO(I4)
     %%%%%% %%%%%% %%%%%% %%%%%%
       HEAT RELEASE OUTPUT TO FEED HEAT2C*   ADDITIONAL OUTPUT FOR
         AUTOIG.EQUATIONS IS IN HEAT2C.
      HRC=DECHEM*RO(I4)*VOL(I4)
      GLCHEM=GLCHEM+HRC
      GLCHDT=GLCHDT+HRC/DT
     %%%%%% %%%%%% %%%%%% %%%%%% %%%%%%
      DECHK=ABS(DECHEM/SIE(I4))
      SIE(I4)=SIE(I4)+DECHEM
      TCHEM=AMAX1(TCHEM,DECHK)
970    CONTINUE
      UPDATE THE STATE VARIABLES AFTER EACH TIME SUBSTEP TO FOLLOW
      THE TEMPERATURE PULSE
           (EXERPTED FROM SUBROUTINE STATE LINES 13-39)
      IF (TEMP(I4).GT.5000.) GO TO 8000
      IF (ICS.EQ.1) GO TO 75
      IT=INT(0.01*TEMP(I4))
8010  ELO=0.
      EHI=0.
      DO 8020 ISP=1,NSP
      ELO=ELO+SPD(I4,ISP)*EK(IT+1,ISP)
      EHI=EHI+SPD(I4,ISP)*EK(IT+2,ISP)
8020  CONTINUE
      ELO=ELO/RO(I4)
      EHI=EHI/RO(I4)
      IF (SIE(I4).LE.EHI) GO TO 8030
      IT=IT+1
      IF (IT.GT.49) GO TO 8000
      GO TO 8010
8030  IF (SIE(I4).GE.ELO) GO TO 8040
      IT=IT-1
      IF (IT.LT.0) GO TO 8000
      GO TO 8010
8040  FR=(SIE(I4)-ELO)/(EHI-ELO)
      TEMP(I4)=(FLOAT(IT)+FR)*100.
      CV=(EHI-ELO)*0.01
      P(I4)=0.
      DO 8045 ISP=1,NSP
      P(I4)=P(I4)+SPD(I4,ISP)*RMW(ISP)
8045  CONTINUE
      P(I4)=P(I4)*RGAS*TEMP(I4)
      GAMMA(I4)= 1.+P(I4)/(RO(I4)*CV*TEMP(I4))
      GO TO 75
8000  WRITE(59,8110) T,NCYC,I,J,K,I4,TEMP(I4),SIE(I4),IT,CRANK
      WRITE(12,8110) T,NCYC,I,J,K,I4,TEMP(I4),SIE(I4),IT,CRANK
      CALL EXITA(7)
8110  FORMAT(' TEMPERATURE OVERFLOW AT T=',E12.5,' CYC',I5,'I=',I3,
     1  'J=',I3,'K=',I2,'I4=',I5/' TEMP=',E12.5,' SIE=',E12.5,
     2  'IT=',I5,' CRANK=',OPF7.2)
75     CONTINUE
       END SUBCYCLE LOOP ON CHEMISTRY
76        CONTINUE
      DESIE= ABS((SIE(I4)-SISTOC)/SIE(I4))
      TCHEM=AMAX1(TCHEM,DESIE)
   END HEAT RELEASE COMPUTATION
D,CHEM,85,CHEM,101
I,NEWCYC,57
       IF(MOD(NCYC,MINO(25,NCFILM)).EQ.0) WRITE(59,9050)ICSLOG,ICSLC
9050       FORMAT(5X,'ICS FROM CHEM SUBCYCLE IS', I5,'AT I4=',I4)
D,RINPUT,8,11
     DATA(IDSP(N),N=1,9)/8H  C12H26,8H       O2,8H       N2,
     1                   8H      CO2,8H      H2O,8H    RDOT,
     2                   8H        E,8H        O,8H      CO/
D,RINPUT,16,17
D,RINPUT,48,77
       IGNORE CONTRIBUTION OF TRACE SPECIES TO SPECIFIC HEAT OF GAS
      DATA (HK(N,6),N=1,51) / 51*0.0/
      DATA (HK(N,7),N=1,51) / 51*0.0/
      DATA (HK(N,8),N=1,51) / 51*0.0/
     MOVE CO FROM POSITION 11 TO 9
D,RINPUT,78
      DATA(HK(N,9),N=1,51) /-2.072,-1.379,-.683,.013,.711,1.417,2.137,
D,RINPUT,84,89
I,NEWCYC,8
       COMMON/CHUBS/ICSLOG,ICSLC
```

A.2 Update Control File for 2-D Autoigniting Spray

```
READ KUEXPORT
READ HOB
READ HKMESHR
READ INJSOW
READ JVBC
READ TKEFUDRR
READ UPDF
READ KILLRZ
READ DROPPEN
READ SHELSUB
READ HEAT2C
/.{{{{{{{{{{{{{{{{{{{{{{{{{{{{{{{{{{{{{{{{{{{{{{{{{{{{{{{{{{{{{{{{{{{{{{{{{{{{{{{
/.  UPDATES FOR SHELL AUTOIGNITION MODEL IN SPRAY INJECTION
/.   FOR 2D REGION WITH HEAT RELEASE.  FORM FOLLOWS SCHAPERTONS AND
/.   LEE SAE 850502.
/.       SHELSUB PROVIDES SUBCYCLING IN ROUTINE CHEM
/}}}}}}}}}}}}}}}}}}}}}}}}}}}}}}}}}}}}}}}}}}}}}}}}}}}}}}}}}}}}}}}}}}}}}}}}}}}}}}}
```

A.3 Parameter Adjustments

```
IDENT HOB
/.
/.      UPDATES TO USE AUTOIGNITION EQUATIONS. SET NO. OF
/.      VAPOR PRESSURE POINTS. ETC.
/.            THIS VERSION FOR DODECANE FUEL WITH LVAP=66
D.EXPORT.1
D.COMD.8
      PARAMETER(NV=2000.LNXPYP=1000.LNSP=9.LNRK=7.LNRE=1.NPAR=1200.
     1          LP=50.LCHOP=50.LVAP=67)
```

A.4 Stretched Axial Grid for 2-D Sprays

```
IDENT HKMESHR
/. ##################################################################
/. SPECIAL UPDATE TO PERFORM 2D FUEL JET SIMULATION OF
/. HIROYASU AND KADOTA ('74) EXPERIMENT
/. WRITTEN BY R A GENTRY , MODIFIED 10/17/85, CORR. 10/21/85
/. ##################################################################
I.SETUP.9
      DIMENSION ZMSH(27)
I.SETUP.82
      ZMSH(1)=0.
      ZMSH(2)=1.2052
      ZMSH(3)=2.3055
      ZMSH(4)=3.3101
      ZMSH(5)=4.2273
      ZMSH(6)=5.0647
      ZMSH(7)=5.8292
      ZMSH(8)=6.5272
      ZMSH(9)=7.1808
      ZMSH(10)=7.7928
      ZMSH(11)=8.3658
      ZMSH(12)=8.9023
      ZMSH(13)=9.4047
      ZMSH(14)=9.8751
      ZMSH(15)=10.3155
      ZMSH(16)=10.7279
      ZMSH(17)=11.1141
      ZMSH(18)=11.4756
      ZMSH(19)=11.8142
      ZMSH(20)=12.1311
      ZMSH(21)=12.4279
       ZMSH(22)=12.7058
       ZMSH(23)=12.9660
       ZMSH(24)=13.2097
       ZMSH(25)=13.4378
       ZMSH(26)=13.6514
       ZMSH(27)=13.8514
D.SETUP.87,SETUP.119
      X(I4)=RPO(I)
      Z(I4)=ZMSH(K)
```

A.5 Square-Wave Injection

```
IDENT INJSQW
/. ##################################################################
/. UPDATE TO CREATE SQUARE WAVE FUEL INJECTION PULSE
/. WRITTEN BY R A GENTRY 9/9/85
/. ##################################################################
D.INJECT.21
      TM1INJ=TSPMAS
      IF(T.LE.T2INJ) TM1INJ=TM1INJ*(T-T1INJ)/(T2INJ-T1INJ)
```

A.6 O'Rourke Boundary Conditions for 2-D Spray

```
IDENT JVBC
/. #####################################################
/. UPDATE TO ADD SPECIAL BOUNDARY CONDITIONS FOR CELL CONTAINING
/. THE FUEL NOZZLE EXIT
/. VELOCITY BOUNDARY CONDITIONS USE O ROURK S ALGORITHM
/. WRITTEN BY R A GENTRY 9/3/85
/.    CONDITIONS 880K.31ATMA.DODEC 12/15
/. #####################################################
I,BC.144
      I4=(NZ-1)*NXPNYP+1
      W(I4)=-0.9801*VELINJ
      W(I4+NXP)=-0.9801*VELINJ
      W(I4+1)=-0.9801*VELINJ
      W(I4+NXP+1)=-0.9801*VELINJ
      U(I4+1)=-0.09312*VELINJ
      U(I4+NXP+1)=-0.09312*VELINJ
      U(I4+NXPNYP+1)=-0.09312*VELINJ
      U(I4+NXP+NXPNYP+1)=-0.09312*VELINJ
D.TIMSTP.54
      DTGROW=CVMGZ(DT,1.05*DT,NCYC)
```

A.7 Axial Penetration Measurement for Droplets

```
IDENT DROPPEN
/.%%%%%%%%%%%%%%%%%%%%%%%%%%%%%%%%%%%%%%%%%%%%%%%%%%%%%%%%%%%%%%%%%%%%%%%%%%%%%%%%
/.    FIND AND PRINT OUT THE MAX Z DISTANCE PENETRATION OF ANY
/.     DROPLET PARCEL
/.           MAT 10/22/85 FOR HIROYASU EXPERIMENTS
/.%%%%%%%%%%%%%%%%%%%%%%%%%%%%%%%%%%%%%%%%%%%%%%%%%%%%%%%%%%%%%%%%%%%%%%%%%%%%%%%%
I.NEWCYC.49
/.          ZREF IS TOP OF CYLINDER= Z MAX, (O PENETRATION)
         ZREF=Z((NZP-1)*NXPNYP+1)
         ZMIN=ZREF
I.NEWCYC.50
               IF (ZP(N).LT.ZMIN) ZMIN=ZP(N)
I.NEWCYC.52
         ZPEN=ZREF-ZMIN
D.EXPORT.226
    1 T,DT,NS,NVS,GRIND,IDSP(1),TSPM(1),PM,AVP,PGS,IDDT,ZPEN
D.EXPORT.229
    2 4H PM=,E11.4,5H AVP=,E11.4,5H PGS=,E11.4,2X,A1/4H PN=,E11.4)
```

A.8 Maintain Stretched Grid Through the REZONE Subroutine

```
IDENT KILLRZ
/.   DISABLE REZONE COMMAND IN MAIN LOOP.   FIXES NONSTANDARD MESH.
/.              MAT 10/21/85       HIROYASU EXPERIMENTS
D.REZONE.15
D.EXPORT.498
           WG(I4)=0.0
D.REZONE.31
```

A.9 Constant Diffusivity Turbulence

```
IDENT TKEFUDRR
/.%%%%%%%%%%%%%%%%%%%%%%%%%%%%%%%%%%%%%%%%%%%%%%%%%%%%%%%%%%%%%%%%%%%%%%%
/. UPDATE TO SPECIFY LOCAL TURBULENT KINETIC ENERGY AS A FRACTION OF
/. THE LOCAL CENTERLINE KINETIC ENERGY.  ALSO SPECIFYTHE TURBULENCE
/. LENGTH SCALE AND RESULTING TIME SCALES.
/.  20% OF MEAN FLOW ENERGY IS ASSIGNED TO TKE IN THIS VERSION.
/.       PROBLEM: HIROYASU INJECTION EXPERIMENTS
/.     WRITTEN BY R.A. GENTRY 9/11/85, MODIFIED 10/22/85
/.    CONDITIONS 880K,31ATM ABS, DODECANE
/.%%%%%%%%%%%%%%%%%%%%%%%%%%%%%%%%%%%%%%%%%%%%%%%%%%%%%%%%%%%%%%%%%%%%%%%
D,PMOVTV.40,PMOVTV.42
          IF (IMOM.GT.99999.OR.TURBT(N).GT.T) GO TO 30
          QT=0.10*(U(IMOM)*U(IMOM)+V(IMOM)*V(IMOM)+W(IMOM)*W(IMOM))
          TEDDYSZ=169.5/(SQRT(QT)+1.E-10)
          TSC1=TEDDYSZ/(SQRT(QT)+1.E-10)
D,PMOVTV.45
          TSC2=TEDDYSZ/(VRELED+1.E-10)
```

A.10 Particle Diffusion Modification

```
IDENT PARDIF
/. KO71885 PARTICLE DIFFUSION MODIFICATION 102385/1355
D,PMOVTV.48
     IF(TSCALE.GE.DT) GO TO 25
     RELVEL(N)=SQRT((UN(IMOM)-UP(N))**2+(VN(IMOM)-VP(N))**2
    1              +(WN(IMOM)-WP(N))**2)
     I4=I4P(N)
     VRELT=RELVEL(N)
     TG=TP(N)+THIRD*(TEMP(I4)-TP(N))
     VISCP=AIRMU1*TG*SQRT(TG)/(TG+AIRMU2)
     REYP=AMAX1(1.0E-10,2.0*RO(I4)*RADP(N)*VRELT/VISCP)
     CD=CVMGT(.424,24.0/REYP*(1.0+SIXTH*REYP**TWOTHD),REYP.GT.1000.)
     DRAGDT=.375*RO(I4)*VRELT*CD*DT/(RHOP*RADP(N))
     ATD=DRAGDT/DT*TSCALE
     EXPATD=EXP(ATD)
     EXPMATD=1./EXPATD
     EXP2ATD=EXPATD**2
     TERM1=(1.-EXPMATD)**4
     TERM2=EXP2ATD/(EXP2ATD-1.)
     DTOTD=DT/TSCALE
     EXPADT=EXP(DRAGDT)
     TERM3=DTOTD-(1.-1./EXPADT**2)/(1.-EXPMATD**2)
     TERM4=(ATD-1.+EXPMATD)**2*DTOTD
     FSUBX=SQRT(TERM1*TERM2*TERM3+TERM4)
     FSUBXO=DRAGDT-1.+1./EXPADT
     TURVEL=TURVEL*FSUBX/FSUBXO
  25 ETA1=1.-2.*FRAN(0.)
I,PMOVTV.63
     IF(TSCALE.LT.DT) GO TO 40
```

A.11 3-D Swirl Profile

```
IDENT SWIRL
/. ##########################################################################
/. UPDATE TO CREATE NON-WHEEL FLOW SWIRL
/. WRITTEN BY R A GENTRY 12/10/85
/. ##########################################################################
D.SETUP.216,SETUP.218
      SWIRLFAC=3.1*(X(I4)*X(I4)+Y(I4)*Y(I4))**0.5
      SWIRLFAC=0.5*SWIRLFAC/RPO(NPO)
      SWIRLSUM=SWIRLFAC
      TERMK=SWIRLFAC
      DO 1950 KK=1,10
      KKFL=FLOAT(KK)
      TERMK=-TERMK*SWIRLFAC*SWIRLFAC/(KKFL*(KKFL+1.))
      SWIRLSUM=SWIRLSUM+TERMK
1950  CONTINUE
      EFFVEL=1450*SWIRLSUM
      U(I4)=-Y(I4)*EFFVEL/(X(I4)*X(I4)+Y(I4)*Y(I4)+1.E-10)**0.5
      V(I4)=X(I4)*EFFVEL/(X(I4)*X(I4)+Y(I4)*Y(I4)+1.E-10)**0.5
```

A.12 Global Diagnostics for Heat Transfer and Gross Heat Release

```
IDENT HEAT2
/.&&&&&&&&&&&&&&&&&&&&&&&&&&&&&&&&&&&&&&&&&&&&&&&&&&&&&&&&&&&&&&&&&&&&&&&&&&&&
/.      GLOBAL DIAGNOSTICS OUTPUT FOR ENGINE COMBUSTION
/.
/.      THIS UPDATE CAUSES KIVA TO WRITE TAPE11 CONTAINING THE
/.      FOLLOWING DIAGNOSTICS: (GLOBAL I.E. SUMMED OVER ALL ACTIVE CELLS)
/.         > CHEMICAL HEAT RELEASE RATE (GROSS)
/.         > INTEGRATED CHEMICAL HEAT RELEASE (GROSS)
/.         > WALL HEAT TRANSFER RATE
/.         > INTEGRATED WALL HEAT TRANSFER
/.         > SPACE-AVERAGE CYLINDER PRESSURE
/.
/.     TAPE 11 MUST BE POST-PROCESSED USING HEATPLT, WHICH USES
/.     DISSPLA GRAPHICS TO PRODUCE TIME HISTORIES OF THE LISTED
/.     VARIABLES.  WRITE INSTRUCTIONS TO TAPE11 OCCUR IN
/.     SUBROUTINE NEWCYC, AT INTERVALS OF 25 CYCLES.  THE DIMENSION
/.     STATEMENTS IN POSTPROCESSOR HEATPLT MUST
/.     ACCOMODATE NCLAST/25 + 2 DATA POIINTS.
/.
/.       INTEGRATED GLOBAL VARIABLES ARE STORED ON TAPE8
/.       DURING A DUMP AND READ FROM TAPE7 UPON RESTART.
/.              MAT 11/4/85  . MODIFIED 11/5/85
/.&&&&&&&&&&&&&&&&&&&&&&&&&&&&&&&&&&&&&&&&&&&&&&&&&&&&&&&&&&&&&&&&&&&&&&&&&&&&
/.    OPEN COMMUNICATION WITH TAPE11 FOR GLOBAL PARAMETERS
D,KIVA.2
     PROGRAM KIVA (ITAPE,TAPE5=ITAPE,TAPE7,TAPE8,TTY,TAPE59=TTY,
    1TAPE11)
I,COMD.55
      COMMON/GLBBAL/AAA8(1),GLCHEM,GLCHDT,IGLC,GLHEAT,
    1   GLHTDT,AVP,TLITE,IGLOG,IGLOGO,IGLOG2,ZZZ8
I,NEWCYC.53
      IF(MOD(NCYC,MINO(25,NCFILM)).NE.O)  GO TO 9000
      IGLC=IGLC+1
      WRITE(11) IGLC  ,T,GLCHEM,GLCHDT,AVP,GLHEAT,GLHTDT
      CALL FEMPTY(11)
9000  CONTINUE
I,SETUP.297
       IGLC=O
       GLCHDT=O.O
       GLCHEM=O.O
      GLHEAT=O.O
      GLHTDT=O.O
             WRITE(11) (NAME(N),N=1,10)
/.     ZERO THE HEAT RELEASE RATE PRIOR TO THIS TIME STEP
/.       (FOR 1 EXECUTION EACH OF CHEM AND CHEMEO)
I,CHEM.9
             GLCHDT=O.
I,CHEM.79
             HRC=DECHEM*RO(I4)*VOL(I4)
             GLCHEM=GLCHEM+HRC
             GLCHDT=GLCHDT+HRC/DT
I,CHEMEO.22
      SIESTO=SIE(I4)
I,CHEMEO.125
      HRC=(SIE(I4)-SIESTO)*RO(I4)*VOL(4)
      GLCHEM=GLCHEM+HRC
      GLCHDT=GLCHDT+HRC/DT
I,LAWALL.6
/.     ZERO THE HEAT TRANSFER RATE PRIOR TO THIS TIME STEP
      GLHTDT=O.
I,LAWALL.99
      HRC=FRICTN*(1.-TKESW)*CELLM
      GLHEAT=GLHEAT-HRC
      GLHTDT=GLHTDT-HRC/DT
I,LAWALL.103
      HRC=DT*FLUX*AREA
      GLHEAT=GLHEAT+HRC
      GLHTDT=GLHTDT+HRC/DT
I,LAWALL.176
      HRC=FRICTN*(1.-TKESW)*CELLM
      GLHEAT=GLHEAT-HRC
      GLHTDT=GLHTDT-HRC/DT
I,LAWALL.180
      HRC=DT*FLUX*AREA
      GLHEAT=GLHEAT+HRC
      GLHTDT=GLHTDT+HRC/DT
I,LAWALL.256
      HRC=FRICTN*(1.-TKESW)*CELLM
      GLHEAT=GLHEAT-HRC
      GLHTDT=GLHTDT-HRC/DT
```

```
I,LAWALL,260
      HRC=DT*FLUX*AREA
      GLHEAT=GLHEAT+HRC
      GLHTDT=GLHTDT+HRC/DT
/.     READ GLOBAL VALUES FROM THE RESTART TAPE
I,TAPERD,31
      NWLCM=LOCF(ZZZ8)-LOCF(AAA8)+1
      READ(7) (AAA8(N),N=1,NWLCM)
/.     RE-ZERO COUNTER FOR GLOBAL PLOTTING ROUTINE AT RESTART
I,TAPERD,39
      IGLC=0
      WRITE(11) (NAME(N),N=1,10)
/.     WRITE GLOBAL VALUES ON THEDUMP TAPE
I,TAPEWR,26
      NWLCM=LOCF(ZZZ8)-LOCF(AAA8)+1
      WRITE(8) (AAA8(N),N=1,NWLCM)
```

A.13 Postprocessor for Global Diagnostics Output (Runs after KIVA)

```
DECK HEATPLT
      PROGRAM HEATPLT(TAPE11,TAPE13,TTY,TAPE59=TTY)
C*****************************************************************
C          POSTPROCESSOR FOR GLOBAL TIME SERIES PLOTS FROM KIVA WITH
C          HEAT.  PLOTS PRODUCED USING DISSPLA LIBRARY.
C        PLOT 1:  GROSS HEAT RELEASE AND RELEASE RATE VS TIME
C        PLOT 2:  HEAT TRANSFER AND TRANSFER RATE VS TIME
C        PLOT 3:  NET HEAT RELEASE AND RELEASE RATE VS TIME
C    ALL 3 PLOTS INCLUDE THE SPACE-AVG CYLINDER PRESSURE TRACE.
C
C    UNITS:  PRESSURE -BAR, TIME-MSEC, RATES-KJ/S, INTEGRALS-J
C
C      PROGRAM READS TAPE11 FROM KIVA
C    PROGRAM WRITES TAPE13 AS A MONITOR--COULD BE DELETED
C
C     ADJUST DIMENSION PARAMETERS TO BE AT LEAST NCLAST/25 +2
C
C               MAT 11/4/85
C*****************************************************************
C
            PARAMETER (NDATA=200)
        DIMENSION T(NDATA),P(NDATA),GLCHEM(NDATA),GLHEAT(NDATA),
     1    GLCHDT(NDATA),GLHTDT(NDATA),NET1(NDATA),NET2(NDATA),NAME(10)
      REAL NET1,NET2,NT1MN,NT2MN,NT1MX,NT2MX
        DATA PMIN,PMAX/0.,110./
        DATA SIZEX,SIZEY/5.0,8.0/
      DATA EPSILON/ 1./
       CALL GPLOT(1HU,4HGLOB,4)
       CALL LIBDISP
           READ(11) (NAME(N),N=1,10)
               WRITE(13,110) NAME
20    READ(11) IGLC,T(IGLC),GLCHEM(IGLC),GLCHDT(IGLC),P(IGLC),
     1                GLHEAT(IGLC),GLHTDT(IGLC)
      IF (EOF(11)) 30,25
      IF (EOI(11)) 30,25
25       WRITE(13,100) IGLC,T(IGLC),P(IGLC)
100   FORMAT(5X,I5,4E12.4)
     WRITE(13,105) GLCHEM(IGLC),GLCHDT(IGLC),GLHEAT(IGLC),GLHTDT(IGLC)
        IGOOD=IGLC
105   FORMAT(1X,7E10.4)
110   FORMAT(10A8)
       GO TO 20
30    CONTINUE
      IGLC=IGOOD
      CONVERT PRESSURE FROM DYNE/CM**2 TO BAR
      CONVERT TIME TO MILLISECONDS
       CONVERT HEAT RELEASE AND TRANSFER RATES TO KJ/S
       CONVERT HEAT RELEASE AND TRANSFER VALUES TO J.
       FIND MIN AND MAX VALUES FOR SCALING PLOTS
      GLMAX= -1.E25
      GLDTMX= -1.E25
      NT1MX= -1.E25
      NT2MX= -1.E25
      NT1MN=1.E25
      NT2MN=1.E25
      HTMX= -1.E25
      HDMX= -1.E25
      GLMIN=1.E25
      GLDTMN=1.E25
      HDMN=1.E25
      HTMN=1.E25
          DO 50 I=1,IGLC
      GLCHEM(I)= 1.E-7*GLCHEM(I)
      GLCHDT(I)= 1.E-10*GLCHDT(I)
      GLHEAT(I)= 1.E-7*GLHEAT(I)
      GLHTDT(I)= 1.E-10*GLHTDT(I)
      IF (GLCHDT(I).GT.GLDTMX) GLDTMX=GLCHDT(I)
      IF (GLCHDT(I).LT.GLDTMN) GLDTMN=GLCHDT(I)
      IF (GLCHEM(I).GT.GLMAX) GLMAX=GLCHEM(I)
      IF (GLCHEM(I).LT.GLMIN) GLMIN=GLCHEM(I)
      NET1(I)= GLCHEM(I)-GLHEAT(I)
      NET2(I)= GLCHDT(I)-GLHTDT(I)
      IF (NET1(I).GT.NT1MX) NT1MX=NET1(I)
      IF (NET2(I).GT.NT2MX) NT2MX=NET2(I)
      IF (NET1(I).LT.NT1MN) NT1MN=NET1(I)
      IF (NET2(I).LT.NT2MN) NT2MN=NET2(I)
      IF (GLHEAT(I).GT.HTMX) HTMX=GLHEAT(I)
      IF (GLHEAT(I).LT.HTMN) HTMN=GLHEAT(I)
      IF (GLHTDT(I).GT.HDMX) HDMX=GLHTDT(I)
      IF (GLHTDT(I).LT.HDMN) HDMN=GLHTDT(I)
```

```
      T(I)=1.E3*T(I)
50        P(I)=1.0E-6*P(I)
      IF (GLMAX.EQ.GLMIN) GLMAX=GLMIN+EPSILON
      IF (GLDTMX.EQ.GLDTMN) GLDTMX=GLDTMN+EPSILON
      IF (HTMX.EQ.HTMN) HTMX=HTMN+EPSILON
      IF (HDMX.EQ.HDMN) HDMX=HDMN+EPSILON
      IF (NT1MX.EQ.NT1MN) NT1MX=NT1MN+EPSILON
      IF (NT2MX.EQ.NT2MN) NT2MX=NT2MN+EPSILON
      TIMMAX=T(IGLC)
      TIMMIN=T(1)

*****************************************************************
    PLOT 1
       CALL PAGE(8.5,11.)
       CALL NOBRDR
            CALL XNAME(' TIME -MSEC $',100)
            CALL YNAME(' GROSS CHEM. HEAT RELEASE RATE -KJ/SEC$',100)
                 CALL AREA2D(SIZEX,SIZEY)
      CALL GRAF(TIMMIN,'SCALE',TIMMAX,GLDTMN,'SCALE',GLDTMX)
            CALL CURVE(T,GLCHDT,IGLC,0)
      CALL YGRAXS(GLMIN,'SCALE',GLMAX,8.,
     1  'GROSS CHEM. HEAT RELEASE -J$',-100,5.0,0.0)
                 CALL DASH
            CALL CURVE(T,GLCHEM,IGLC,0)
       CALL YGRAXS(PMIN,10.,PMAX,8.,'PRESSURE-BAR$',-100,0.,0.)
            CALL DOT
             CALL CURVE(T,P,IGLC,0)
            CALL ENDPL(0)
+++++++++++++++++++++++++++++++++++++++++++++++++++++++++++++++++++++++++
      PLOT 2
      CALL PAGE(8.5,11.)
     CALL NOBRDR
     CALL XNAME(' TIME -MSEC $',100)
     CALL YNAME('HEAT TRANSFER RATE -KJ/SEC$',100)
     CALL AREA2D(SIZEX,SIZEY)
      CALL GRAF(TIMMIN,'SCALE',TIMMAX,HDMN,'SCALE',HDMX)
      CALL RESET('DOT')
     CALL CURVE(T,GLHTDT,IGLC,0)
     CALL YGRAXS(HTMN,'SCALE',HTMX,8.,
    1'INT. HEAT TRANSFER -J$',-100,5.0,0.0)
      CALL DASH
      CALL CURVE(T,GLHEAT,IGLC,0)
      CALL YGRAXS(PMIN,10.,PMAX,8.,'PRESSURE -BAR$',-100,0.,0.)
      CALL DOT
      CALL CURVE(T,P,IGLC,0)
      CALL ENDPL(0)
*****************************************************************
     PLOT 3
      CALL PAGE(8.5,11.)
      CALL NOBRDR
      CALL XNAME(' TIME -MSEC $',100)
      CALL YNAME(' NET HEAT RELEASE RATE -KJ/SEC$',100)
      CALL AREA2D(SIZEX,SIZEY)
     CALL GRAF(TIMMIN,'SCALE',TIMMAX,NT2MN,'SCALE',NT2MX)
      CALL RESET('DOT')
      CALL CURVE(T,NET2,IGLC,0)
       CALL YGRAXS(NT1MN,'SCALE',NT1MX,8.,
    1 'NET HEAT RELEASE -J$',-100,5.,0.)
      CALL DASH
      CALL CURVE(T,NET1,IGLC,0)
      CALL YGRAXS(PMIN,10.,PMAX,8.,'PRESSURE -BAR$',-100,0.,0.)
       CALL DOT
      CALL CURVE(T,P,IGLC,0)
     CALL ENDPL(0)

     AFTER ALL PLOTS FINISHED GO
          CALL DONEPL

       CALL EXIT
       END
```

APPENDIX B

Input List for a 2-D Autoigniting Spray of Dodecane Fuel

```
1 SHELL MODEL:SPRAY - DODECANE FUEL, HIROYASU COMBUSTION BOMB 12/85
 NX         20
 NY         01
 NZ         26
 LWALL       0
 NCHOP       1
 LPR         0
 USECTR      1
 NCFILM   050
 NCTAP8  9999
 NCLAST  2000
 CAFILM    9.99E+9
 CAFIN    +28.0
 ANGMOM      1.0
 CYL         1.0
 DY          0.0
 PGSSW       1.0
 SAMPL       0.0
 DTI         1.0E-6
 DTMAX       1.0E-5
 TLIMD       1.0
 TWFIN        .035
 FCHEM       0.25
 STROKE      0.0
 SQUISH    13.8514
 RPM         0.0
 ATDC        0.0
 CONROD    16.269
 OFFSET      0.0
 SWIRL       0.0
 THSECT    72.0
 THNOZL    08.0
 SSSF        2.5
 TEMPI   850.0
 AO          0.75
 BO          1.0
 ANC4        0.00
 ARTVIS      1.0
 UVFREE      1.0
 ADIA        0.0
 CHARLF      2.0
 ANUO        7.100
 VISRAT-.66666667
 RGAS    8.3143E+7
 TCUT     300.0
 TCUTE   5000.0
 EPSCHM      0.02
 OMGCHM      1.0
 TKEI        0.00
 ATKE        0.00
 DTKE        1.0
 AIRMU1   1.457E-5
 AIRMU2   110.0
 AIRLA1   252.0
 AIRLA2   200.0
 AIRDIF    2.00E-6
 EXPDIF      0.6
 TWALL    353.00
 RPR         1.0
 RSC         1.0
 XIGNIT      1.0E+4
 T1IGN     -1.0
 T2IGN     -1.0
 CA1IGN   -27.0
 CA2IGN   -17.4
 IIGNL1      4
 IIGNR1      4
 JIGNF1     13
 JIGND1     14
 KIGNB1      7
 KIGNT1      7
 IIGNL2      0
 IIGNR2      0
 JIGNF2      0
 JIGND2      0
 KIGNB2      0
 KIGNT2      0
 KWIKEO      1
 KOLIDE      1
 EVAPP       1.0
```

```
T1INJ      +0.0
T2INJ     3.00E-3
CA1INJ   -52.0
CA2INJ   -39.328
TSPMAS     0.0439
TNPARC   1200.
RHOP       0.7452
TPI      296.0
VELINJ    1.00E+4
CONE     010.0
DCONE     05.0
TILT       0.0
SMR       3.00E-4
SURTEN    25.04
TCRIT    659.00
TURB       1.0
NPO       21
NUNIF     21
  1    1    0.0       0.0
  2    1  0.0500      0.0
  3    1  0.1050      0.0
  4    1  0.1655      0.0
  5    1   .2320      0.0
  6    1   .3053      0.0
  7    1   .3858      0.0
  8    1   .4744      0.0
  9    1   .5718      0.0
 10    1   .6790      0.0
 11    1   .7969      0.0
 12    1   .9266      0.0
 13    1  1.0692      0.0
 14    1  1.2261      0.0
 15    1  1.3987      0.0
 16    1  1.5886      0.0
 17    1  1.7975      0.0
 18    1  2.0272      0.0
 19    1  2.2800      0.0
 20    1  2.5579      0.0
 21    1  2.8637      0.0
 NSP         9
RHO1       0.0      MW1     170.33     HTF1    -52.77
RHO2   2.9877E-3    MW2      32.0      HTF2       0.0
RHO3   9.8350E-3    MW3      28.0      HTF3       0.0
RHO4       0.0      MW4      44.00     HTF4    -93.965
RHO5       0.0      MW5      18.00     HTF5    -57.103
RHO6       0.0      MW6     101.00     HTF6       0.0
RHO7       0.0      MW7     202.0      HTF7       0.0
RHO8       0.0      MW8     202.0      HTF8       0.0
RHO9       0.0      MW9      28.0      HTF9    -27.200
 NRK         7
CF1    1.2000E12  EF1    1.7600E+4  ZF1        0.0
CB1       0.0     EB1       0.0     ZB1        0.0
AM1     1    1     0     0     0     0     0     0     0     0     0
BM1     0    0     0     0     0     2     0     0     0     0     0
AE1    1.000    1.000    0.000    0.000    0.000    0.000    0.000    0.000
       0.
BE1    0.000    0.000    0.000    0.000    0.000    0.000    0.000    0.000
       0.
CF2    1.0000E00  EF2    1.0000E00  ZF2        0.0
CB2    0.0        EB2       0.0     ZB2        0.0
AM2     1    1     0     0     0     1     0     0     0     0     0     0
BM2     0    0     0     1     1     1     1     1     1     0     0
AE2    0.000    0.000    0.000    0.000    0.000    1.000    0.000    0.000
       0.
BE2    0.000    0.000    0.000    0.000    0.000    0.000    0.000    0.000
       0.00
CF3    1.00       EF3    1.00       ZF3        0.0
CB3    0.0        EB3    0.0        ZB3        0.0
AM3     0    0     0     0     0     1     0     1     0     0     0
BM3     0    0     0     0     0     1     1     0     0     0     0
AE3    0.000    0.000    0.000    0.000    0.000    1.000    0.000    1.000
       0.0
BE3    0.000    0.000    0.000    0.000    0.000    0.000    0.000    0.000
       0.0
CF4    4.4000E17  EF4    2.2700E+4  ZF4        0.0
CB4       0.0     EB4       0.0     ZB4        0.0
AM4     0    0     0     0     0     0     1     0     0     0     0     0
BM4     0    0     0     0     0     2     0     0     0     0     0     0
AE4    0.000    0.000    0.000    0.000    0.000    0.000    1.000    0.000
       0.0
```

```
BE4    0.000    0.000    0.000    0.000    0.000    0.000    0.000    0.000
      0.0
CF5   1.0        EF5  1.0         ZF5      0.0
CB5   0.0        EB5  0.0         ZB5      0.0
AM5     0     0     0     0     0     1     0     0     0
BM5     0     0     1     0     0     0     0     0     0
AE5    0.        0.        0.        0.        0.        1.        0.        0.
       0.
BE5    0.        0.        0.        0.        0.        0.        0.        0.
       0.
CF6   3.0000E12 EF6   0.0         ZF6      0.0
CB6      0.0     EB6         0.    ZB6      0.0
AM6     0     0     0     0     0     2     0     0     0
BM6     0     0     1     0     0     0     0     0     0
AE6    0.        0.        0.        0.        0.        2.        0.        0.
       0.
BE6    0.        0.        0.        0.        0.        0.        0.        0.
       0.
CF7   5.0000E12 EF7   15780.      ZF7      0.0
CB7   0.0        EB7   0.0         ZB7      0.0
AM7     2    37     0     0     0     0     0     0     0     0
BM7     0     0     0    24    26     0     0     0     0     0
AE7    1.0       1.0       0.        0.        0.        0.        0.        0.
       0.
E7     0.        0.        0.        0.        0.        0.        0.        0.
       0.
 NRE        0
```

APPENDIX C

Tables of Physical Properties of Fuels for Use in "KIVA"

C.1 Heptane Fuel

```
IDENT HEPTA
/.+++++++++++++++++++++++++++++++++++++++++++++++++++++++++++++++++++++++++++++
/.
/.   UPDATE TO CONVERT FUEL IN KIVA TO HEPTANE C7H16
/.     --MATCHES TO KIVA VERSION NPL822+KUEXPORT
/.              M.THEOBALD 12/09/85
/.   DATA FROM VERGAFTIK PP. 266-267:
/.         LINEAR EXTRAPOLATIONS FOR:  LATENT HEAT BELOW 300K
/.                                     ENTHALPY ABOVE 1500K
/.
/.     OTHER DATA FOR HEPTANE:       TCRIT= 540K
/.                                   SURTEN AT 293K IS 20.86 (CGS)
/.                                   MOLECULAR WEIGHT= 100.2
/.                                   LIQUID DENSITY= 0.6836 (CGS) AT 293K.
/.                                   PCRIT= 2.736E7
/.+++++++++++++++++++++++++++++++++++++++++++++++++++++++++++++++++++++++++++++
/.   INSERT THE HEPTANE ENTHALPY TAPLE
/.
D,RINPUT.18,RINPUT.23
 +++
 +++ INPUT THE ENTHALPIES OF THE SPECIES FROM THE JANNAF TABLES
 +++ UNITS ARE KCAL/MOLE. 1=HEPTANE, 2=O2, 3=N2, 4=CO2, 5=H2O,
 +++ 6=H, 7=H2, 8=O, 9=N, 10=OH, 11=CO, 12=NO
 +++
      DATA (HK(N,1),N=1,51)/0.,2.56,5.12,7.69,12.20,17.73,24.15,
     1  31.33,39.19,47.60, 56.50, 65.83,75.536,85.552,95.838,106.35,
     2  115.95,125.56,135.17,144.77,154.38,163.99,173.59,183.20,192.81
     3  202.42,212.02,221.63,231.24,240.84,250.45,260.06,269.66,279.27,
     4  288.88,298.48,308.09,317.70,327.30,336.91,346.52,356.12,365.73,
     5  375.34,384.94,394.55,404.16,413.76,423.37,432.98,442.58/
/.
/.   LATENT HEAT FOR HEPTANE EVERY 100K
/.
D,RINPUT.92,RINPUT.96
 +++ HEPTANE LATENT HEAT VALUES IN RANGE   0-500K
   +++           VALUES IN ERGS/GRAM
      DATA (HLATU(N),N=1,51) /4.857E9,4.44E9,4.023E9,3.606E9,
     1                2.95E9,1.763E9,        45=0.0/
/.
/.   HEPTANE VAPOR PRESSURE EVERY 10K FROM 0-540K
/.
D,RINPUT.99,RINPUT.107
 +++ LVAP=55 TCRIT=540K
 +++ DATA FROM VERGAFTIK + SCALING LISTED ABOVE
 +++
      DATA (PVAP(N),N=1,LVAP) /28=0.0,2.74E4,4.72E4,7.78E4,1.23E5,
     1        1.89E5,2.80E5,4.05E5,5.70E5,7.86E5,1.06E6,1.41E6,
     2        1.83E6,2.35E6,2.98E6,3.72E6,4.60E6,5.600E6,6.780E6,
     3        8.140E6,9.710E6,1.151E7,1.354E7,1.586E7,1.847E7,2.14E7,
     4        2.4650E7,2.736E7/
/.
/.     END UPDATE FOR HEPTANE
```

C.2 Dodecane Fuel

```
IDENT DODEC
/.+++++++++++++++++++++++++++++++++++++++++++++++++++++++++++++++++++++++++++++
/.
/.  UPDATE TO CONVERT FUEL IN KIVA TO DODECANE C12H26
/.    --MATCHES TO KIVA VERSION NPL822+KUEXPORT
/.            M.THEOBALD 12/02/85
/.  DATA FROM VERGAFTIK PP. 284-285:
/.       LINEAR EXTRAPOLATIONS FOR: LATENT HEAT BELOW 300K
/.                                  ENTHALPY ABOVE 1500K
/.       VAPOR PRESSURE SCALED WITH TEMP. USING EQN (SEE REID.PROP.
/.         OF LIQ. AND GAS. EQN 6-2.4.2.5)
/.         LN(PV)-LN(PVO)=(LN(PV1)-LN(PVO))((T -TO)/(T1-TO))(T1/T)
/.             WITH OT1=TCRIT, TO=520.
/.
/.    OTHER DATA FOR DODECANE:     TCRIT= 659K
/.                                 SURTEN AT 298K IS 25.04 (CGS)
/.                                 MOLECULAR WEIGHT= 170.328
/.                                 LIQUID DENSITY= 0.7452 (CGS) AT 298K.
/.                                 PCRIT= 1.813E7
/.+++++++++++++++++++++++++++++++++++++++++++++++++++++++++++++++++++++++++++++
/.  INSERT THE DODECANE ENTHALPY TAPLE
/.
D,RINPUT.18,RINPUT.23
 +++
 +++ INPUT THE ENTHALPIES OF THE SPECIES FROM THE JANNAF TABLES
 +++ UNITS ARE KCAL/MOLE. 1=DODECANE, 2=O2,3=N2, 4=CO2, 5=H2O,
 +++ 6=H, 7=H2, 8=O, 9=N, 10=OH, 11=CO, 12=NO
 +++
      DATA (HK(N,1),N=1,51)/0.,4.23,8.47,12.7,20.33,29.67,40.47,
     1  52.54,65.76,79.29, 94.82,110.43,126.70,143.45,160.64,178.20,
     2  195.50,212.60,229.90,247.10,264.30,281.50,299.,315.90,333.10,
     3  350.30,367.50,384.70,401.90,419.10,436.30,453.50,470.70,487.90,
     4  505.10,522.30,539.50,556.70,573.90,591.10,608.30,625.50,642.70,
     5  659.90,677.10,694.30,711.50,728.70,745.90,763.10,780.20/
/.
/.  LATENT HEAT FOR DODECANE EVERY 100K
/.
D,RINPUT.92,RINPUT.96
 +++ DODECANE LATENT HEAT VALUES IN RANGE 300-600K
   +++          VALUES IN ERGS/GRAM
      DATA (HLATO(N),N=1,51) /5.160E9,4.64E9,4.120E9,3.600E9,
     1               3.08E9,2.560E9,9.40E8,44*0.0/
/.
/.  DODECANE VAPOR PRESSURE EVERY 10K FROM 0-660K
/.
D,RINPUT.99,RINPUT.107
 +++ LVAP=67 TCRIT=659K
 +++ DATA FROM VERGAFTIK + SCALING LISTED ABOVE
 +++
      DATA (PVAP(N),N=1,LVAP) /27*0.0,1.23E1,3.73E1,9.73E1,2.37E2,
     1       5.32E2,1.11E3,2.19E3,4.07E3,7.24E3,1.23E4,2.02E4,
     2       3.20E4,4.91E4,7.34E4,1.07E5,1.52E5,2.13 E5,2.91 E5,
     3       3.917E5,5.186E5,6.765E5,8.706E5,1.106E6,1.389E6,1.73E6,
     4       2.1227E6,2.571E6,3.093E6,3.695E6,4.386E6,5.176E6,6.07E6,
     5       7.087E6,8.228E6,9.505E6,1.093E7,1.251E7,1.427E7,1.620E7,
     6            1.813E7/
/.
/.    END UPDATE FOR DODECANE
```

C.3 Tridecane Fuel

```
IDENT TRIDEC
/.+++++++++++++++++++++++++++++++++++++++++++++++++++++++++++++++++++++++++++++
/.
/.   UPDATE TO CONVERT FUEL IN KIVA TO TRIDECANE    (FOR SAE PAPER 810259)
/.     --MATCHES TO KIVA VERSION NPL822+KUEXPORT
/.              M.THEOBALD 11/16/85, CORRECTED 12/4/85
/.   DATA FROM VERGAFTIK PP. 285-286:
/.         LINEAR EXTRAPOLATIONS FOR: LATENT HEAT BELOW 300K
/.                                    ENTHALPY ABOVE 1500K
/.        VAPOR PRESSURE SCALED WITH TEMP. USING EQN (SEE REID,PROP.
/.          OF LIQ. AND GAS. EQN 6-2.4.2.5)
/.          LN(PV)-LN(PVO)=(LN(PV1)-LN(PVO))((T-TO)/(T1-TO))*T1/T
/.              WITH T1=TCRIT, TO=510K
/.
/.     OTHER DATA FOR TRIDECANE:    TCRIT= 677K
/.                                  SURTEN AT 298K IS 25.69 (CGS)
/.                                  PCRIT= 1.72E7
/.                                  MOLECULAR WEIGHT= 184.35
/.                                  LIQ. DENSITY= 0.7527 AT 298K
/.+++++++++++++++++++++++++++++++++++++++++++++++++++++++++++++++++++++++++++++
/.   INSERT THE TRIDECANE ENTHALPY TAPLE
/.
D,RINPUT.18,RINPUT.23
 +++
 +++ INPUT THE ENTHALPIES OF THE SPECIES FROM THE JANNAF TAPBLES
 +++ UNITS ARE KCAL/MOLE. 1=TRIDECANE, 2=O2,3=N2, 4=CO2, 5=H2O,
 +++ 6=H, 7=H2, 8=O, 9=N, 10=OH, 11=CO, 12=NO
 +++
      DATA (HK(N,1),N=1,51)/0.,4.57,9.13,13.7,21.95,32.06,43.72,
     1  56.79,71.07,86.31,102.48,119.35,136.94,155.03,173.65,192.58,
     2  211.35,230.13,248.91,267.68,286.46,305.23,324.,342.78,361.56,
     3  380.33,399.11,417.88,436.66,455.43,474.21,492.98,511.76,530.53,
     4  549.31,568.08,586.86,605.63,624.41,643.18,661.96,680.73,699.51,
     5  718.28,737.06,755.83,774.61,793.38,812.16,830.93,849.71/
/.
/.   LATENT HEAT FOR TRIDECANE EVERY 100K
/.
D,RINPUT.92,RINPUT.96
 +++ TRIDECANE LATENT HEAT VALUES IN RANGE 300-600K
   +++          VALUES IN ERGS/GRAM
      DATA (HLATO(N),N=1,51) /5.207E9,4.67E9,4.132E9,3.595E9,
     1                3.06E9,2.521E9,1.29E9,44*0.0/
/.
/.   TRIDECANE VAPOR PRESSURE EVERY 10K FROM 0-680K
/.
D,RINPUT.99,RINPUT.107
 +++ LVAP=69 TCRIT=677K
 +++ DATA FROM VERGAFTIK + SCALING LISTED ABOVE
 +++
      DATA (PVAP(N),N=1,LVAP) /34*0.0,1.67E3,3.11E3,5.55E3,9.47E3,
     1       1.56E4,2.47E4,3.81E4,5.72E4,8.37E4,1.20E5,1.68E5,
     2       2.30E5,3.11E5,4.13E5,5.41E5,6.99E5,8.913E5,1.123E6,
     3       1.389E6,1.705E6,2.076E6,2.511E6,3.015E6,3.598E6,4.27E6,
     4       5.0330E6,5.903E6,6.886E6,7.994E6,9.237E6,1.062E7,1.22E7,
     5       1.388E7,1.577E7,1.72E7/
/.
/.     END UPDATE FOR TRIDECANE
```

C.4 Hexadecane (Cetane) Fuel

```
IDENT HEXA
/.+++++++++++++++++++++++++++++++++++++++++++++++++++++++++++++++++++++++++
/.
/.  UPDATE TC CONVERT FUEL IN KIVA TO HEXADECANE C16H34
/.    --MATCHES TO KIVA VERSION NPL822+KUEXPORT
/.            M.THEOBALD 12/09/85
/.  DATA FROM VERGAFTIK PP. 289-290:
/.       LINEAR EXTRAPOLATIONS FOR:  LATENT HEAT BELOW 300K
/.                                   ENTHALPY ABOVE 1500K
/.       VAPOR PRESSURE SCALED WITH TEMP. USING EQN (SEE REID.PROP.
/.         OF LIQ. AND GAS. EQN 6-2.4.2.5)
/.         LN(PV)-LN(PVO)=(LN(PV1)-LN(PVO))((T -TO)/(T1-TO))(T1/T)
/.
/.    OTHER DATA FOR HEXADECANE:  TCRIT= 725K
/.                                SURTEN AT 298K IS 27.22 (CGS)
/.                                MOLECULAR WEIGHT= 226.43
/.                                LIQUID DENSITY= 0.7700 (CGS) AT 298K.
/.                                PCRIT= 1.420E7
/.+++++++++++++++++++++++++++++++++++++++++++++++++++++++++++++++++++++++++
/.  INSERT THE HEXADECANE ENTHALPY TAPLE
/.
D.RINPUT.18.RINPUT.23
 +++
 +++ INPUT THE ENTHALPIES OF THE SPECIES FROM THE JANNAF TABLES
 +++ UNITS ARE KCAL/MOLE.  1=HEXADECANE, 2=O2,3=N2, 4=CO2, 5=H2O,
 +++ 6=H, 7=H2, 8=O, 9=N, 10=OH, 11=CO, 12=NO
 +++
      DATA (HK(N,1),N=1,51)/0.,5.57,11.1,16.7,26.83,39.22,53.51.
    1  69.51,87.01,105.7,125.46,146.13,167.62,189.76,212.47,235.68,
    2  257.60,279.52,301.43,323.35,345.27,367.18,389.,411.02,432.93,
    3  454.85,476.76,498.68,520.60,542.51,564.43,586.35,608.26,630.18,
    4  652.09,674.01,695.93,717.84,739.76,761.68,783.59,805.51,827.42,
    5  849.34,871.26,893.17,915.09,937.00,958.92,980.84,1002.75/
/.
/.  LATENT HEAT FOR HEXADECANE EVERY 100K
/.
D.RINPUT.92.RINPUT.96
 +++ HEXADECANE LATENT HEAT VALUES IN RANGE   0-700K
   +++           VALUES IN ERGS/GRAM
      DATA (HLATO(N),N=1,51) /5.094E9,4.59E9,4.087E9,3.583E9,
     1               3.08E9,2.576E9,1.72E9,3.446E8,43=0.0/
/.
/.  HEXADECANE VAPOR PRESSURE EVERY 10K FROM 0-730K
/.
D.RINPUT.99.RINPUT.107
 +++ LVAP=74 TCRIT=725K
 +++ DATA FROM VERGAFTIK + SCALING LISTED ABOVE
 +++
      DATA (PVAP(N),N=1,LVAP) /36=0.0,9.35E2,1.60E3,2.65E3,4.29E3,
     1       6.77E3,1.05E4,1.58E4,2.35E4,3.42E4,4.90E4,6.92E4,
     2       9.77E4,1.36E5,1.86E5,2.47E5,3.26E5,4.25 E5,5.464E5,
     3       6.960E5,8.729E5,1.073E6,1.309E6,1.587E6,1.911E6,2.29E6,
     4       2.720OE6,3.218E6,3.786E6,4.433E6,5.164E6,5.989E6,6.91E6,
     5       7.950E6,9.103E6,1.038E7,1.180E7,1.336E7,1.420E7/
/.
/.    END UPDATE FOR HEXADECANE
```